SPIE.

The Optomechanical Constraint Equations

THEORY AND APPLICATIONS

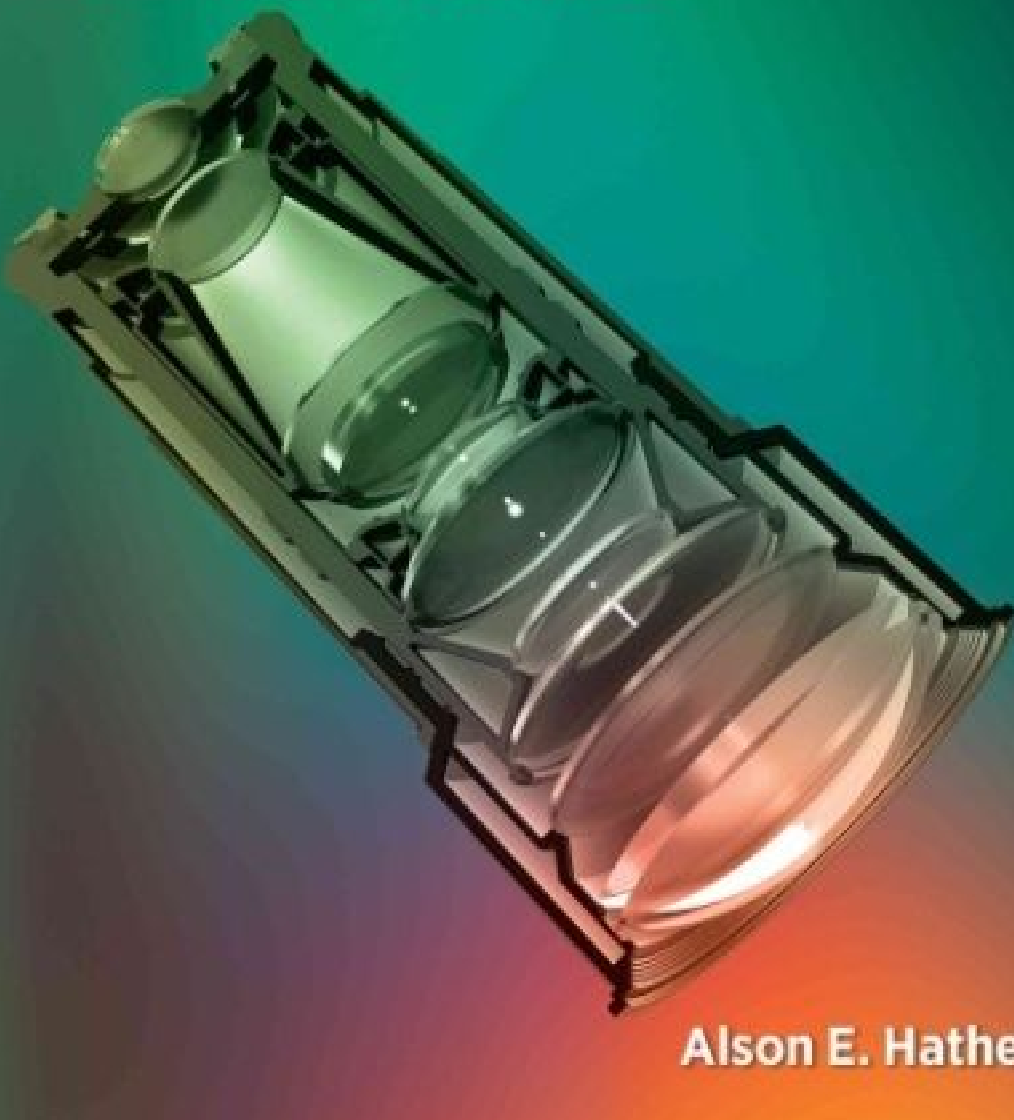

Alson E. Hatheway

The Optomechanical Constraint Equations

THEORY AND APPLICATIONS

The Optomechanical Constraint Equations

THEORY AND APPLICATIONS

Alson E. Hatheway

SPIE PRESS
Bellingham, Washington USA

Library of Congress Cataloging-in-Publication Data

Names: Hatheway, Alson E., author.
Title: The optomechanical constraint equations : theory and applications / Alson E. Hatheway.
Description: Bellingham, Washington : SPIE Press, [2016] | Includes bibliographical references and index.
Identifiers: LCCN 2016015871 | ISBN 9781510601758 (print) | ISBN 1510601759 (print) | ISBN 9781510601765 (pdf) | ISBN 1510601767 (pdf) | ISBN 9781510601772 (epub) | ISBN 1510601775 (epub) | ISBN 9781510601789
(Kindle/mobi) | ISBN 1510601783 (Kindle/mobi)
Subjects: LCSH: Optomechanics—Mathematics. | Mechanical engineering. | Optical instruments—Design and construction. | Constraints (Physics)—Mathematical models.
Classification: LCC TA1520 .H39 2016 | DDC 621.3601/51—dc23 LC record available at https://lccn.loc.gov/2016015871

Published by

SPIE
P.O. Box 10
Bellingham, Washington 98227-0010 USA
Phone: +1 360.676.3290
Fax: +1 360.647.1445
Email: books@spie.org
Web: http://spie.org

The content of this book reflects the work and thought of the author. Every effort has been made to publish reliable and accurate information herein, but the publisher is not responsible for the validity of the information or for any outcomes resulting from reliance thereon.

Cover photograph courtesy of Shutterstock, Inc.

Printed in the United States of America.
First printing.
For updates to this book, visit http://spie.org and type “PM268” in the search field.

To

Robin

The light of my life

Contents

Preface

This is an engineering treatise for mechanical engineers who design and analyze optical systems. It also will be of interest to structural engineers in the optical industry and to other optics professionals. As with most engineering treatises, the book is based on both the physical science of, and the practical realities of, designing, analyzing, building, testing, and servicing real optical products.

The overwhelming majority of optical challenges that a mechanical engineer faces are associated with the position, orientation, and size of the image at the detector, the image's first-order properties. Control of these properties throughout the mechanical design activity is essential for successful assembly and test of the first systems. If the optical elements of a system are manufactured and aligned in accordance with the dimensions in the physical optical prescription, the performance degradation due to small deviations from the prescription is dominated by misregistration of the first-order image on the detector rather than by a shift in the "balance" of the higher-order terms. The contribution of these higher-order terms (the aberrations) is usually relatively small, as shown in the following analysis of the image of a well-corrected optical system:

- It is assumed that the optical designer has given the mechanical engineer the physical optical prescription data. These data define the geometric properties of all of the optical surfaces in the system as well as the index of refraction properties for all of the materials that transmit the light. This optical prescription defines the conditions under which the optical system provides a suitable optical image, i.e., the preferred position, orientation, and size for the image, and acceptable image quality (image sharpness) over the desired field of view.
- The image formation by the optical system might be as shown in Fig. 1, which is a telescope system observing an object that is some distance to the left of the figure. The system's principal planes are shown, as are its entrance and exit pupils. The light from points on the object (not shown) leaves the exit pupil in nearly spherical wavefronts that converge to small regions in the right side of the figure, the system's point images. The system's detector, which is usually in a flat plane, is located among

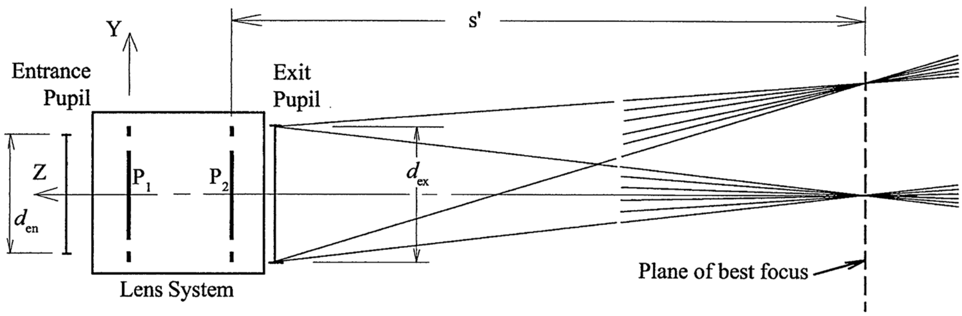

Figure 1 The image of an optical system.[1]

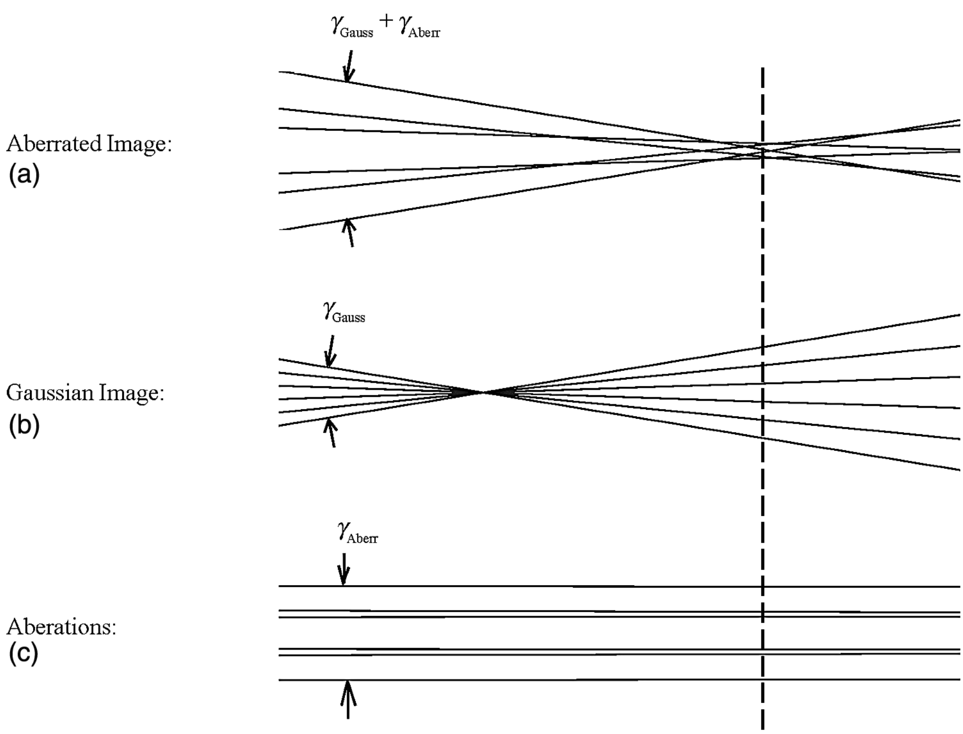

Figure 2 (a) Aberrated image, (b) Gaussian image, and (c) aberrations.[1]

the converged image regions. Since the converged regions do not necessarily all lie on a flat plane, the detector is located to provide the best point images over its full area. This location is known as the *plane of best focus*.

- Details of the light forming one of the system's image points—the point on the optical axis of the system—are shown in Fig. 2(a). This figure shows an *aberrated* point image in longitudinal cross section. The best image of the point happens to be registered on the detector at the plane of best focus. It can be seen that the light rays from the exit pupil do not converge at a single point as would be required to form a perfect point image of a point on the system's object. This defect in the image is due to the fact that the light from the exit pupil does not form a perfect spherical wavefront.

- Knowing the physical optical prescription of the optical system permits the calculation of the theoretically perfect image point, the Gaussian image (Karl Fredrick Gauss, 1841). The Gaussian image of this point is shown in Fig. 2(b). Note that the Gaussian image does not necessarily register exactly on the detector at the plane of best focus for the system.
- Subtracting the Gaussian image rays of Fig. 2(b) from the system's aberrated image rays [Fig. 2(a)] results in Fig. 2(c), a plot of all of the ray aberrations in the system's image at this point in the plane of best focus.
- If the cone angle of the Gaussian image is defined as γ_{Gauss}, and the cone angle of the aberrations is defined as γ_{Aberr}, it can be observed that

$$\gamma_{\mathrm{Gauss}} \gg \gamma_{\mathrm{Aberr}},$$

  such that the cone angle of the aberrated image is dominated by the cone angle of the Gaussian image. This is true for all well-corrected optical imaging systems over their designed full fields of view.
- It follows that, in the vicinity of the plane of best focus, the changes in the position, orientation, and size of the system's "best" image are dominated by the Gaussian image's corresponding changes. It also follows that, while at the plane of the "best" image, the measure of the quality or sharpness of the image [say, the diameter of the circle of ray intercepts at the detector in Fig. 2(a)] is dominated by the aberrations, the changes in that measure of sharpness are dominated by changes in the axial position of the Gaussian image.

Since the optical designer's physical optical prescription describes the conditions for the best possible optical performance, and because the mechanical engineer can neither perfectly create nor perfectly maintain those conditions in a real system, the engineer must be sensitive to the magnitude of the imaging errors being introduced by the mechanical design.

The present work deals with what are termed the first-order, or Gaussian, optical imaging effects. Gaussian imaging is specifically defined in the opening sections that discuss the nature of optical imaging and define the coordinate systems and sign conventions to be used throughout this work. These conventions are slightly different from those used by optical designers and physicists, and are based on common practice in the mechanical design arts. It is assumed that the reader has some familiarity with the physics of optical imaging from university training and perhaps some additional experience in the optical industry. The purpose of the opening sections is not so much to teach optical physics to the uninitiated but rather to adapt the optical imaging equations to the coordinate systems and sign conventions that are convenient for mechanical engineers.

What the mechanical engineer needs in order to manage the mechanical design process is the influence that each optical element has on the position, orientation, and size of the image. This treatise develops the influence functions between the positions and dimensions of all of the optical elements in an optical system and the resultant position, orientation, and size of the optical image at the detector. These functions are derived from the equations of optical imaging as adapted to the coordinate systems and sign conventions of the mechanical design.

Optical design usually begins with a defined object of interest and proceeds from there through the optical elements to the detector. The optical design assumes that the Z axis propagates with the light from the object toward the detector. Mechanical design, however, might not consider the object of the optical system at all; the object is often at infinity or some other distant location. Rather, mechanical design begins somewhere in the instrument, perhaps at the detector, and propagates outward from there, toward the incoming light. To maintain the mechanical features in a positive hemisphere, the mechanical Z axis is usually in the direction *opposite* that assumed in optical design, from the detector toward the system object. This work, intended for mechanical engineers, assumes sign conventions and coordinate systems convenient for mechanical design. The familiar equations of optics have been adapted to these conventions. Most of the influence functions developed here are independent of the assumed coordinate systems. Differences are noted in the text where they occur.

Some of the influence functions are linear, while others are nonlinear. The permitted deviations from the dimensions in the published physical optical prescription are usually very small. The significance of the nonlinearities diminishes quickly as the deviations (from the prescription) are reduced in size. A system is developed that segregates the linear and nonlinear components of the influence functions. This facilitates a quick solution of the linearized image motion problem but still permits the engineer to assess the magnitudes of related nonlinear effects. If they are sufficiently small, the nonlinearities might not materially reduce the margins of safety on optical performance. Otherwise, the engineer can arrange to accommodate them appropriately in the mechanical design.

The optical system's influence functions are organized into seven equations representing the three translations, three rotations, and the change in size of the image at the detector. These equations are called the *optomechanical constraint equations* because they constrain the changes in the system's image to those effects that are driven by changes in the position, orientation, and focal length of each of the optical elements. The way the equations are used is entirely up to the engineer. The influence coefficients are often used longhand or with a 10-key calculator to estimate the effects of local positioning errors during project meeting or design reviews. The optomechanical constraint equations can be developed in a computer spreadsheet program to make easy calculations for multi-element systems. Computer codes can be written that automate the preparation of the optomechanical constraint equations from the physical optical prescription data. The optomechanical constraint equations can also be imported into finite element models to evaluate the effects of elastic deflection and temperature changes in dynamic environments.

Use of the optomechanical constraint equations assumes that the Gaussian image is a reasonable proxy for the image of the system. Questions in this regard should be referred to the optical designer. The influence coefficients are presented for a number of common optical elements, and the method for convolving the individual elements into the system's influence coefficients is shown. Finally, simple examples are provided that apply the influence coefficients to common mechanical engineering problems in optical systems.

The author hopes that the reader will find this treatise a valuable addition to the literature of optomechanics and a useful addition to the engineer's toolbox.

Alson Hatheway
May 2016

Chapter 1
Optical Functions

Optical physics defines a number of mathematical functions that govern the direction of propagation of light. A few of such *optical functions* (Fig. 1.1) are refraction,

$$n \sin \phi = n' \sin \phi',$$

reflection,

$$\phi = -\phi',$$

and scalar diffraction at a grating,

$$\sin \phi + \sin \phi' = \frac{m\lambda}{d},$$

where m is the diffraction order, λ is the wavelength, and d is the grating spacing. By carefully controlling the propagation of light, the light can be collected from some object and concentrated in some other desired location in a process known as optical imaging.

Each of these optical functions relates a local mechanical geometric variable (for instance, the angle of incidence, ϕ) to an optical variable (for instance, the angle of reflection, ϕ'). One of the tasks of an optical designer is to determine the optimal physical geometry to achieve the preferred optical performance (image quality). The optical designer's solution to this problem is published in the physical optical prescription.

The challenge for the mechanical engineer is to understand how small variations in the physical geometry (due to tolerances, elastic deflections, or temperature changes, for example) will affect the optical variables, and thus the image, in the design. With this understanding the mechanical engineer will be positioned to guide the mechanical design to minimize the adverse effects that the mechanical variables will have on the optical performance of the system.

If a generalized optical function, *OF*, is defined in terms of its mechanical variables, $\ldots m_j, m_k, \ldots,$

$$OF = f(\ldots m_j, m_k, \ldots),$$

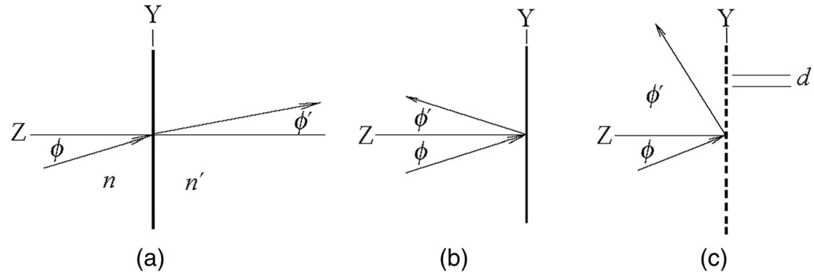

Figure 1.1 (a) Refraction, (b) reflection, and (c) diffraction.[1]

a generalized *influence function*, IF_j, can be defined as the change in the OF, caused by a change in one of the mechanical variables, such as m_j:

$$IF_j = \frac{\Delta OF}{\Delta m_j}.$$

If an optical function is dependent on more than one mechanical variable, it has as many influence functions as it has independent mechanical variables.

Some optical functions are nonlinear functions of the mechanical variables. In these cases it is convenient to adopt a uniform style for the influence function. In this book, that convention is

$$IF_j = \frac{c_j}{1 + e_j}.$$

In this convention, the term c_j is the *influence coefficient* and is numerically equal to the first partial derivative of the influence function with respect to the mechanical variable of interest:

$$c_j = \partial OF/\partial m_j.$$

The influence coefficient contains the linear properties of the influence function in the vicinity of the desired value of the mechanical variable.

The term e_j is the *deviation fraction* and contains the nonlinear properties of the influence function in the vicinity of the desired value of the mechanical variable. The value of the deviation fraction is the fractional amount by which a linear estimate, based on the influence coefficient, is in error with respect to the full nonlinear influence function. If the deviation fraction is –0.15, the linear estimate will be low by 15%.

This treatise shows the engineer how to evaluate both the influence coefficients and the deviation fractions for all of the optical elements in a system. Adopting this standard style for the influence functions is convenient for the mechanical engineer. It allows independent quantification of nonlinear effects in the optical phenomena of interest to the optical system. The tight dimensional requirements imposed on the mechanical design of optical instruments usually result in relatively small deviations from linearity.

However, if any of the deviations are judged to be substantial, the engineer can then address them in the design process.

The balance of this treatise develops the influence functions (in the preferred style) for imaging optical systems and shows how these functions can be applied to the mechanical design of optical systems.

1.1 The Imaging Properties of a Lens

Any physical body that receives some light from points in space and concentrates that light at other points in space can be considered to be a *lens*. The source of the light is the *object* of the lens, and the region where the light is concentrated is the *image* of the lens. The lens can employ any of a number of methods (physical phenomena) for effecting the concentration of the light at the image; refraction, reflection, and diffraction are a few of such phenomena. For our initial purposes, the lens is assumed to use refraction.

A *refractive lens* can be formed from a piece of clear glass by polishing two convex spherical surfaces on opposite sides of the glass (Fig. 1.2). An image is formed from the light that the lens receives from the object and then concentrates (by refraction, in this case) into a local spatial region, the image. The lens forms observable and recognizable images of distant objects.

Assuming that the object is some distance to the left of the lens, the image is some distance to the right of the lens (Fig. 1.3). The distance from the lens to the object is the *object distance*, s, and is considered to be positive, being in the positive direction along the Z axis. The distance from the lens to the image is the *image distance*, s', and is (in this case) considered to be negative, being in the negative direction along the Z axis. The Z axis lies along the axis of symmetry of the lens as defined by its spherical surfaces, positive being to the left. The origin is at the lens, and the Y-axis direction is upward with the light flowing from left to right. This description will be further refined.

The image can be observed on a screen, a ground glass plate, photographic film, a semiconductor detector, or in blown smoke. This is called a *real image* because it can be directly observed. The image is *inverted*;

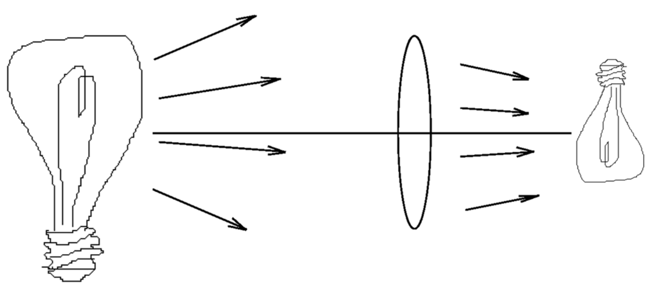

Figure 1.2 A refractive lens.[2]

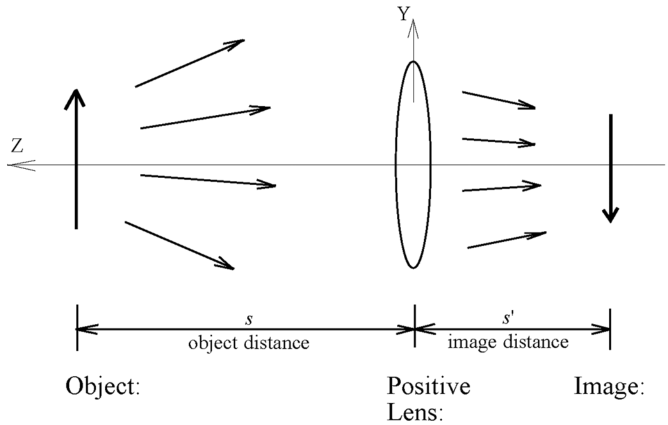

Figure 1.3 Object and image of a positive refractive lens.[2]

i.e., it is upside-down with respect to the object. If the object is an arrow pointing up, the image is an arrow pointing down.

If a screen is placed in the plane of the sharpest image, one can observe the extent, or size, of this image in the plane of the screen. If the positions of the object and image are reversed, i.e., rotated so that the first surface of the lens becomes the second and the second surface becomes the first (with light traveling from right to left), one can also observe the extent, or size, of this reverse image in the new plane of the relocated screen. Careful measurement of the two images thus observed discloses that they are of about the same extent, or size, in the plane of the screen. Thus, it may be said that the size of a lens' image is the same whether the light is transiting the lens from front to back or from back to front.

If the object moves, the image is also observed to move. Returning to the original left-to-right arrangement (Fig. 1.3), if the object moves up, the image moves down. If the object moves toward the viewer, the image moves away from the viewer. Note that in these two cases the image moves in the direction exactly opposite to that of the object. However, if the object moves to the left, the image also moves to the left, in the same direction as the object. As the object continues to move to the left, the image continues to move left also but at a slower and slower rate. As the object distance grows very large, approaching infinity, the image approaches a fixed position on the opposite side of the lens. The position of the image when the object is at infinity is called a *focal point* of the lens. The distance from this focal point to the back vertex of the lens is the *back focal length* of the lens. This biconvex lens, which produces a real, inverted image of a distant object, is considered to be a *positive lens* and is characterized as having a positive focal length.

A *negative lens* can be made by polishing *concave* surfaces (Fig. 1.4) in the glass instead of the convex ones used above. Assuming that the object is

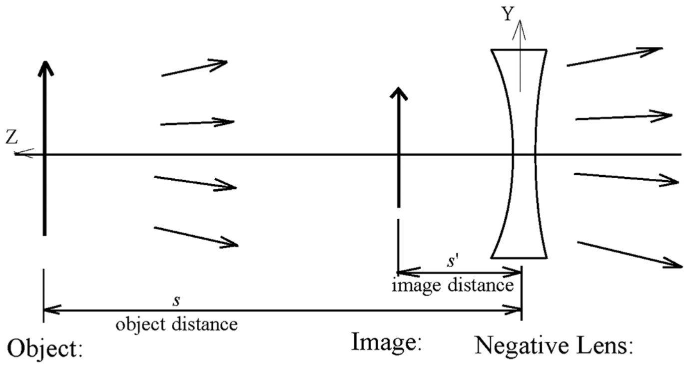

Figure 1.4 Object and image of a negative refractive lens.[2]

some distance to the left, as with the positive lens, the image is also some distance to the left, just the reverse of the positive lens: the object and the image will be on the same side of the lens. Both s and s' are positive. This image is not directly observable unless the observer looks through the lens from the right side, in which case it will be sensed to be on the opposite side (the object side) of the lens itself. This is called a *virtual image*. It will also be observed to be an *erect image*, its vertical orientation being the same as that of the object.

If the object of a negative lens moves, the image is also observed to move. If the object moves up, the image also moves up. If the object moves toward the viewer, the image also moves toward the viewer. In these two cases, the object and the image move in the same direction. If the object of a negative lens moves to the left, the image moves to the right. In this case, the image and object move in opposite directions. As the object distance for a negative lens grows very large, approaching infinity, the image approaches a fixed position on the same side of the lens as the object. The position of the image when the object is at infinity is a *focal point* for the negative lens. The distance from the focal point to the second vertex of the lens is the back focal length of the negative lens. This biconcave lens, which produces a virtual, erect image of a distant object, is considered to be a *negative lens* and is characterized as having a negative focal length.

These qualitative observations will be refined and quantified in the following sections.

1.2 Optical Ray Tracing

The imaging properties of a lens are often visualized by drawing lines in the direction that the light is propagating. The lines are called *light rays*, and these rays can trace the path that the light follows from the object, through the lens, and to the image.

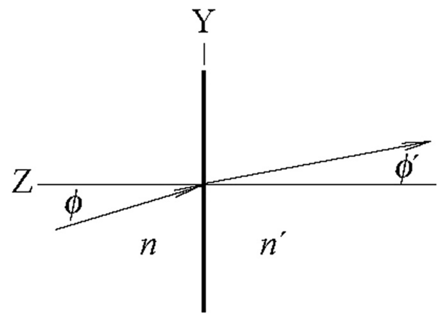

Figure 1.5 Refraction at an air-to-glass surface.[1]

Glass lenses bend the light at the air-to-glass surfaces according to the effect of *refraction*. Refraction is quantified by Snell's law (Willebrord Snellius, 1620) (Fig. 1.5):

$$n \sin \phi = n' \sin \phi',$$

where n is the *index of refraction* of the first material (usually air), n' is the index of refraction of the second material (usually a glass), ϕ is the *angle of incidence* of a ray incident at the surface (measured from the incident side's surface normal), and ϕ' is the *angle of refraction* of the ray transmitted at that surface (measured from the opposite surface normal).

In optical design practice, Snell's law can be simplified by using a *relative index of refraction*, n_R, which is defined as the index of refraction of the glass divided by the index of refraction of the surrounding medium (usually air):

$$n_R = n'/n.$$

Snell's law then becomes simply

$$\sin \phi = n_R \sin \phi'.$$

The symbol n is redefined here to represent the relative index of refraction for the glass; i.e.,

$$n \equiv n_R = n'/n,$$

where n had previously been the index of refraction of air, so that Snell's law in the form

$$\sin \phi = n \sin \phi'$$

will be adopted when going from air to glass, and

$$n \sin \phi = \sin \phi'$$

will be adopted when going from glass to air.

When tracing a ray through a glass lens situated in air, refraction occurs at both surfaces. The ray comes from some point on the object through the air to the first surface. At this surface the refractive effect is that of going from air into glass. Then the ray travels through the glass to the second surface where the refractive effect is that of going from glass into air. The ray then travels through the air to the image.

1.3 The Imaging Properties of a Lens, Concluded

Returning to the positive refractive lens, the centers of curvature of the two spherical surfaces define an axis of symmetry, the *optical axis*, for this imaging system, which includes the object, the lens, and the image. A special case exists for the ray that lies along the optical axis: its angle of incidence is zero; therefore, its angle of refraction is zero. Consequently, all of its segments lie along the straight line that is the optical axis and are independent of the indexes of refraction. The image position associated with any optical ray that is initially parallel to the optical axis can therefore be defined as the intersection of that ray with the ray along the optical axis.

Additionally, the intersection of the optical axis with the first surface is the *first vertex*, V_1, of the lens, and its intersection with the second surface is the *second vertex*, V_2, of the lens.

Consider the imaging behavior of a lens with two unequal convex spherical surfaces when the object is a great distance away; i.e., all of the rays entering the first surface are effectively parallel to the optical axis (Fig. 1.6).

If Snell's law is applied to incident rays that are parallel to the optical axis, it is found that as they get closer and closer to the optical axis, their image positions (where the refracted rays cross the optical axis) approach a fixed point on the axis. This point is the *second focal point*, f_2. The distance from the lens' second focal point to the lens' second vertex is the *back focal length* (*bfl*).

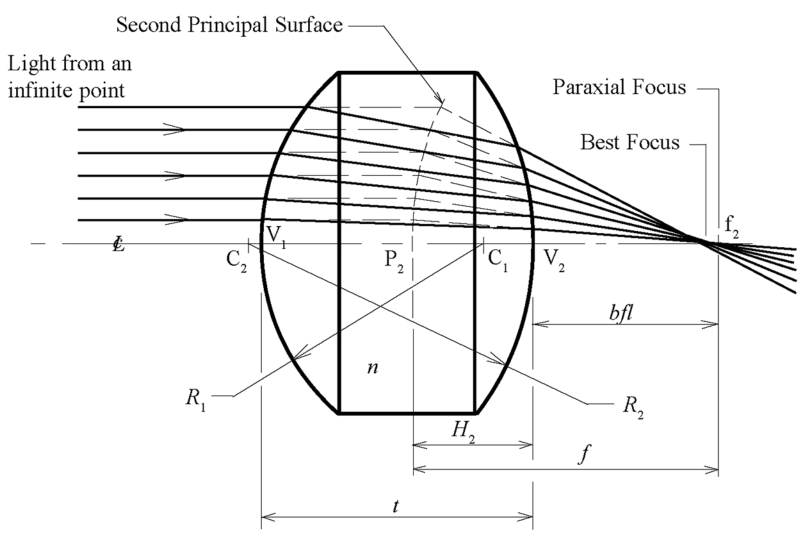

Figure 1.6 Image formation by a positive refractive lens.[1]

Not all of the rays transiting the lens cross the optical axis at the second focal point. As a result, the image is not perfectly sharp. The plane of best focus occurs along the Z axis where the height in the Y direction to the farthest ray is a minimum. This height defines the *circle of least confusion* in the region of this image. The second focal point defined in the preceding paragraph is more appropriately called the *paraxial second focal point* since it is defined by the imaging properties on the optical axis of the element, a region called the *paraxial zone* of the lens. Other zones of the lens might have imaging properties that slightly differ from those of the paraxial zone.

Now, we reverse the positions of the object and the image, repeat the operation, and find a new paraxial focal point, the *first paraxial focal point*, f_1, on the opposite side of the lens. The distance from the lens' first vertex to the lens' first focal point is the *front focal length* (*ffl*).

In general, the front focal length is different from the back focal length (except in symmetrical lenses), even though they produce the same-sized images (see above). It is clear that neither the front focal length nor the back focal length controls the size or extent of the image.

Let's reconsider the first case, in which we determined the back focal length of the lens. If an incident ray parallel to the optical axis is projected through the lens into the air on the image side of the lens, and if the corresponding imaged ray at the second focal point is projected forward through the lens into the air on the object side of the lens, the two rays cross at a point. This point is on a surface called the *second principal surface*. The second principal surface is fully defined by the intersections of all of the incident rays that are parallel to the optical axis with their corresponding rays coming forward from their second focal points. The point where the optical axis intersects the second principal surface is the *second principal point*, P_2. The distance from the V_2 to P_2 is H_2. The distance from P_2 to the second focal point is the *second focal length*, f_2, of the lens.

Now, let us reverse the positions of the object and image again, and project the corresponding incident and imaging rays to determine the *first principal surface*. The point where the optical axis intersects the first principal surface is the *first principal point*, P_1. The distance from the first vertex, V_1, to P_1 is H_1.

The distance from the first principal point to the first focal point is the *first focal length*, f_1. It can be seen that the first and second focal lengths are equal but opposite in sign, such that

$$f_1 = -f_2 \equiv f,$$

where f is the *effective focal length* of the lens. The effective focal length is symmetrical with respect to the lens and controls the image formation.

A lens such as this one, with two convex surfaces, produces a *real* and *inverted* image of a distant object. Such lenses are said to have a *positive focal length* and are called *positive lenses*. The image is real in that a screen or detector can be placed at the image location and can sense or record the image. The image is inverted because it is on the side of the optical axis that is opposite to the object. If the object comes inside f_1 close enough to the lens to fall between the first focal point and the first principal point, the image is on the same side of the lens as the object, and the image is be said to be *virtual* and *erect*. The image is virtual in that it cannot be directly observed or sensed without looking back through the lens. It is erect because it is on the same side of the optical axis as the object.

Lenses with a *negative focal length* (perhaps with two concave surfaces) produce virtual and erect images of distant objects. These are called *negative lenses*. They produce real and inverted images only if the object is beyond f_1, which is very rare because the positions of the two focal points is reversed for negative lenses, f_2 being on the object side of the lens and f_1 on the image side.

Since the focal length of a lens is generally large compared to its diameter, the principal surfaces tend to be relatively shallow and are usually represented by flat planes through the principal points and normal to the optical axis. These are called the *first* and *second principal planes*.

We have now found conditions of symmetry that are consistent with our initial observation that the images are of the same size. We have also found a property of the lens, the effective focal length f that describes the imaging properties of the lens. Additionally, we have found geometric locations in the lens, the principal points (P_1 and P_2) that determine the position of the focal points (f_1 and f_2) with respect to the lens' vertices. The imaging properties of a lens are considered to be concentrated at the principal points.

1.4 Image and Object Relative Positions

If the object of the positive lens is some distance to the left of the lens and beyond f_1, the image is on the opposite side of the lens, beyond f_2, and inverted from the object, as in Fig. 1.7(b). As the object recedes to infinity [Fig. 1.7(a)], the image approaches f_2. If the motion of the object is reversed and the object approaches f_1 [Fig. 1.7(c)], the image moves away from the lens and approaches negative infinity. As the object crosses f_1, the image suddenly flips to positive infinity and assumes an erect posture [Fig. 1.7(d)]. Finally, as the object approaches the first principal plane, the image approaches the second principal plane [Fig. 1.7(e)]. Note that in this final situation the object and image are the same size.

1.5 The Ray Aberration Polynomial

The ray aberration polynomial puts optical imaging into a more rigorous context. This polynomial was developed to describe the characteristics of an imaging optical element in the image plane, including the errors (aberrations).[3] Spherical surfaces produce pretty good images, but none are perfect. The polynomial helps to quantify the imperfections.

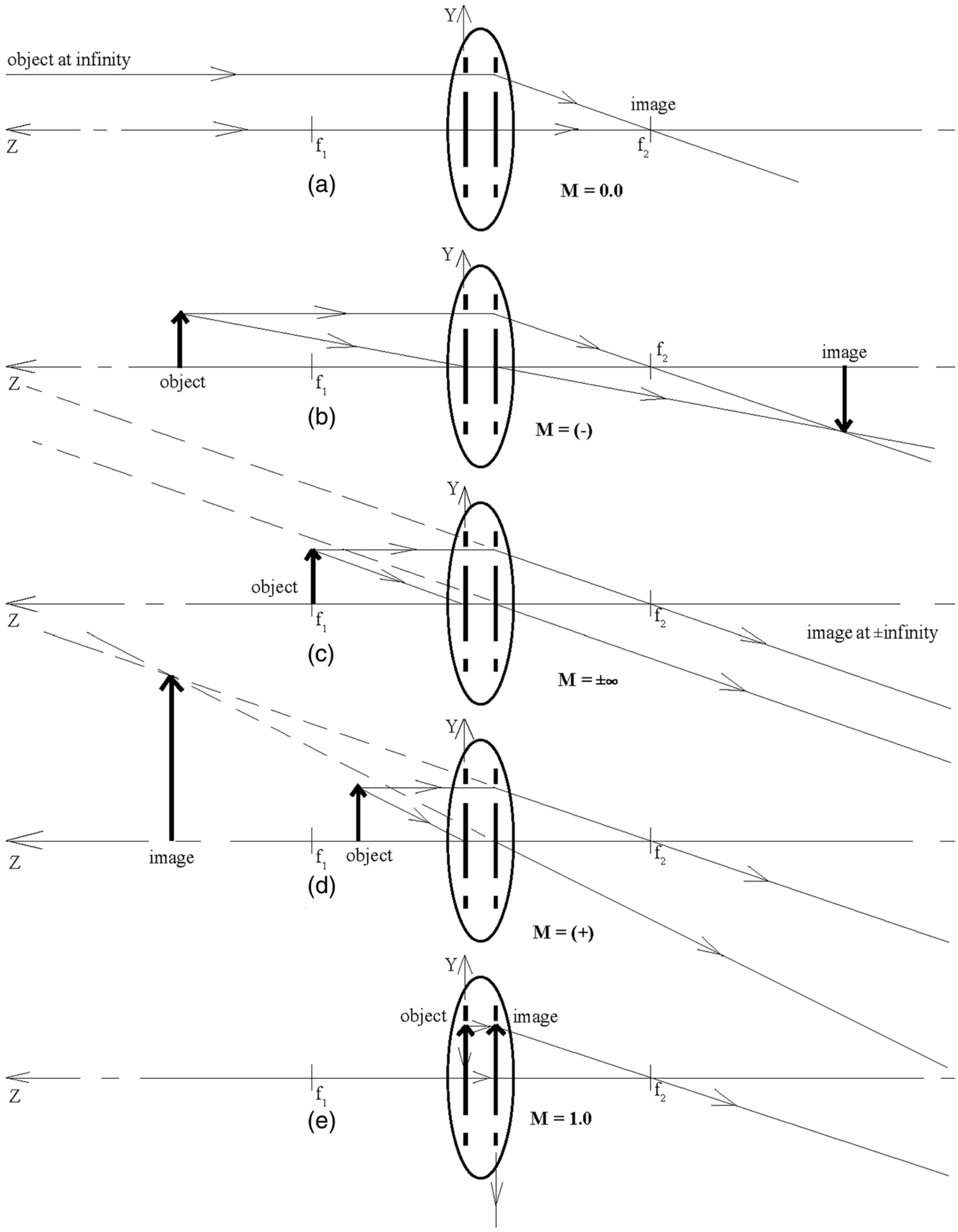

Figure 1.7 Image and object relative positions.[2] (See text in Section 1.4 for details.)

If (as in Fig. 1.8) we have a thin lens (i.e., P_1 and P_2 are collocated) with an object point at a distance s along the Z axis from the lens and offset a distance $-h$ along its Y axis, we can trace a ray from the object point, through the lens, and onto some intercept plane at some distance z along the Z axis. The ray intercepts the thin lens at some radius, ρ, from the optical axis and some angle γ

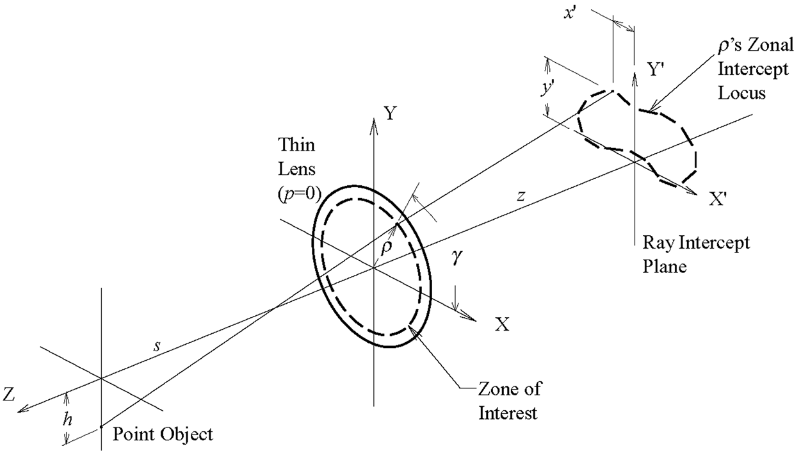

Figure 1.8 Ray tracing through a zone ρ of a lens.[1]

from the element's X axis. The ray is refracted through some angle at the lens' principal plane and proceeds to the ray intercept plane. The ray intercepts the ray intercept plane at some coordinates (x', y') in that plane.

In generalized terms, the coordinates in the ray intercept plane can be described by the following *polynomial equations*:

$$
\begin{aligned}
x' =& A_1\rho \sin\gamma \\
&+ B_1\rho^3 \sin\gamma + B_2\rho^2 h \sin\gamma + (B_3 + B_4)\rho h^2 \sin\gamma \\
&+ C_1\rho^5 \sin\gamma + C_3\rho^4 h \ \sin 2\gamma + (C_5 + C_6\cos^2\gamma)\rho^3 h^2 \sin\gamma + C_9\rho^2 h^3 \sin 2\gamma \\
&\quad + C_{11}\rho h^4 \sin\gamma \\
&+ D_1\rho^7 \sin\gamma \ldots,
\end{aligned}
$$

$$
\begin{aligned}
y' =& \mathrm{A}_1\rho \cos\gamma + \mathrm{A}_2 h \\
&+ B_1\rho^3 \cos\gamma + \mathrm{B}_2\rho^2 h(2 + \cos 2\gamma) + (3\mathrm{B}_3 + \mathrm{B}_4)\rho h^2 \cos\gamma + \mathrm{B}_5 h^3 \\
&+ \mathrm{C}_1\rho^5 \cos\gamma + (\mathrm{C}_2 + \mathrm{C}_3 \cos 2\gamma)\rho^4 h + (\mathrm{C}_4 + \mathrm{C}_5 \cos^2\gamma)\rho^3 h^2 \cos\gamma \\
&\quad + (\mathrm{C}_7 + \mathrm{C}_8 \cos 2\gamma)\rho^2 h^3 + \mathrm{C}_{10}\rho h^4 \cos\gamma + \mathrm{C}_{12}\mathrm{h}^5 \\
&+ \mathrm{D}_1\rho^7 \cos\gamma \ldots.
\end{aligned}
$$

The terms of the equations are grouped according to the degree of their independent terms, ρ, h, and the groups are usually referred to by their differential *order*, which is equivalent to their algebraic degree. The first row is first order, the second row is third order, the third row is fifth order, etc. The orders of all of the terms are odd numbers; the even numbers having been removed by the assumption of dihedral symmetry defined by the Y-Z plane. Each of the equations (for x' and y') has an infinite number of terms.

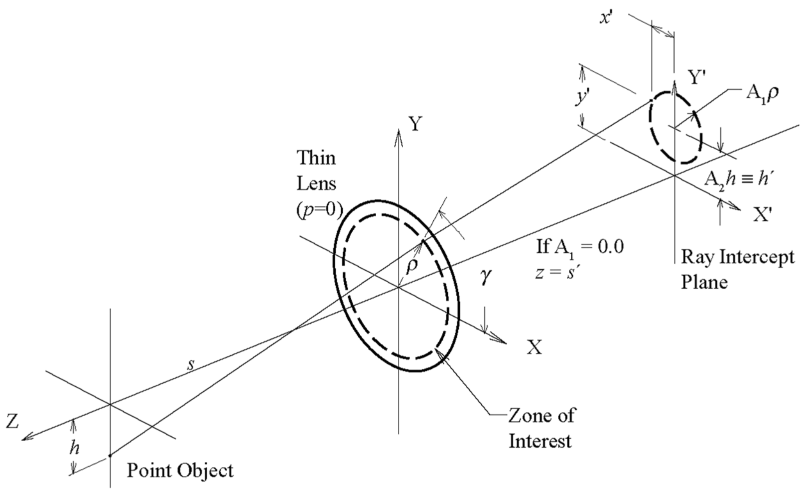

Figure 1.9 The effect of the first-order polynomial terms.[1]

If the intercept point at the lens is allowed to rotate about the optical axis at a constant radius, ρ, the locus of the corresponding points on the ray intercept plane at z form a closed curve in that plane. The ray aberration polynomials provided above can describe any closed curve (that is symmetrical with respect to the Y-Z plane) in the ray intercept plane by varying the coefficients on each of the terms.

The first-order terms from above are

$$x' = \mathrm{A}_1\rho \sin\gamma,$$

$$y' = \mathrm{A}_1\rho \cos\gamma + \mathrm{A}_2 h.$$

Considered by themselves, these terms describe a circle on the ray intercept plane (Fig. 1.9) that has a radius of $\mathrm{A}_1\rho$, the center of which is offset from the axis by $\mathrm{A}_2 h$. If the distance z is varied so that A_1 goes to zero, then the radius of the intercept circle goes to zero, and the locus of all points reduces to a single point offset from the axis by $\mathrm{A}_2 h$. Under these circumstances, the ray intercept plane becomes the image plane, the z distance becomes the image distance s', and the height of the image h' becomes $\mathrm{A}_2 h$. As a result,

$$z \equiv s',$$

$$\mathrm{A}_2 = h'/h \equiv M,$$

where M is the magnification at which the thin lens is working.

In the Y-Z plane, the slope (referred to the optical axis) of the ray incident at the lens is u, and the slope of the exiting ray is u'. Since A_1 is zero, it follows that

$$u - u' = -\Delta u = \frac{\rho - h}{s} - \frac{\rho - h'}{s'},$$

and since, by similar triangles,

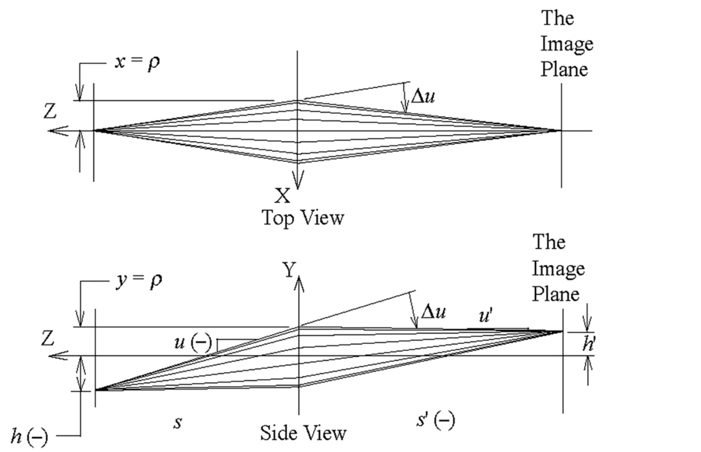

Figure 1.10 The imaging constant $-\Delta u/\rho$ of the first-order polynomial terms.[1]

$$h/s = h'/s',$$
$$1/s - 1/s' = -\Delta u/\rho = \text{a constant},$$

where Δu is the change in slope of the ray, referred to the optical axis, going through the lens, and ρ is the radial zone of the lens. The expression $-\Delta u/\rho$ defines the imaging properties of the lens (Fig. 1.10).

All of the polynomial terms above the first order (third, fifth, seventh, etc.) are added to the first-order terms. In the image plane, the sum of these higher-order terms forms a vector, $\mathbf{g}'$, from the image point at (h', s') to another point in the image plane. The locus of $\mathbf{g}'$ for a given radius, ρ, at the lens forms a closed curve in the vicinity of the image point (Fig. 1.11). This vector defines the aberrations associated with the image.

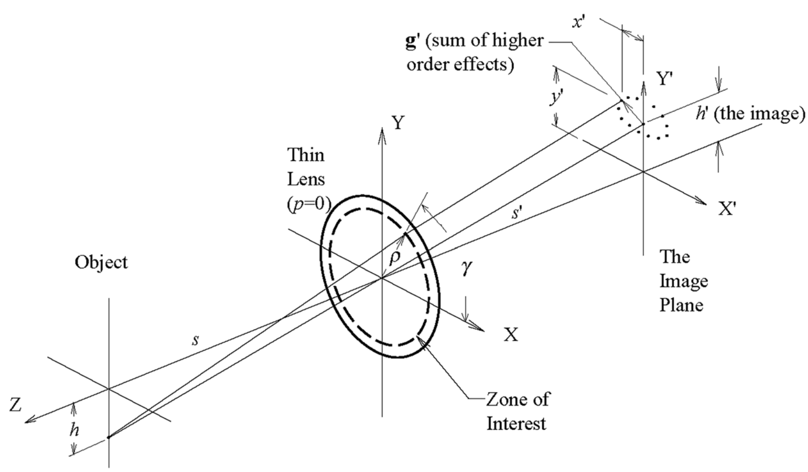

Figure 1.11 The aberration vector $\mathbf{g}'$ of the higher-order polynomial terms.[1]

In imaging systems, the magnitude of $\mathbf{g}'$ must be small in order to observe the optical image. In well-corrected systems, this magnitude is very small. Since there is an infinite number of terms in each of the aberration polynomials and their sum must be small, it follows that the magnitude of the terms must fall very quickly as their orders increase.

This review of the ray aberration polynomials shows that the influence of the aberrations must be small compared to the image if the imaging system is to have a distinct image. Part of an optical designer's task is to balance the (positive and negative) aberration contributions from the various surfaces in an optical system to reduce the net effect of the aberrations at the final system image.

It follows that, in a well-corrected imaging system, the dominant effect of misaligned optics is from the first-order terms. Once the elements are located such that the position, orientation, and size of the image are correct (according to the physical optical prescription), the system needs little or no further adjustments. This is because the imaging properties of most optical elements are very strong compared to their aberration properties.

1.6 Paraxial Lens Equations

If Snell's law is applied to the rays near the optical axis of a lens (the lens' *paraxial zone*) the positions of f_2 and P_2 can be established along the optical axis. In Fig. 1.12, the location of P_2 with respect to f_2 is the effective focal length f of the lens. The effective focal length is determined from the physical properties of the lens by the *paraxial lens equation*,

$$\frac{1}{f} = (n-1)\left[\frac{1}{R_2} - \frac{1}{R_1} + \frac{t(n-1)}{nR_1R_2}\right],$$

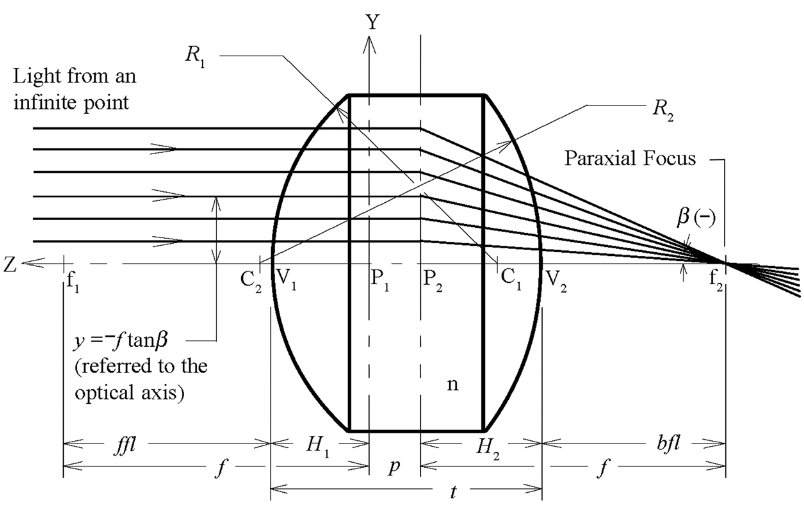

Figure 1.12 The imaging properties of the paraxial zone of a lens.[1]

where R_1 is the radius of curvature of the first surface, R_2 is the radius of curvature of the second surface, t is the thickness of the lens at the vertices, and n is the relative index of refraction of the lens material.

From this application of Snell's law, the position H_2 of the second principal point with respect to the second vertex is found to be

$$H_2 = \frac{-f\,t(n-1)}{nR_1}.$$

If the rays are run in the opposite direction, we can calculate the position H_1 of the first principal point with respect to the first vertex as

$$H_1 = \frac{-f\,t(n-1)}{nR_2}.$$

Knowing the physical thickness t of the lens between the vertices, the principal thickness, p (the distance from P_2 to P_1), can be determined by

$$p = t\left[1 - f(n-1)\left(\frac{1/R_2 - 1/R_1}{n}\right)\right].$$

Note that the principal thickness is not a physical thickness. The principal thickness is usually positive but under some conditions of radii, thickness, and index of refraction, it can be negative. But whether it is positive or negative, it serves to accurately locate the image along the Z axis of the system. Note also that in Fig. 1.12, if we let y equal ρ, then $\tan\beta$ equals u of Fig. 1.10.

The + and – signs in these equations might differ from the equations used by optical designers because mechanical sign conventions are being used in this work.

1.7 Gauss' Equation of Image Formation

In 1841 Karl Fredrick Gauss proposed an equation that calculates the location of the image along the Z axis (Fig. 1.13):

$$1/s - 1/s' = 1/f,$$

where s is the object distance from the first principal point, s' is the image distance from the second principal point, and f is the focal length of the lens. The minus sign in this equation differs from lens design convention because the mechanical Z axis is reversed from the optical Z axis.

Recalling that the first-order terms of the aberration polynomial lead to a similar expression,

$$1/s - 1/s' = -\Delta u/\rho = \text{a constant},$$

it can be seen that

$$1/f = -\rho/\Delta u.$$

Gauss' equation with a little first-order ray tracing allows the calculation of the magnification, M, at which the lens is working.

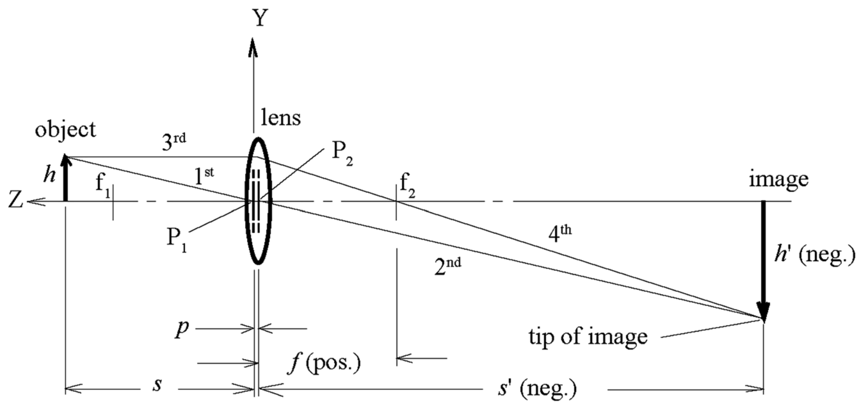

Figure 1.13 The Gaussian imaging properties of a lens.[1]

Referring to Fig. 1.13, if an object of height h is set at some location s along the Z axis, the height of the image h' can be determined, along with its Z-axis location, by ray tracing. From the tip of the object at (s, h) draw a first ray (1^{st}) to the first principal point P_1. Then, from the second principal point P_2, draw a second ray (2^{nd}) parallel to the first ray but extending out toward the image, away from the lens. Next, draw a third ray (3^{rd}) from the tip of the object at (s, h) parallel to the optical axis to an intersection with the second principal plane. Finally, draw a fourth ray (4^{th}) from the intersection of the third ray and the second principal plane through the second focal point f_2 and out toward the image away from the lens.

The point at the intersection of the second and fourth rays is the image of the tip of the object. This point is located at $z = s'$ and $y = h'$, both of which are negative.

Note that in paraxial ray tracing, rays always pass from the first principal plane to the second principal plane along a line parallel to the optical axis. Incident rays that are parallel to the optical axis go from the second principal plane through the second focal point. Rays incident at P_1 at any angle of incidence exit the lens at P_2 undeviated in direction (that is, parallel to the incident ray).

Now we can calculate the focal length of the lens from the lens equation (see Section 1.6) and the physical optical prescription data. Knowing the object distance, s, calculate the image distance, s', from Gauss' equation. Observing the ray trace from object to image in Fig. 1.13, we see that the triangle along the optical axis at the object is geometrically similar to the triangle along the optical axis at the image. Consequently, the height of the image and the magnification at which the lens is working can be determined from

$$h' = h\left(\frac{s'}{s}\right),$$

$$\frac{h'}{h} = \frac{s'}{s} \equiv M,$$

where M is the lateral magnification in the image's X-Y plane. A longitudinal (or depth) magnification along the Z axis M_Z is also used by optical designers. Taking the first partial derivative of Gauss' equation with respect to s, we find that

$$\frac{-1}{s^2} + \frac{\partial s'/\partial s}{s'^2} = 0,$$

$$\frac{\partial s'}{\partial s} = \left(\frac{s'}{s}\right)^2 = M^2 \equiv M_Z.$$

Gauss' equation defines a linear transformation between the object's X-Y plane and the image's X-Y plane, but there is a nonlinear transformation between the object's Z axis and the image's Z axis.

Gauss' equation is entirely general for imaging systems. Although it has been applied here only to symmetrical systems, it can be applied to asymmetrical and off-axis imaging systems as well.

The Gaussian properties of a lens as developed here are for the zone of a lens that is very near the optical axis. As the center of the light bundle of interest moves away from the optical axis, the imaging properties change, and this new set of properties is associated with the new location of the light bundle. If the center of the bundle at the lens is off axis by a distance y, then the imaging properties are associated with a circular zone of the lens that has a radius of y. These properties are then used in Gauss' equation for calculating the image positions and magnifications through the optical system.

In this book, the term *Gaussian* can be substituted for the term *paraxial* to indicate that the material is not necessarily limited to axially symmetric systems nor to the paraxial zone of the elements.

1.8 The Location of the Principal Points

The paraxial properties H_1 and H_2 are used to locate the principal points with respect to the vertices of the lens. Figure 1.14 shows how the principal points can change locations depending on the values of the physical optical prescription variables of the lens. In general, for a biconvex [Fig. 1.14(a)] or biconcave [Fig. 1.14(b)] lens, both principal points are between the two vertices. For plano-convex [Fig. 1.14(c)] and plano-concave [Fig. 1.14(d)] lenses, one principal point is at the vertex of the curved surface, and the other principal point is inside the lens between the vertices. For a positive meniscus lens [Fig. 1.14(d)], one or both of the principal points is outside the convex surface of the lens. For a negative meniscus lens [Fig. 1.14(e)], one or both of the principal points is outside the concave surface of the lens. In rare cases, the principal points might be reversed, P_2 being to the left of P_1 (not illustrated).

1.9 Lens Prescriptions

Lenses are defined by their *prescriptions*. An optical designer will publish a *physical optical prescription* for the lens, which consists of:

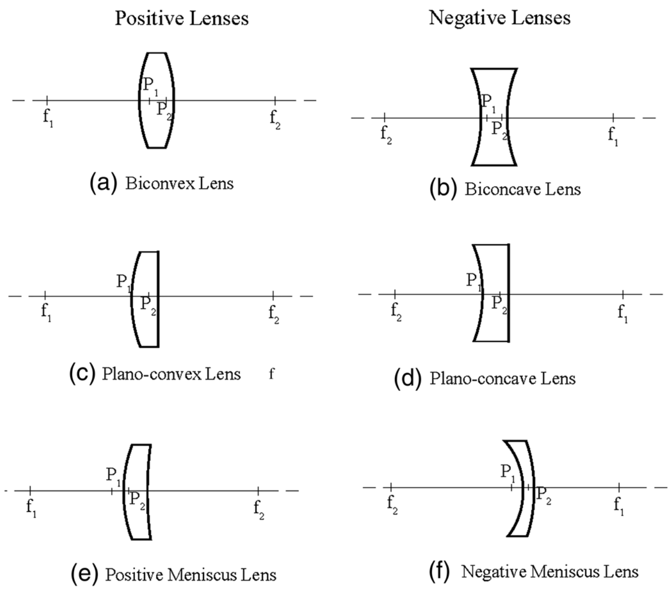

Figure 1.14 The principal points of common lens forms (see text in Section 1.8 for details).

R_1, the first radius,
R_2, the second radius,
t, the thickness at the vertices, and
n, the relative index of refraction.

The physical optical prescription can also specify higher-order polynomial functions superimposed on the spherical surfaces. These are used primarily to control high-order defects (aberrations) in the system's image and have little effect on the first-order (Gaussian) performance of interest here.

The radii and thickness are the information that the lens maker will need to fabricate the lens. However, this prescription does not directly tell the engineer about the image-forming capability of the lens. Based on the imaging properties of a lens provided above, it is possible to define an alternative functional form of prescription for the lens, consisting of:

f, the focal length,
H_1, the distance from V_1 to P_1, and
H_2, the distance from V_2 to P_2.

These properties are brought into geometric congruence with the physical optical prescription by also prescribing

p, the *principal thickness*, or the distance from P_2 to P_1.

This latter form is called the *paraxial* (or *Gaussian*) *prescription* because it is based on both the lens imaging properties near the optical axis (the *paraxial zone*) of the lens and Karl Gauss' definition of the image. The Gaussian prescription properties (f, p, H_1, and H_2) can be developed for other zones of the lens, but defining their relationship to the physical optical prescription is beyond the scope of this work.

These two forms of the prescription are complimentary; the physical optical prescription describes the solid body of the lens and its material, while the paraxial prescription describes the lens' imaging capabilities and refers those properties to the vertices of the lens.

Note that in the paraxial zone of a lens, the higher-order surface terms are not used. Outside the paraxial zone they might need to be considered by tracing a ray through the center of the zone of interest and calculating the equivalent Gaussian properties (f, p, H_1 and H_2) for the zone.

Each physical lens prescription has a unique paraxial (or other zonal) prescription that is determined from that particular physical optical prescription. However, the inverse is not true: each paraxial prescription can have an infinite number of possible physical optical prescriptions that can satisfy it.

1.10 Coordinate Systems for the Lens

Optical designers use coordinate systems to define optical surfaces. It is their convention that: (1) the light travels from left to right on the paper or screen, (2) the initial Z axis is aligned with the initial light bundle (left to right), (3) the Y axis is pointed upward on the paper or screen, and (4) the X axis completes a right-handed coordinate system. The coordinate origin is at the vertex of the surface, i.e., where the axis of symmetry intersects the surface. It is also conventional that the orientation of the Z axis reverses at every reflective surface. Following these conventions presents some design challenges for mechanical engineers.

Compared to optical design, in mechanical design it is more convenient (1) for the object of an optical system to be in the positive Z hemisphere of the design space and (2) to avoid changing dimensional orientation ($+$ and $-$) at reflective surfaces throughout the design space. It is also more convenient in mechanical design if material thickness, such as a lens thickness, is always positive. This work adopts mechanically oriented sign conventions and coordinates systems, applying them at each optical element, each optical object, and each optical image (Fig. 1.15).

Light will be incident from left to right at each optical element. The element will have its own coordinate system centered at its first principal point, P_1. The element's Z axis will be normal to the first principal plane and directed to the left, against the incident light. The element's Y-axis orientation will be upward in the first principal plane, and the element's X axis will complete a right-handed coordinate system.

For the lens:

- R_1 is the Z-axis distance from the first vertex to its center of curvature ($+$ or $-$),

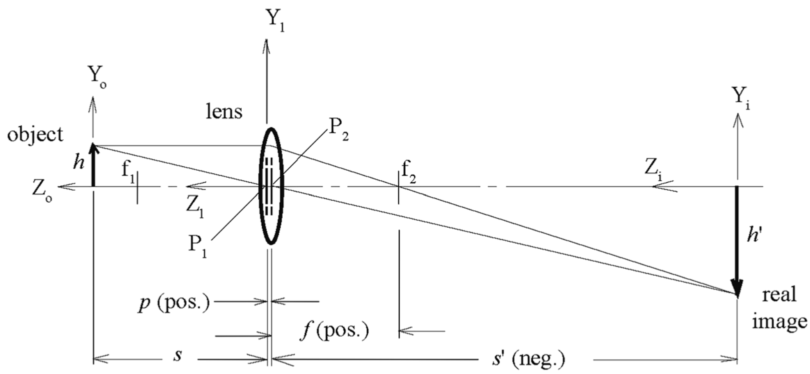

Figure 1.15 The coordinate systems for the lens, its object, and its image.[1]

- R_2 is the Z-axis distance from the second vertex to its center of curvature (+ or −),
- t is the thickness at the vertices (always positive), and
- n is the relative index of refraction (always positive).

The object of each element will have its own coordinate system at its intersection with the optical axis:

- The object's Z axis will be directed to the left, against the emitted light.
- The object's Y axis will be directed upward.
- The object's X axis will complete a right-handed coordinate system.

The image of each element will have its own coordinate system at its intersection with the optical axis (as reflected, if the element is a mirror):

- The image's Z axis will be directed along the optical axis against the incident light.
- The image's Y axis will be directed upward, on the same side of the optical axis as the object's Y axis.
- The image's X axis will complete a right-handed coordinate system.

1.11 Definitions and Sign Conventions for the Lens

Index of refraction n:
This is the relative index of refraction of the lens material, i.e., the absolute index of refraction of the lens material divided by the absolute index of refraction of the medium in which the lens is immersed, assumed to be air at standard conditions ($n_{\text{air}} = 1.000292$).

Surfaces S_1, S_2:
The geometric features (assumed to be spherical) of a lens that contribute to its imaging property. They are subscripted in the sequence that light passes through them.

Centers of curvature C_1, C_2:
The points in space that are the centers of the spherical surfaces. The centers of curvature derive their subscripts from their associated surfaces.

Optical axis:
The straight line defined by the centers of curvature of the spherical surfaces.

Vertices V_1, V_2:
The points of intersection of the optical axis and the spherical surfaces. The vertices derive their subscripts from the associated surfaces.

Radii of curvature R_1, R_2:
The distances in the element coordinate system from vertices to their centers of curvature. The radii of curvature derive their subscripts from the associated surfaces.

Thickness t:
Either the distance between the vertices of a lens or the distance between vertices of adjacent lenses. The thickness is always positive.

Focal points f_1, f_2:
Points on the optical axis at which infinite points (also on the optical axis) are imaged. All refractive lenses have two focal points: the first is associated with an object point that is infinitely far along the negative Z axis, and the second is associated with an object point that is infinitely far along the positive Z axis.

Principal points P_1, P_2:
Points on the optical axis at which the focusing properties of the surfaces of a lens can be assumed to be concentrated. All refractive lenses have two principal points.

The Z-axis distances from a vertex to the associated principal point in the element coordinate system can be calculated from

$$H_1 = z_{P1} - z_{V1} = \frac{-f\,t(n-1)}{nR_2},$$

$$H_2 = z_{P2} - z_{V2} = \frac{-f\,t(n-1)}{nR_1}.$$

Principal thickness p:
The distance from the second principal point to the first principal point in the element coordinate system. The principal thickness is usually positive but is not a physical thickness (such as t) and may occasionally be a negative value.

Effective focal length f:
The distance from the first principal point to the first focal point in the element coordinate system. Positive lenses have positive focal lengths, and negative lenses have negative focal lengths.

Chapter 2
Optomechanical Influence Functions

In the mechanical engineering of optical systems, the preferred position, orientation, and size of the image are determined by the optical designer. It is the mechanical engineer's responsibility to locate all of the elements in the system with sufficient accuracy to maintain the optical designer's intentions. To that end, the mechanical engineer must be able to know the influence that each of the optical elements, including the object, has on the position, orientation, and size of the system's image.

The mathematical functions that relate the motions of the image to the motions of the lens and the motions of its object are called *optomechanical influence functions*. These functions can be developed using Gauss' equation and the Gaussian properties of the lens.

Figure 2.1 shows a positive lens forming an image of a nearby object. The coordinate systems for the image, the lens, and the object are all parallel to each other and co-axial along their Z axes. Since the object coordinates and lens coordinates are parallel, the rotation angle θ of the object with respect to the lens is 0.0. These geometric assumptions will be used throughout this chapter.

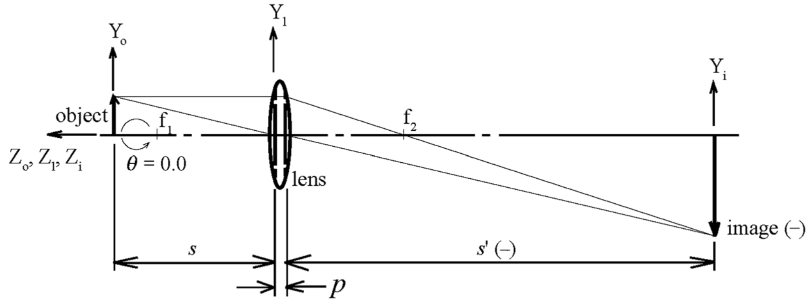

Figure 2.1 A positive lens forming an image of a nearby object.

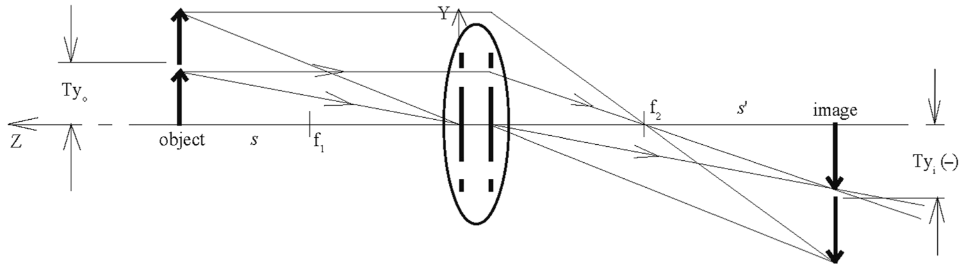

Figure 2.2 Vertical object motions.[1]

In this work, angular motions of objects, elements, and images (*Rx*, *Ry* and *Rz*) will be assumed to be in radians (rad).

2.1 The Object's Influence Functions

2.1.1 Vertical object motions

As noted in Section 1.7, Gauss' equation defines a linear transformation between the object's *Y* axis and the image's *Y* axis. In Fig. 2.2 it can be seen that the ratio of the image's motion, Ty_i, to the object's motion, Ty_o, equals the magnification, *M*. Therefore, the object's influence function in the vertical direction is exactly

$$Ty_i/Ty_o = M.$$

2.1.2 Horizontal object motions

Similarly, in the horizontal direction, Gauss' equation defines a linear transformation between the object's motion, Tx_o, and the image's motion, Tx_i. The ratio between the image and the object equals the magnification, *M*. Therefore, the object's influence function in the horizontal direction is exactly

$$Tx_i/Tx_o = M.$$

2.1.3 Longitudinal object motions

Longitudinal motions of the object, Tz_o, cause both a longitudinal motion of the image, $\Delta s'$, and a change in its size, $\Delta h'$ (Fig. 2.3).

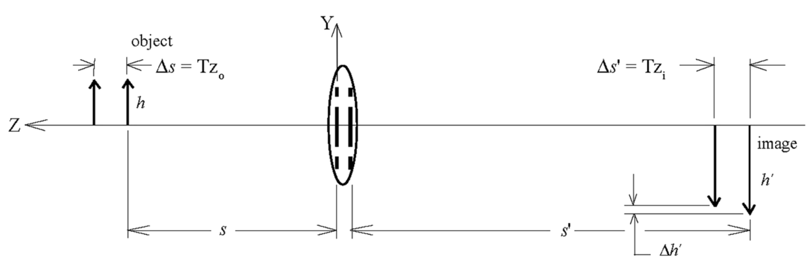

Figure 2.3 Longitudinal object motions.[1]

2.1.3.1 Image motion

The object's longitudinal influence function determines how much the image will move in the Z direction, Tz_{i}, of the image's coordinate system when the object is moved in the Z direction, Tz_{o}, in the object's coordinate system. If Gauss' equation is set up with the following finite-sized displacements:

$$\frac{1}{f}=\frac{1}{s+Tz_{\mathrm{o}}}-\frac{1}{s'+Tz_{\mathrm{i}}},$$

and noting that

$$Tz_{\mathrm{i}}=\Delta s', \quad Tz_{\mathrm{o}}=\Delta s,$$

it can be seen that

$$\frac{1}{s+\Delta s}-\frac{1}{s'+\Delta s'}=\frac{1}{f}.$$

Multiplying through by s' gives

$$\frac{s'/s}{1+(\Delta s/s)}-\frac{1}{1+(\Delta s'/s')}=\frac{s'}{f}.$$

Since $M = s'/s$,

$$\frac{M}{1+(\Delta s/s)}-\frac{1}{1+(\Delta s'/s')}=\frac{s'}{f}.$$

Then, since

$$\frac{1}{s}-\frac{1}{s'}=\frac{1}{f}, \qquad \frac{s'}{s}-\frac{s'}{s'}=\frac{s'}{f}, \qquad M-1=\frac{s'}{f},$$

it follows that

$$\frac{M}{1+(\Delta s/s)}-\frac{1}{1+(\Delta s'/s')}=M-1.$$

Re-arranging gives

$$\frac{\Delta s'}{\Delta s}=\frac{M^2}{1+[\Delta s(1-M)]/s}.$$

Then, since

$$\frac{1}{s}-\frac{1}{s'}=\frac{1}{f}, \qquad \frac{s}{s}-\frac{s}{s'}=\frac{s}{f}, \qquad 1-\frac{1}{M}=\frac{s}{f},$$

multiplying through by M gives

$$\frac{1-M}{s}=\frac{-M}{f},$$

and

$$\frac{\Delta s'}{\Delta s}=\frac{M^2}{1-(M\Delta s/f)}.$$

Noting again that $\Delta s' = Tz_i$ and $\Delta s = Tz_o$ leads to the Tz_i/Tz_o influence function:

$$\frac{Tz_i}{Tz_o} = \frac{M^2}{1 - (MTz_o/f)}.$$

This is a nonlinear function since the independent variable Tz_o occurs on both sides of the equation. Note that the numerator of the function (the influence coefficient) M^2 agrees with the first partial derivative that we called the longitudinal magnification (see Section 1.7). The nonlinearity is controlled by the term in the denominator, $-MTz_o/f$.

If this term is small with respect to 1 (the other term in the denominator), the value of a linear assumption based on the numerator M^2 will be correspondingly close to the value of the full nonlinear influence function. However, if this term is large, the nonlinear effect might need to be accommodated by the engineer.

For mechanical engineering purposes, it is useful to track the linear and nonlinear portions of this function separately. The linear portion, in this case the numerator M^2, is called the *influence coefficient*, c, and the nonlinear portion in the denominator $-MTz_o/f$ is called the *deviation fraction*, e. The engineering utility of this approach is that if the deviation fraction is sufficiently small, the effects of nonlinearity on engineering decisions will be correspondingly small and can be knowledgeably either ignored or accommodated as the case requires.

The absolute error (or *deviation*), in dimensional displacement quantities such as millimeters, associated with assuming linear behavior can be assessed by subtracting the exact value from the linear assumed value:

$$\begin{aligned} \text{deviation} &= M^2 Tz_o - \left[\frac{M^2}{1 - (MTz_o/f)}\right] Tz_o \\ &= \frac{(M^3 Tz_o^2)/f}{1 - (MTz_o/f)}. \end{aligned}$$

From this expression it can be seen that if the deviation fraction $-MTz_o/f$ is small compared to 1.0, then dimensional error in a linear estimate will be proportional to M^3, $Tz_o{}^2$, and $1/f$.

Since the magnitude of the permissible motion Tz_o is generally orders of magnitude smaller than the focal length of the lens, and since the magnification for an individual lens is usually modest, the errors due to nonlinearity in a linear estimate tend to be small. In all cases, it is appropriate for the engineer to check the magnitude of these errors to assure the quality of the linear estimate and make adjustments as necessary. Separating the deviation fractions from the influence coefficients facilitates this assessment.

2.1.3.2 Image size

Longitudinal object motions also cause a change in the image's size. To determine this influence function, the change in magnification, ΔM, and finite longitudinal displacements are put into both Gauss' equation and the definition of magnification:

$$\frac{1}{f} = \frac{1}{s + Tz_o} - \frac{1}{s' + Tz_i}, \qquad M + \Delta M = \frac{s' + Tz_i}{s + Tz_o},$$

and solved simultaneously. The result is

$$\frac{\Delta M}{MTz_o} = \frac{M/f}{1 + (MTz_o/f)}.$$

Note that the influence function $\Delta M/Tz_o$ has been divided by M in order to reflect the change in size, bigger or smaller, regardless of whether the image is erect or inverted. This is also a nonlinear influence function. The influence coefficient is M/f, and the deviation fraction is MTz_o/f.

2.1.4 Horizontal object rotations

Gauss' equation can be used to determine the effect on the image of rotating the object about its horizontal axis. This is performed by calculating the Z-axis motion at the tips of the object and the image as shown in Fig. 2.4. The object plane is extended until it intersects the first principal plane. The image plane is also extended until it intersects the second principal plane. Both intersections are at the same height y_0. This is known as the Scheimpflug condition.

It follows from Fig. 2.4 that

$$\tan(Rx_o) = -s/y_0, \quad \tan(Rx_i) = -s'/y_0.$$

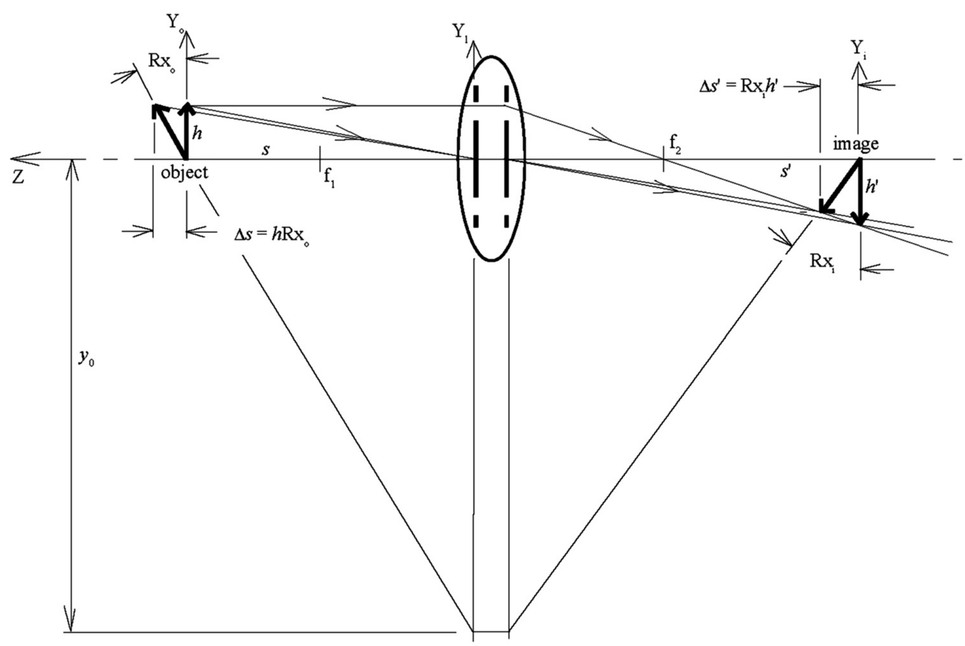

Figure 2.4 Horizontal object rotations.[2]

Assuming small angles, i.e., $\tan\phi = \sin\phi = \phi$,

$$Rx_o = -s/y_0, \quad Rx_i = -s'/y_0,$$

and

$$\frac{Rx_i}{Rx_o} = \frac{-s'/y_0}{-s/y_0} = \frac{s'}{s}.$$

The result is exactly

$$Rx_i/Rx_o = M.$$

2.1.5 Vertical object rotations

Repeating the analysis for vertical rotations, Ry_o, leads to a similar result of exactly

$$Ry_i/Ry_o = M.$$

2.1.6 Longitudinal object rotations

The effect on the image of rotating the object about the Z axis can be determined by simple logic: if the object is rotated about Z by some amount, the image will be rotated by exactly the same amount. Therefore,

$$Rz_i/Rz_o = 1.0,$$

exactly.

2.1.7 Summary: The object's influence on the lens' image

The object's influence functions can be arranged in an array of six object motions driving seven image motions, as shown in Table 2.1. These results can be summarized for engineering purposes by putting the influence coefficients and the deviation fractions into two separate arrays of variables [Tables 2.2(a) and (b), respectively].

Table 2.1 The object's influence functions.

Image Motions \ Object Motions	Tx_o	Ty_o	Tz_o	Rx_o	Ry_o	Rz_o
Tx_i	M					
Ty_i		M				
Tz_i			$\frac{M^2}{1-(MTz_o/f)}$			
Rx_i				M		
Ry_i					M	
Rz_i						1.0
$\Delta M/M$			$\frac{M/f}{1+(MTz_o/f)}$			

Table 2.2(a) The object's influence coefficients.

Image Motions	Tx_o	Ty_o	Tz_o	Rx_o	Ry_o	Rz_o
Tx_i	M					
Ty_i		M				
Tz_i			M^2			
Rx_i				M		
Ry_i					M	
Rz_i						1.0
$\Delta M/M$			M/f			

Object Motions

Table 2.2(b) The object's deviation fractions.

Image Motions	Tx_o	Ty_o	Tz_o	Rx_o	Ry_o	Rz_o
Tx_i						
Ty_i						
Tz_i			$-MTz_o/f$			
Rx_i						
Ry_i						
Rz_i						
$\Delta M/M$			MTz_o/f			

Object Motions

Note that among the object influence functions there are five linear functions and two nonlinear functions. The deviation fractions for the two nonlinear functions are of the same magnitude but opposite sense.

Separating the influence coefficients from the deviation fractions allows the engineer to make estimates of the linear and nonlinear effects separately, and to accommodate the nonlinearities as seems appropriate.

2.2 The Lens' Influence Functions

2.2.1 Vertical lens motions

The vertical motion influence function for the lens can be derived through a thought experiment, which leads to a solution by the superposition of two effects. We start with the object, lens, and image in their initially aligned positions [Fig. 2.5(a)]. Then we move all three components in the Y direction by one unit of length ($Ty_o = Ty_l = Ty_i = 1$) [Fig. 2.5(b)]. Finally, we move the object back down to its original position so that $Ty_o = 0$ [Fig. 2.5(c)].

The image motion from moving the entire system up [Fig. 2.5(b)] is given as

$$Ty_i = 1.$$

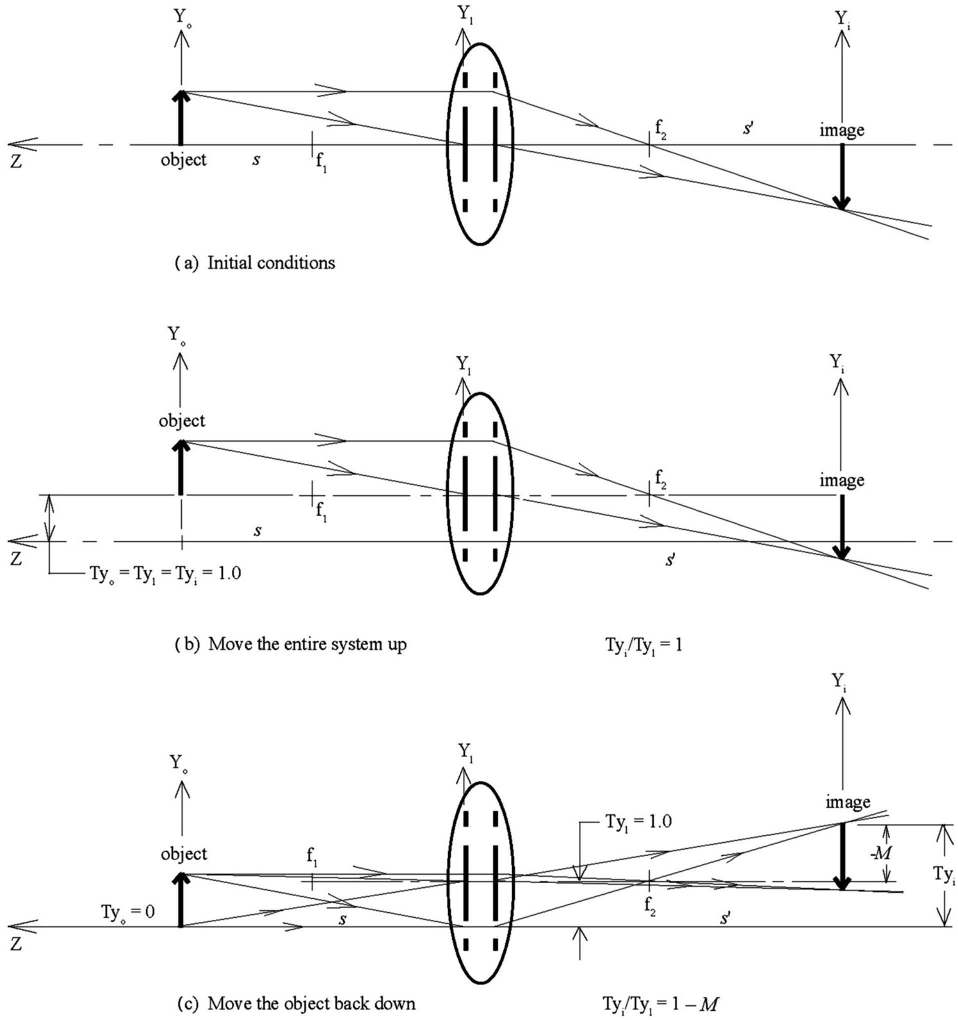

Figure 2.5 Vertical lens motions.

The image motion from moving the object back down to its original position [Fig. 2.5(c)] was derived in Section 2.1.1 as

$$Ty_\mathrm{i} = -M.$$

The net effect of these two operations is exactly their sum:

$$Ty_\mathrm{i}/Ty_1 = 1 - M.$$

2.2.2 Horizontal lens motions

A similar thought experiment and superposition in the horizontal direction yields exactly

$$Tx_i/Tx_l = 1 - M.$$

2.2.3 Longitudinal lens motions

Longitudinal motions of the lens, Tz_l, cause both a longitudinal motion of the image and a change in its size.

2.2.3.1 Image motions

A thought experiment and superposition similar to that in Section 2.2.1 applied in the longitudinal direction yields

$$\frac{Tz_i}{Tz_1} = 1 - \left[\frac{M^2}{1 + (MTz_1/f)}\right].$$

In this expression the initial "1" on the right side of the equation is *not* in the numerator with the M^2 term. When the expression is rearranged into that preferred form,

$$\frac{Tz_i}{Tz_1} = \frac{1 - M^2}{1 - M^3 Tz_1/(f + Tz_1 - fM^2)},$$

the influence coefficient becomes $1 - M^2$, and the deviation fraction becomes $-M^3 Tz_l/(f + MTz_l - fM^2)$.

The complicated form of this deviation fraction is due to singularities near the magnifications of $+1.0$ and -1.0. Under these conditions, the true image motion goes to 0.0. Since the true image motion goes into the denominator of the deviation fraction,

$$e = (\text{linear image motion} - \text{true image motion})/(\text{true image motion}),$$

the true image motion sends the value of the deviation fraction to infinity as any of the variables drive the magnification to approach ±1.0. Although the fraction grows very large in the vicinity of $M = \pm 1.0$, the actual image motion is very small, and the nonlinear deviation in dimensional terms is similarly very small.

The nonlinear deviation in dimensional terms, millimeters, or inches, can be accurately calculated from the object motion's deviation fraction

$$e = -MTz_o/f$$

since the magnitude of the nonlinear effect is independent of object or the lens movement.

2.2.3.2 Image size

Longitudinal lens motions also cause a change in the image's size. Application of the thought experiment and superposition, noting that Tz_l in the lens' case equals $-Tz_o$ in the object case, yields

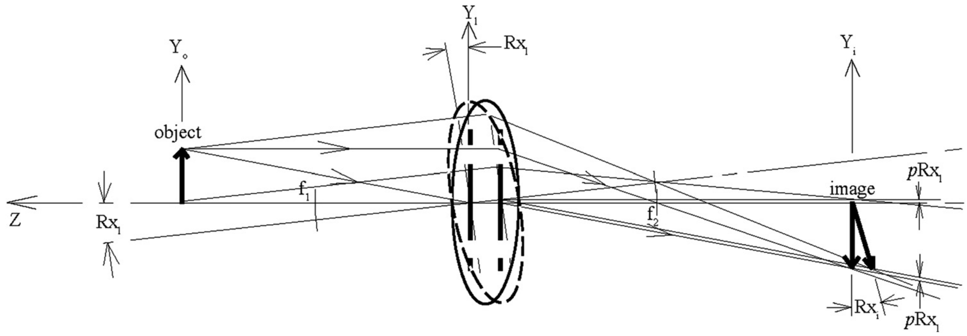

Figure 2.6 Horizontal lens rotations.[1]

$$\frac{\Delta M}{MTz_1} = \frac{(-M/f)}{1-(MTz_1/f)},$$

in which the influence coefficient is $-M/f$, and the deviation fraction is $-MTz_1/f$.

2.2.4 Horizontal lens rotations

Application of the thought experiment and superposition to horizontal rotation of the lens (Fig. 2.6) leads to exactly

$$Rx_i/Rx_1 = 1 - M.$$

However, there is another component of motion. Since the lens is being rotated about its first principal point, there is also a Y-direction displacement of the image that is exactly proportional to the principal thickness, p:

$$Ty_i/Rx_1 = p.$$

2.2.5 Vertical lens rotations

Application of the thought experiment and superposition to rotation about the vertical Y axis lead to similar results:

$$Ry_i/Ry_1 = 1 - M,$$

exactly, and

$$Tx_i/Ry_1 = -p,$$

exactly.

2.2.6 Longitudinal lens rotation

For the case of longitudinal lens rotation, no thought experiment is necessary. Since the lens is rotationally symmetric, its longitudinal rotation has no effect on the image:

$$Rz_i/Rz_1 = 0.0,$$

exactly.

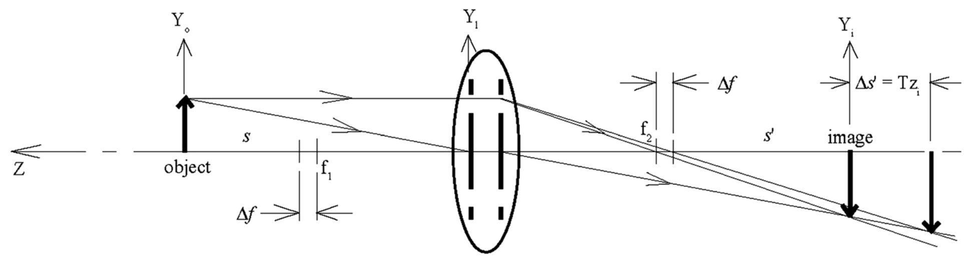

Figure 2.7 Change of lens focal length.[1]

2.2.7 Changes in the lens focal length

2.2.7.1 Image motion

When the focal length changes, the image position also changes (Fig. 2.7). First, Gauss' equation can be written to include the change in focal length and the change in the image position:

$$\frac{1}{s} - \frac{1}{s' + \Delta s'} = \frac{1}{f + \Delta f}.$$

Second, the solution must also obey Gauss' law for the undisturbed configuration:

$$\frac{1}{s} - \frac{1}{s'} = \frac{1}{f}.$$

Solving for $\Delta s'$ in the first equation in this section yields

$$\Delta s' = \frac{sf + s\Delta f + s's - s'f - s'\Delta f}{-s + f + \Delta f}.$$

Re-arrangement of the second equation in this section yields

$$s' = (M - 1)f,$$

and

$$s = \frac{(M - 1)f}{M}.$$

Substituting s' and s into $\Delta s'$ gives

$$\Delta s' = -\left[\frac{(M - 1)^2 \Delta f}{1 + (M\Delta f)/f}\right],$$

from which one obtains

$$\frac{\Delta s'}{\Delta f} = -\left[\frac{(M - 1)^2}{1 + (M\Delta f)/f}\right].$$

Noting that $\Delta s' = Tz_i$, the $Tz_i/\Delta f$ influence function becomes

$$\frac{Tz_{\rm i}}{\Delta f} = \frac{-(M-1)^2}{1+(M\Delta f/f)},$$
$$\frac{Tz_{\rm i}}{\Delta f} = \frac{-(1-M)^2}{1+(M\Delta f/f)}.$$

The influence coefficient is $-(1-M)^2$, and the deviation fraction is $M\Delta f/f$. Note that the influence coefficient's initial minus sign is outside the parenthesis, so this coefficient is always negative.

2.2.7.2 Change in size

There is also a change in image size with the change in focal length. Rewriting Gauss' equation with the finite displacements yields

$$\frac{1}{s} - \frac{1}{s' + Tz_{\rm i}} = \frac{1}{f+\Delta f}.$$

The solution must also obey Gauss' law for the undisturbed configuration:

$$\frac{1}{s} - \frac{1}{s'} = \frac{1}{f}.$$

Noting that $\Delta s'/s = \Delta M$ and $s'/s = M$, it follows that

$$M + \Delta M = \frac{s' + \Delta s'}{s}, \qquad \frac{\Delta M}{M} = \frac{\Delta s'/s}{s'/s} = \frac{\Delta s'}{s'},$$

and

$$\Delta s' = \frac{s'\Delta M}{M}.$$

From Section 2.2.7.1 it can be seen that

$$s' = (M-1)f,$$

such that

$$\Delta s' = \frac{(M-1)f\Delta M}{M},$$

and

$$\frac{\Delta s'}{\Delta f} = \frac{(M-1)f\Delta M}{M\Delta f},$$

Since $Tz_{\rm i} = \Delta s'$, it follows that

$$\frac{Tz_{\rm i}}{\Delta f} = \frac{(M-1)f\Delta M}{M\Delta f} = \frac{-(M-1)^2}{1+(M\Delta f/f)}$$

from which one obtains

Table 2.3 The lens' influence functions.

Image Motions	Tx_1	Ty_1	Tz_1	Rx_1	Ry_1	Rz_1	Δf_1
Tx_i	$1-M$				$-p$		
Ty_i		$1-M$		p			
Tz_i			$\dfrac{1-M^2}{1-M^3Tz_1/(f+Tz_1-fM^2)}$				$\dfrac{-(M-1)^2}{1+(M\Delta f/f)}$
Rx_i				$1-M$			
Ry_i					$1-M$		
Rz_i						0.0	
$\Delta M/M$			$\dfrac{-M/f}{1-MTz_1/f}$				$\dfrac{(1-M)/f}{1+M\Delta f/f}$

Lens Motions

$$\frac{\Delta M}{M\Delta f}=\frac{1-M}{f[1+(M\Delta f/f)]}.$$

The influence coefficient is $(1-M)/f$, and the deviation fraction is $M\Delta f/f$.

2.2.8 Summary: The lens' influence on its image

The lens' influence functions can be arranged in an array of seven lens motions, including the change in focal length, driving seven image motions (Table 2.3).

These results can be summarized for engineering purposes by putting the influence coefficients and the deviation fractions into two separate arrays of variables [Tables 2.4(a) and (b), respectively]. Note the long expression in Table 2.4(b) in the Tz_1 column of lens motions; see the comments on this expression in Section 2.2.3.1.

2.2.9 The magnitudes of the nonlinearities

It was stated in Section 2.2.3.1 that the nonlinearities described by the complicated deviation fraction for Tz_i/Tz_1 can be accurately calculated from the simpler deviation fractions for Tz_i/Tz_o. If we develop the dimensional deviation, δ, for both the object's Z motion and the lens' Z motion,

Table 2.4(a) The lens' influence coefficients.

Image Motions	Tx_1	Ty_1	Tz_1	Rx_1	Ry_1	Rz_1	Δf_1
Tx_i	$1-M$				$-p$		
Ty_i		$1-M$		p			
Tz_i			$1-M^2$				$-(M-1)^2$
Rx_i				$1-M$			
Ry_i					$1-M$		
Rz_i						0.0	
$\Delta M/M$			$-M/f$				$(1-M)/f$

Lens Motions

Table 2.4(b) The lens' deviation fractions.

Image Motions	Tx_1	Ty_1	Tz_1	Rx_1	Ry_1	Rz_1	Δf_1
Tx_i							
Ty_i							
Tz_i			$-\frac{M^3 Tz_1}{f + MTz_1 - fM^2}$				$M\Delta f/f$
Rx_i							
Ry_i							
Rz_i							
$\Delta M/M$			$-MTz_1/f$				$M\Delta f/f$

Lens Motions

$$\delta_{\text{object}} = M^3 T z_o^2 \left(\frac{1}{f - M^2 T z_o} \right),$$

$$\delta_{\text{lens}} = (1 - M^2) T z_1 \left[1 - \left(\frac{1}{1 - \frac{M^3 T z_1}{f + M T z_1 - f(M)^2}} \right) \right],$$

and plot them both (Fig. 2.8) over a range of magnification from -6 to $+6$, for a lens with a focal length of 150 mm, one can see the similarity between the two functions. In fact, if the orientation of one of the magnification axes is reversed, the two functions will be exactly on top of each other. The magnitude of the nonlinearity can be calculated from the simpler expression, but the sense of the magnification at which the lens is working must be reversed.

The curves in the Fig. 2.8 are cubic polynomial functions. This characteristic can be further explored by deriving the dimensional nonlinearity as the difference between the exact solution and the linear approximation in dimensional displacement quantities:

$$Tz_i = \left[\frac{M^2}{1 - (MTz_o/f)} \right] Tz_o \quad \text{(exact)},$$

$$Tz_i = M^2 Tz_o \quad \text{(linear)},$$

$$\begin{aligned}
\delta = \text{linear} - \text{exact} &= M^2 Tz_o - \left[\frac{M^2}{1 - (MTz_o/f)} \right] Tz_o \\
&= \left\{ M^2 \left[\frac{1 - (MTz_o/f) - 1}{1 - (MTz_o/f)} \right] \right\} Tz_o \\
&= \frac{(M^3 Tz_o^2/f)}{1 - (MTz_o/f)} \\
&= \frac{(M^3 Tz_o^2/f)}{1 - e}.
\end{aligned}$$

Therefore, the dimensional nonlinear effects on the registration variables are

- proportional to M^3,

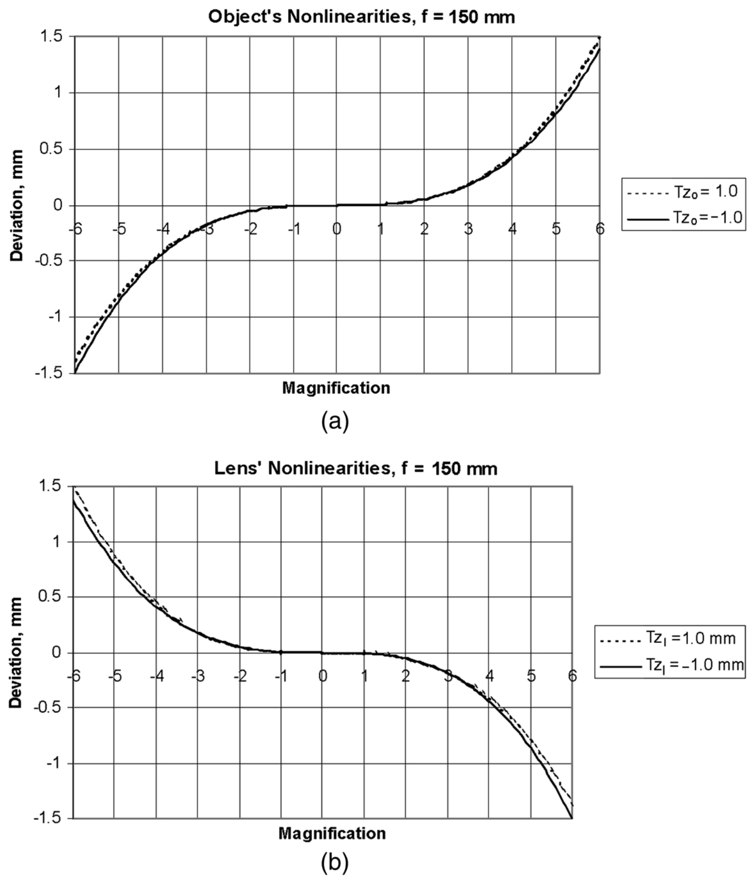

Figure 2.8 The magnitudes of the nonlinearities (a) for the object and (b) for the lens.[1]

- proportional to Tz_o^2, and
- proportional to $1/f$,

if e is small compared to 1.0.

The engineer has the information necessary for checking nonlinearities by recording the ratio of the magnification of an optical element to its focal length:

$$M/f = e/Tz_o.$$

This ratio is called the *nominal* deviation fraction. With this ratio the engineer can estimate nonlinear effects from knowledge (or estimates) of the expected motions Tz_o, Tz_l, and Δf.

2.3 The Lens Design Variables' Influence on the Lens' Image

The above formulation of influence coefficients accommodates a change in focal length as a possible design variable. In lens design, the focal length is rarely specified. Instead, the four physical optical prescription variables—two radii, a thickness, and a material (index of refraction)—are specified.

In turn, these yield a singular set of properties for the Gaussian prescription: the focal length, two principal points, and the principal thickness.

It is true that a change to any one of the physical optical prescription variables will affect all four of the Gaussian prescription variables to some extent. However, as a practical matter, physical optical prescription changes have a much larger effect on the focal length than on any of the other Gaussian prescription variables. This is largely because the focal length is much larger dimensionally (one or two orders of magnitude, typically) than any of the other Gaussian variables, and the physical optical prescription variables have a very strong influence on it.

The starting point is the paraxial prescription equations:

$$\frac{1}{f} = (n-1)\left[\frac{1}{R_2} - \frac{1}{R_1} + \frac{t(n-1)}{nR_1R_2}\right],$$
$$H_1 = \frac{-f\,t(n-1)}{nR_2},$$
$$H_2 = \frac{-f\,t(n-1)}{nR_1},$$
$$p = t\left[1 - f(n-1)\left(\frac{1/R_2 - 1/R_1}{n}\right)\right].$$

Full influence functions will not be developed between these paraxial variables and the physical optical prescription variables. Rather, only the influence coefficients (the first partial derivatives of each of these variables with respect to each of the four physical optical prescription variables) are presented in Table 2.5.

Practical experience has shown that the influence of the lens design variables on image registration errors is dominated by their influence on the focal length of the lens. This is partly due to the fact that the focal length is relatively large compared to the other Gaussian prescription variables so that a fractional change in the focal length will be much larger in absolute value than a comparable fractional change in any of the other Gaussian variables. All of the lens design influence functions are shown in Table 2.5, but only the functions applicable to the focal length will be carried forward in this treatise.

The influence coefficients for an imaging lens can now be summarized in three arrays: one for the object motions, one for the lens motions, and one for the lens design variables (Table 2.6). These arrays allow the engineer to determine the change in position, orientation, and size of the optical image when it has been perturbed by any of the mechanical or optical design variables.

The deviation fractions of the lens can be summarized in two arrays: one for the object motions and one for the lens motions (Table 2.7). These separate arrays allow the engineer to estimate the magnitude of nonlinearities

Table 2.5 Lens design variables' influence on the Gaussian variables.

Gaussian Variables	**Lens Design Variables**			
	Δt	ΔR_1	ΔR_2	Δn
Δf	$-\frac{f^2(n-1)^2}{nR_1R_2}$	$(n-1)f^2\left[\frac{t(n-1)}{nR_1^2R_2}-\frac{1}{R_1^2}\right]$	$(n-1)f^2\left[\frac{t(n-1)}{nR_1R_2^2}+\frac{1}{R_2^2}\right]$	$-\frac{tf^2(n-1)}{n^2R_1R_2}-\frac{f}{n-1}$
ΔH_1	$-\frac{f(n-1)}{nR_2}\left[1-\frac{t(n-1)^2f}{nR_1R_2}\right]$	$\frac{t(n-1)^2f^2}{nR_1^2R_2}\left[1-\frac{t(n-1)}{nR_2}\right]$	$\frac{t(n-1)f}{nR_2^2}\left[1-\frac{(n-1)f}{R_2}-\frac{t(n-1)^2f}{nR_1R_2}\right]$	$\left[\frac{t(n-1)f}{n^2R_2}\right]\left[1+\frac{t(n-1)f}{nR_1R_2}\right]$
ΔH_2	$-\left[\frac{f(n-1)}{nR_1}\right]\left[1-\frac{t(n-1)^2f}{nR_1R_2}\right]$	$\frac{t(n-1)f}{nR_1^2}\left[1-\frac{t(n-1)^2f}{nR_1R_2}+\frac{(n-1)f}{R_1}\right]$	$-\frac{t(n-1)^2f^2}{nR_1R_2^2}\left[1+\frac{t(n-1)}{nR_1}\right]$	$\frac{t(n-1)f}{n^2R_1}\left[1+\frac{t(n-1)f}{nR_1R_2}\right]$
Δp	$1-\left[\frac{(n-1)f}{nR_1R_2}\right]\left[1-\frac{t(n-1)^2f}{nR_1R_2}\right](R_1-R_2)$	$\frac{t(n-1)f}{nR_1^2}\left\{1+f(n-1)\left(\frac{1}{R_1}-\frac{1}{R_2}\right)\left[1-\frac{t(n-1)}{nR_2}\right]\right\}$	$\frac{t(n-1)f}{nR_2^2}\left\{1+f(n-1)\left(\frac{1}{R_1}-\frac{1}{R_2}\right)\left[1+\frac{t(n-1)}{nR_1}\right]\right\}$	$\frac{t(n-1)f}{n^2R_1R_2}\left[1+\frac{t(n-1)f}{nR_1R_2}(R_1-R_2)\right]$

Table 2.6 Influence coefficients for an imaging lens.

Image Motions	Tx_o	Ty_o	Tz_o	Rx_o	Ry_o	Rz_o	Tx_1	Ty_1	Tz_1	Rx_1	Ry_1	Rz_1	Δf_1
	Object Motions						**Lens Motions**						
Tx_i	M						$1 - M$				$-p$		
Ty_i		M						$1 - M$		p			
Tz_i			M^2						$1 - M^2$				$-(1 - M)^2$
Rx_i				M						$1 - M$			
Ry_i					M						$1 - M$		
Rz_i						1.0						0.0	
$\Delta M/M$			M/f						$-M/f$				$(1 - M)/f$

	Δt	ΔR_1	ΔR_2	Δn
	Lens Design Variables			
Δf	$-\dfrac{f^2(n-1)^2}{nR_1R_2}$	$(n-1)f^2\left[\dfrac{t(n-1)}{nR_1^2R_2} - \dfrac{1}{R_1^2}\right]$	$(n-1)f^2\left[\dfrac{t(n-1)}{nR_1R_2^2} + \dfrac{1}{R_2^2}\right]$	$-\dfrac{tf^2(n-1)}{n^2R_1R_2} - \dfrac{f}{n-1}$

Table 2.7 Deviation fractions for an imaging lens.

	Object Motions						Lens Motions						
	Tx_o	Ty_o	Tz_o	Rx_o	Ry_o	Rz_o	Tx_1	Ty_1	Tz_1	Rx_1	Ry_1	Rz_1	Δf_1
Tx_i													
Ty_i													
Tz_i			$-MTz_o/f$						$\dfrac{-M^3 Tz_1}{f + MTz_1 - fM^2}$				$M\Delta f/f$
Rx_i													
Ry_i													
Rz_i													
$\Delta M/M$			MTz_o/f						$-MTz_1/f$				$M\Delta f/f$

in the position, orientation, and size of the optical image, and make any accommodations that seem appropriate.

2.4 The Detector's Influence Functions

To complete a simple imaging optical system, a detector is necessary to record the image. The detector will have two arrays of a form similar to those of the lens. It is assumed that the image of the lens is to be sensed and recorded on the detector. In a form that is analogous to the lens, the image of the lens can be considered as the object of the detector, and the image of the detector can be considered as a visual electronic monitor, a developed piece of photographic film, or a data storage disk.

The influence functions for the detector can be developed very simply by imagining the interaction between the lens' image (the detector's object) and the output from the detector, in whichever form that output may be. If the object of the detector (the image of a lens) moves in the positive Y direction (Fig. 2.9), it will be perceived by the detector to have done just that, moved in the positive Y direction, and passed to the detector's image (the visible monitor). The viewer of the monitor will then perceive that the object of the detector (the image of the lens) has moved in the positive Y direction. Therefore,

$$Ty_i/Ty_o = 1.0.$$

Similar thought experiments for the other object motions (translations and rotations) show that they all directly record the motions of the detector's object. All of their influence functions are also 1.0.

Now consider the effect of moving the detector in the positive Y direction. The recording medium (or the monitor) suggests that the object of the detector has moved in the negative Y direction. Therefore, the influence function for the detector's Y motion is

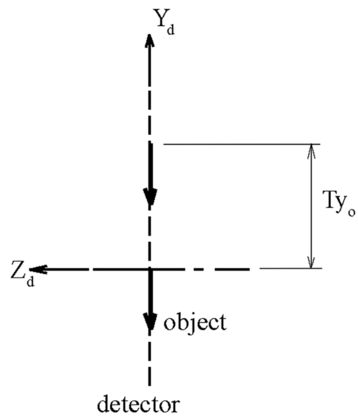

Figure 2.9 The detector's motions.

Table 2.8 Influence coefficients for the detector.

Image Motions	Tx_o	Ty_o	Tz_o	Rx_o	Ry_o	Rz_o	Tx_d	Ty_d	Tz_d	Rx_d	Ry_d	Rz_d
Tx_i	1.0						–1.0					
Ty_i		1.0						–1.0				
Tz_i			1.0						–1.0			
Rx_i				1.0						–1.0		
Ry_i					1.0						–1.0	
Rz_i						1.0						–1.0
$\Delta M/M$												
	Object Motions						**Detector Motions**					

$$Ty_i/Ty_d = -1.0.$$

Again, similar thought experiments for the other detector motions show that they all record a motion opposite to the motion of the detector. All of their influence functions are also -1.0. The arrays of influence coefficients for the detector of the system are presented in Table 2.8. The influence functions for the detector are linear and therefore have no deviation fractions.

Chapter 3
The Optomechanical Constraint Equations

The influence functions for the object, the lens, and the detector control the position, orientation, and size of their image. Their influence functions can be combined into seven equations that control the position, orientation, and size of the images of both simple and complex optical systems. These seven equations are the optomechanical constraint equations and are developed here for a single-lens system and a multilens system.

3.1 A Single-Lens System

With the development of the influence functions for the lens and the detector, it now becomes possible to write seven equations that determine the position, orientation, and size of the recorded image of a simple (single-lens) imaging system (Fig. 3.1).

The system's image motions relative to the detector (the image motions that can be observed at a visual monitor) are called the *registration variables*. Each registration variable equals the sum of all of the terms to its left (for the object, the lens, and the detector) in Table 3.1. There are seven registration variables, and these correspond to the Gaussian image variables: three translations, three rotations, and one change in size. The registration variables are identified in the far-right column of Table 3.1. These seven variables are often referred to, in analysis, as the *dependent variables*.

The mechanical design variables arranged along the bottom of the table are often referred to as the *independent variables*. The independent variables represent the object motions, lens motions, and detector motions, in any combination whatsoever. The independent variables can arise from manufacturing tolerances, gravitational deformations, vibratory excitation, transient heating, or other service conditions that the optics might experience. In this particular case, there are 19 independent variables including the change

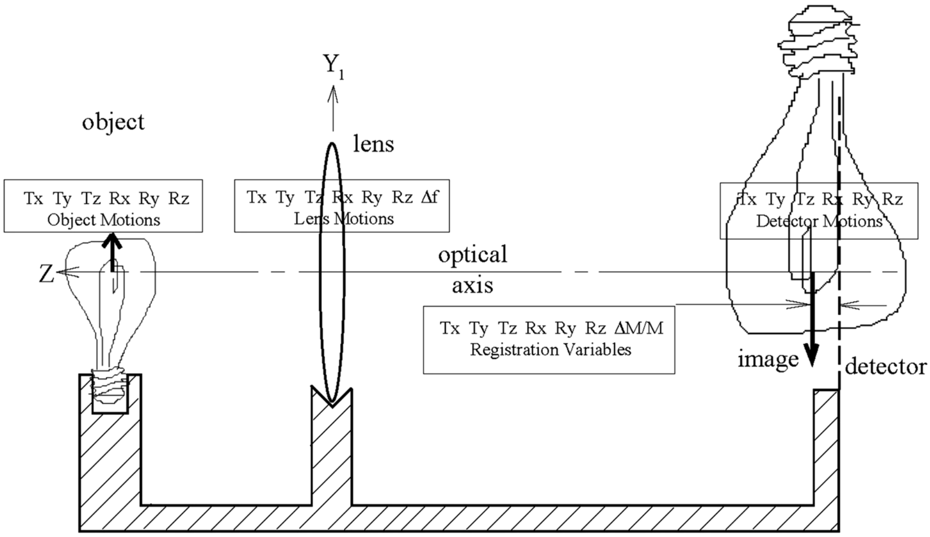

Figure 3.1 A single-lens imaging system.

in focal length, Δf. The effects on the registration variables are summed from left to right along the seven rows (now expressed as equations).

The change in focal length is determined from changes to the four lens design variables using the influence coefficients that were determined in Section 2.3 for the lens (Table 3.2).

Changes to the lens design variables can be from any source, such as manufacturing tolerance on the lens drawings, or dimensional and index of refraction changes caused by temperature changes. The relative index of refraction can also change due to changes in the index of refraction of the immersion medium (assumed to be air at standard conditions).

The seven equations in Table 3.1 control the position, orientation, and size of the Gaussian image on the system's detector and are called *optomechanical constraint equations*. These equations constrain the changes to the optical image that are driven by changes to the independent variables and the lens design variables.

The influence coefficients in the seven equations are determined from the magnification, focal length, and principal thickness of each of the elements. The magnitude of the independent variables is determined from mechanical engineering analysis of the system. The influence coefficients are then multiplied by the appropriate independent variables and summed to determine the value of the registration error in each of the seven registration variables.

3.1.1 Example: A reticle projection system

A company makes imaging systems and wishes to project a reticle onto the charge-coupled device (CCD) of an existing test setup. The optics department has found an existing reticle in stock that will do the job and a plano-convex

Table 3.1 Image motions for a single-lens imaging system.

Tx_o	Ty_o	Tz_o	Rx_o	Ry_o	Rz_o	Tx_1	Ty_1	Tz_1	Rx_1	Ry_1	Rz_1	Δf_1	Tx	Ty	Tz	Rx	Ry	Rz	
M						$1-M$				$-p$			-1.0						$= Tx_i$
	M						$1-M$		p					-1.0					$= Ty_i$
		M^2						$1-M^2$				$-(1-M)^2$			-1.0				$= Tz_i$
			M						$1-M$							-1.0			$= Rx_i$
				M						$1-M$							-1.0		$= Ry_i$
					1.0						0.0							-1.0	$= Rz_i$
		M/f						$-M/f$				$(1-M)/f$							$= \Delta M/M$
Object Motions						**Lens Motions Mechanical Design Variables**							**Detector Motions**						**Registration Variables**

Table 3.2 Influence coefficients on the focal length for a single-lens imaging system.

$\Delta f =$	$-\dfrac{f^2(n-1)^2}{nR_1R_2}$	$(n-1)f^2\left[\dfrac{t(n-1)}{nR_1^2R_2} - \dfrac{1}{R_1^2}\right]$	$(n-1)f^2\left[\dfrac{t(n-1)}{nR_1R_2^2} + \dfrac{1}{R_2^2}\right]$	$-\dfrac{tf^2(n-1)}{n^2R_1R_2} - \dfrac{f}{n-1}$
	Δt	ΔR_1	ΔR_2	Δn
	Lens Design Variables			

lens that will project it onto the CCD. The image of the reticle at the CCD will be two times larger than the physical reticle that will serve as the object of the projector. Since the image will be real, it will also be inverted, so the magnification will be -2. The lens is a commercial stock item with the following catalog values, in mechanical sign conventions:

$$f = 150 \text{ mm} \pm 2\%, \quad H_2 = 4.9 \text{ mm}, \quad t = 7.4 \text{ mm}.$$

In the design for the projector (Fig. 3.2), the convex side of the lens faces the reticle (the object). In this configuration, the first principal point is at the vertex of the first (convex) side, $H_1 = 0.0$ mm. The calculation of the principal thickness is

$$p = t + H_1 - H_2 = 7.4 + 0.0 - 4.9 = 2.5 \text{ mm}.$$

With these data, the optomechanical constraint equations for this single lens system can be written directly (Table 3.3).

The nominal deviation fraction for this lens is

$$e/Tz_o = M/f = 2.0/150 = 0.01333 \text{ mm}^{-1}.$$

While the deviation fraction is dimensionless, the nominal deviation fraction is given in the inverse units of the focal length, inverse millimeters in this case.

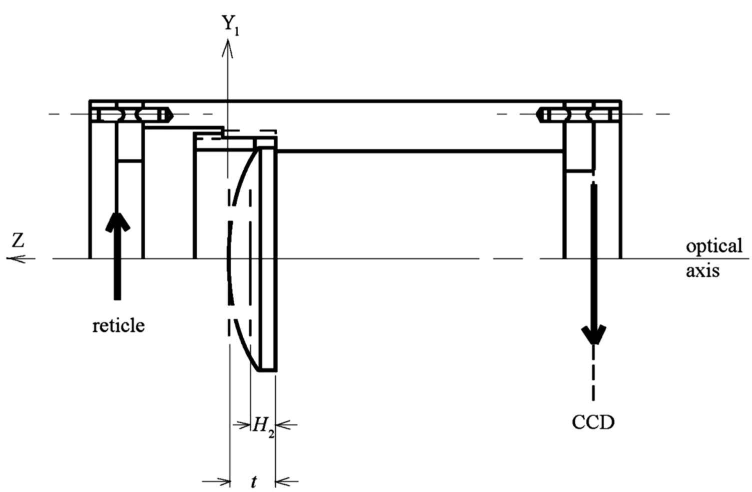

Figure 3.2 A reticle projection system (CCD: 0.0015-in. pixels, 256 × 256, 0.384 in. sq.).

Table 3.3 Optomechanical constraint equations for the reticle projector.

Tx_o	Ty_o	Tz_o	Rx_o	Ry_o	Rz_o	Tx_1	Ty_1	Tz_1	Rx_1	Ry_1	Rz_1	Δf_1	Tx	Ty	Tz	Rx	Ry	Rz	
−2						3				−2.5			−1.0						$= Tx_i$
	−2						3		2.5					−1.0					$= Ty_i$
		4						−3				−9			−1.0				$= Tz_i$
			−2						3							−1.0			$= Rx_i$
				−2						3							−1.0		$= Ry_i$
					1.0						0.0							−1.0	$= Rz_i$
		−0.0133						0.0133				0.0200							$= \Delta M/M$
Object Motions						**Lens Motions**							**Detector Motions**						**Registration Variables**
						Mechanical Design Variables													

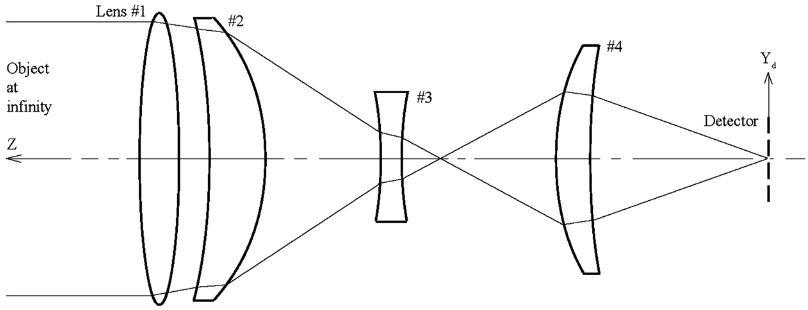

Figure 3.3 A multilens system.[1]

The engineer can determine the effects of the focal length tolerance as follows:

$$\Delta f = \pm 2\% = \pm 3.0 \text{ mm}, \quad Tz_{\mathrm{i}} = \pm(-9.0 \times \pm 3.0) = \pm 27 \text{ mm},$$
$$\Delta M/M = \pm(0.0200 \times \pm 3.0) = \pm 0.0600,$$
$$\text{relative nonlinearity} = 0.01333 \times \pm 3.0 = \pm 0.0400 \text{ or } 4\%.$$

3.2 Multilens Systems

Consider a multilens system (Fig. 3.3) consisting of an object at infinity, four lenses, and a detector. The system's image at the detector can be considered as the sequential product of each of the elements in the system. The object of the first lens produces an image from the first lens; this image becomes the object for the second lens, which, in turn, produces an image from the second lens; this second image becomes the object for the third lens, which produces an image from the third lens; this third image becomes the object for the fourth lens, which produces an image from the fourth lens; and, finally, this fourth image becomes the object for the detector and produces an image from the detector (an image on a screen, on film, in an eye, or on a recording medium). This method passes a right-handed image from one element to the right-handed object of the next element. The two coordinate systems, one for the image of one lens and one for the object of the next lens, are congruent.

The method for developing the optomechanical constraint equation for a multilens system begins by developing the individual arrays for each of the optical elements. An element's coefficients are then convolved into the appropriate object coefficients for each of the elements from it to, and including, the detector. (The convolution process described here is not a conventional matrix multiplication process.) For the $\Delta M/M$ registration variable, the process is both a convolution and superposition of the element's coefficients with all of the elements from it to, and including, the detector, as will be seen in Sections 3.2.1 and 3.2.2. The detector's element array is included in Section 3.2.3.

In the system's optomechanical constraint equations there will be an array for the system's object, an array for each of the system's optical elements, and

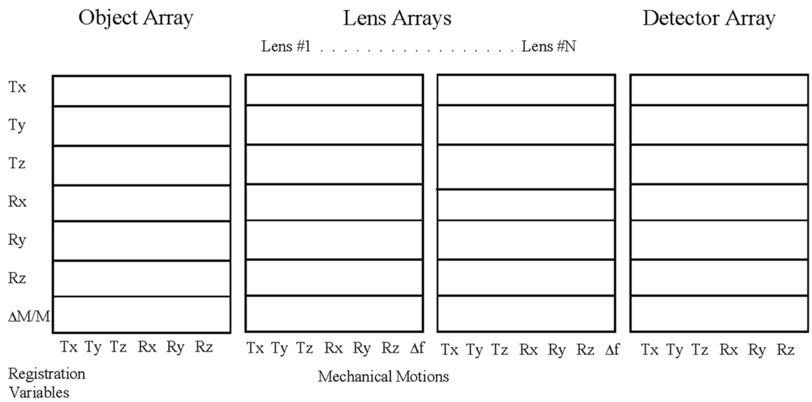

Figure 3.4 Arrays for a multilens system.[1]

an array for the detector. In general, if the system has N optical elements, its constraint equations will have $N+2$ arrays of coefficients (Fig. 3.4).

3.2.1 The system's object

The system's object is the object of the system's first element and has seven influence coefficients, A through G, as shown in Fig. 3.5. Coefficients A through F will be evaluated first.

If this system's object moves in the X direction, Tx_o, the system's image also moves in its X direction, Tx_i, by the amount

$$Tx_\mathrm{i} = Tx_\mathrm{o}(M_1)(M_2)(M_3)(M_4)(1.0).$$

The first four terms in parenthesis in the above equation represent the object influence coefficients Tx_i/Tx_N for each of the lenses, where N ranges from 1 to 4. The final term in parentheses, (1.0), represents the detector. Consequently, the system's influence coefficient A between the system's object and the system's image is

$$A = Tx_\mathrm{i}/Tx_\mathrm{o} = (M_1)(M_2)(M_3)(M_4)(1.0).$$

By similar reasoning, the system's coefficients for the other two translations and three rotations of the object can be derived as

$$B = Ty_\mathrm{i}/Ty_\mathrm{o} = (M_1)(M_2)(M_3)(M_4)(1.0),$$
$$C = Tz_\mathrm{i}/Tz_\mathrm{o} = (M^2{}_1)(M^2{}_2)(M^2{}_3)(M^2{}_4)(1.0),$$
$$D = Rx_\mathrm{i}/Rx_\mathrm{o} = (M_1)(M_2)(M_3)(M_4)(1.0),$$
$$E = Ry_\mathrm{i}/Ry_\mathrm{o} = (M_1)(M_2)(M_3)(M_4)(1.0),$$
$$F = Rz_\mathrm{i}/Rz_\mathrm{o} = (1.0)(1.0)(1.0)(1.0)(1.0).$$

The process here is to multiply the influence coefficient of the optical element being analyzed (the system's object in this case) by the corresponding

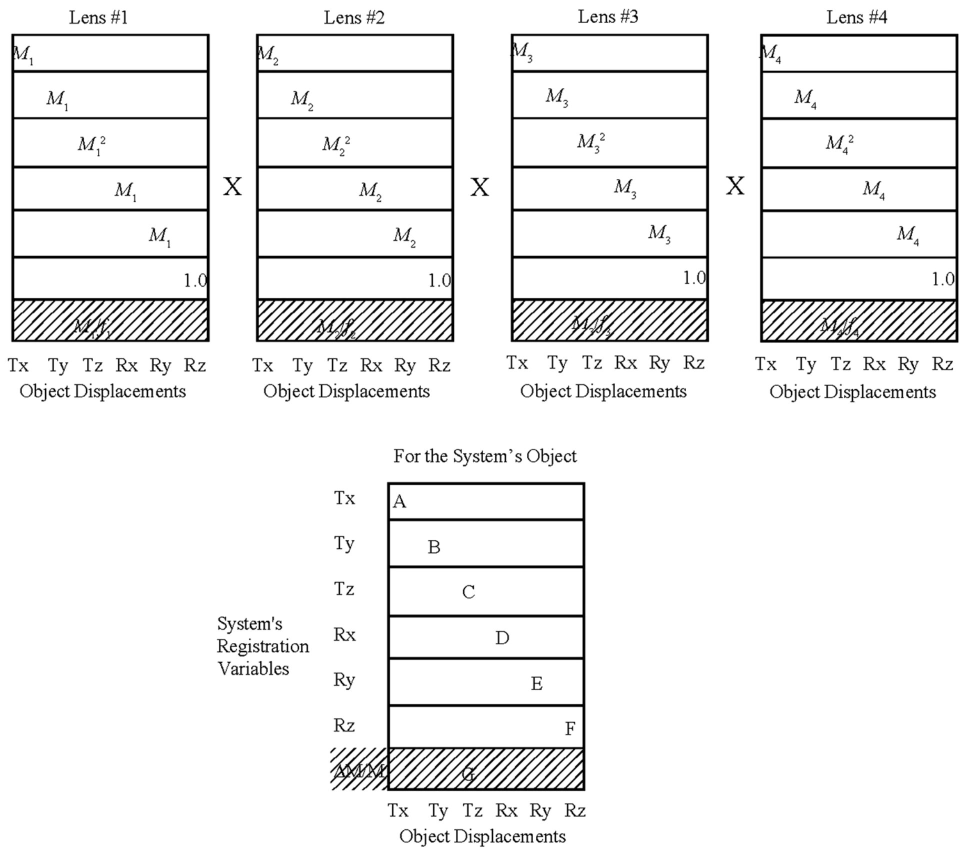

Figure 3.5 Translations and rotations caused by the system's object.[1]

object influence coefficient for each of the optical elements between it and the system's image, the output of the detector.

The seventh object influence function, G in Fig. 3.6, will now be evaluated. The system's influence coefficients for the change in size due to a Z translation of the system's object must be formulated a little differently. The Tz_o motion not only has a direct effect on the size of the image of the first lens, but it also causes a Z translation of the image of the first lens, which, in turn, causes an independent change in size of the image of the second lens. This process continues at each optical element in the system through to the system's image. The resulting system's influence coefficient for change in size contains an expression for the change in size contributed by each optical element:

$$\begin{aligned} G &= \Delta M/MTz_o \\ &= [(M_1/f_1) + (M_1{}^2)(M_2/f_2) + (M_1{}^2)(M_2{}^2)(M_3/f_3) \\ &\quad + (M_1{}^2)(M_2{}^2)(M_3{}^2)(M_4/f_4)](1.0). \end{aligned}$$

The seven equations for A through G summarize the influence of the motions of the system's object on the motions of the system's image.

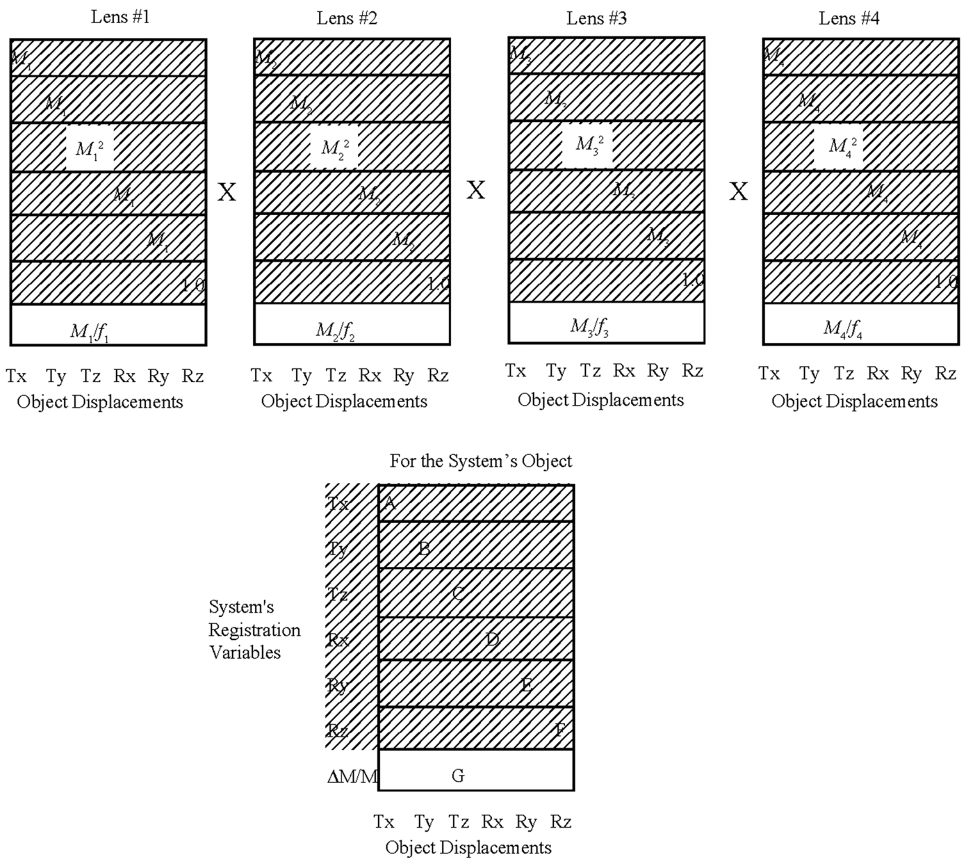

Figure 3.6 Change in size caused by the system's object.[1]

3.2.2 The system's lenses

Each lens in the system has 11 influence coefficients, A through K in Fig. 3.7. Influence coefficients A through I will be evaluated first. The system's influence coefficients for each of the lenses are developed in a fashion similar to that of the system's object except that the lens array is used as the starting point instead of the object array. If the first lens is moved in the X direction, the system's image also moves in the X direction by the amount

$$Tx_{\mathrm{i}} = Tx_1(1 - M_1)(M_2)(M_3)(M_4)(1.0).$$

The final term, (1.0), is the effect of the detector, which is not shown in Figs. 3.5 through 3.8. The lens' influence coefficient A on the system's image is

$$A = Tx_{\mathrm{i}}/Tx_1 = (1 - M_1)(M_2)(M_3)(M_4)(1.0).$$

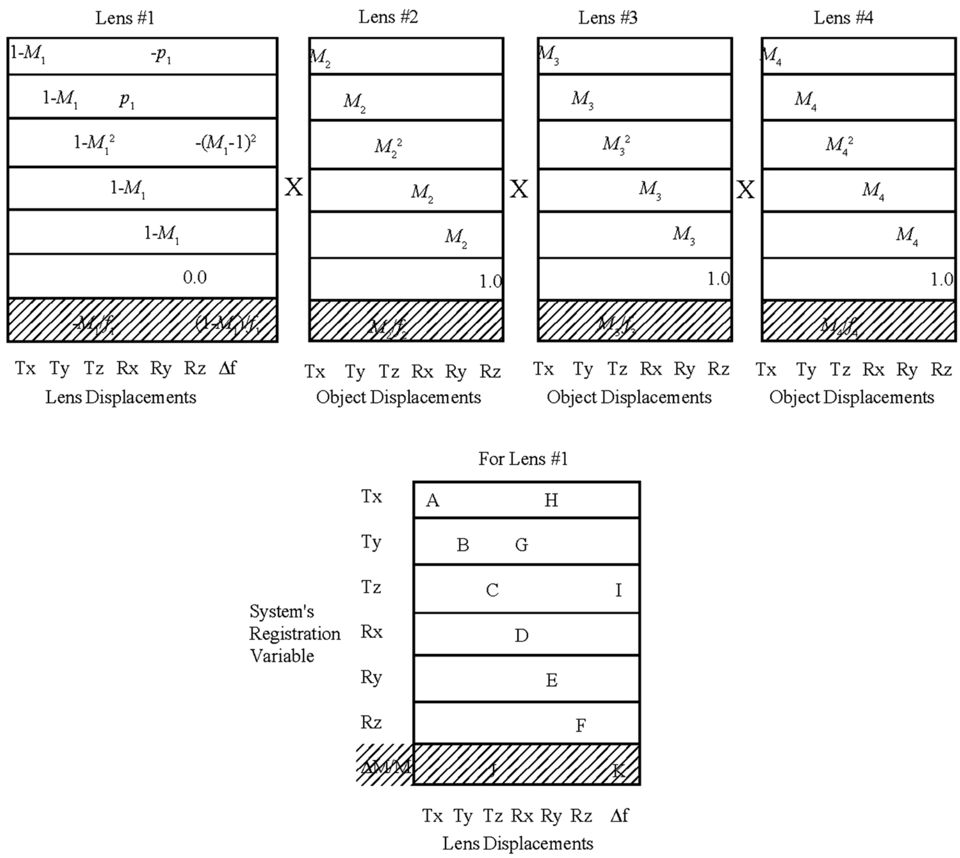

Figure 3.7 Translations and rotations caused by a lens in the system.[1]

The system's influence coefficients for the other two translations and three rotations can be developed by the same process. Note that there are three more coefficients in this group; two are associated with the principal thickness, p, and one with the change in focal length, Δf:

$$B = Ty_i/Ty_1 = (1 - M_1)(M_2)(M_3)(M_4)(1.0),$$
$$C = Tz_i/Tz_1 = (1 - M_1{}^2)(M_2{}^2)(M_3{}^2)(M_4{}^2)(1.0),$$
$$D = Rx_i/Rx_1 = (1 - M_1)(M_2)(M_3)(M_4)(1.0),$$
$$E = Ry_i/Ry_1 = (1 - M_1)(M_2)(M_3)(M_4)(1.0),$$
$$F = Rz_i/Rz_1 = (0.0)(1.0),$$
$$G = Ty_i/Rx_1 = (p_1)(M_2)(M_3)(M_4)(1.0),$$
$$H = Tx_i/Ry_1 = (-p_1)(M_2)(M_3)(M_4)(1.0),$$
$$I = Tz_i/\Delta f_1 = -(1 - M_1)(M_2)(M_3)(M_4)(1.0).$$

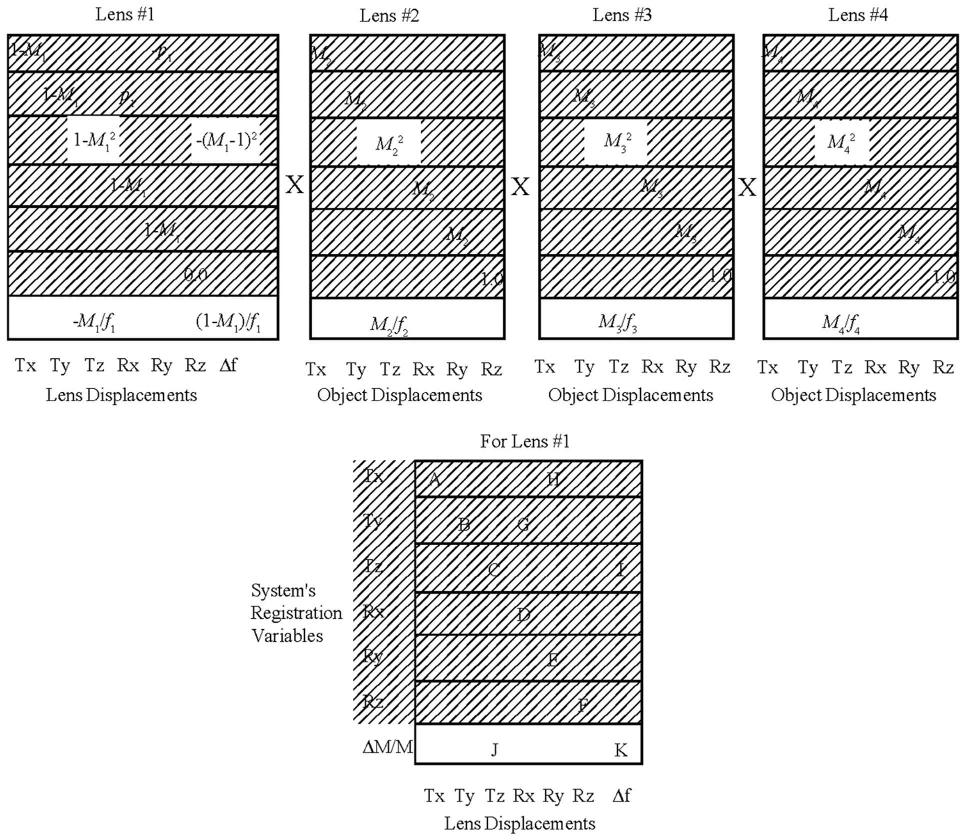

Figure 3.8 Change in size caused by a lens in the system.[1]

There are also two system-level coefficients associated with the change in image size, J and K in Fig. 3.8. The first coefficient is associated with the translation in Z of the lens, and the second is associated with the change in focal length of the lens. These coefficients are developed in a process similar to that of corresponding coefficients for the system object (Section 3.2.1):

$$\begin{aligned} J &= \Delta M/MTz_1 \\ &= [-(M_1/f_1) + (1 - M_1{}^2)(M_2/f_2) + (1 - M_1{}^2)(M_2{}^2)(M_3/f_3) \\ &\quad + (1 - M_1{}^2)(M_2{}^2)(M_3{}^2)(M_4/f_4)](1.0), \end{aligned}$$

$$\begin{aligned} K &= \Delta M/M\Delta f_1 \\ &= [(1 - M_1)/f_1 - (M_1 - 1)^2(M_2/f_2) - (M_1 - 1)^2(M_2{}^2)(M_3/f_3) \\ &\quad - (M_1 - 1)^2(M_2{}^2)(M_3{}^2)(M_4/f_4)](1.0). \end{aligned}$$

3.2.3 The system's detector

The influence coefficients for the system's detector are the same as those for the single lens system:

$$Tx_i/Tx_d = -1$$
$$Ty_i/Ty_d = -1$$
$$Tz_i/Tz_d = -1$$
$$Rx_i/Rx_d = -1$$
$$Ry_i/Ry_d = -1$$
$$Rz_i/Rz_d = -1.$$

3.2.4 Effective focal length of multilens systems

Calculating the effective focal length of a system provides a useful quality metric; it tells the engineer how faithfully the physical optical prescription data has been interpreted.

The effective focal length of a system of lenses can be determined from the Gaussian prescription data of the lenses. The process starts by combining the first two lenses into a doublet and calculating the Gaussian properties of the doublet (Fig. 3.9). If the first lens (lens a) has the Gaussian properties f_a, H_{1a}, H_{2a}, and p_a, and the second lens (lens b) has the Gaussian properties f_b, H_{1b}, H_{2b}, and p_b, then the Gaussian focal length, f_{ab}, of the doublet can be calculated as

$$f_{ab} = f_a f_b/(f_a + f_b - pair_a),$$

where the variable *pair* is the principal air thickness between lenses. The position *Ba* of the doublet's first focus $(f_1)_{ab}$ relative to the first principal point of lens a $(P_1)_a$ can be calculated by

$$Ba = f_{ab}(f_b - pair_a)/f_b,$$

and the position *Bb* of the doublet's second focus $(f_2)_{ab}$ can be calculated by

$$Bb = -f_{ab}(f_a - pair_a)/f_a.$$

The principal thickness of the doublet p_{ab} can be calculated by

$$p_{ab} = Ba + p_a + pair_a + p_b - Bb - 2f_{ab}$$

and

$$pair_{ab} = pair_b + Bb + f_{ab}.$$

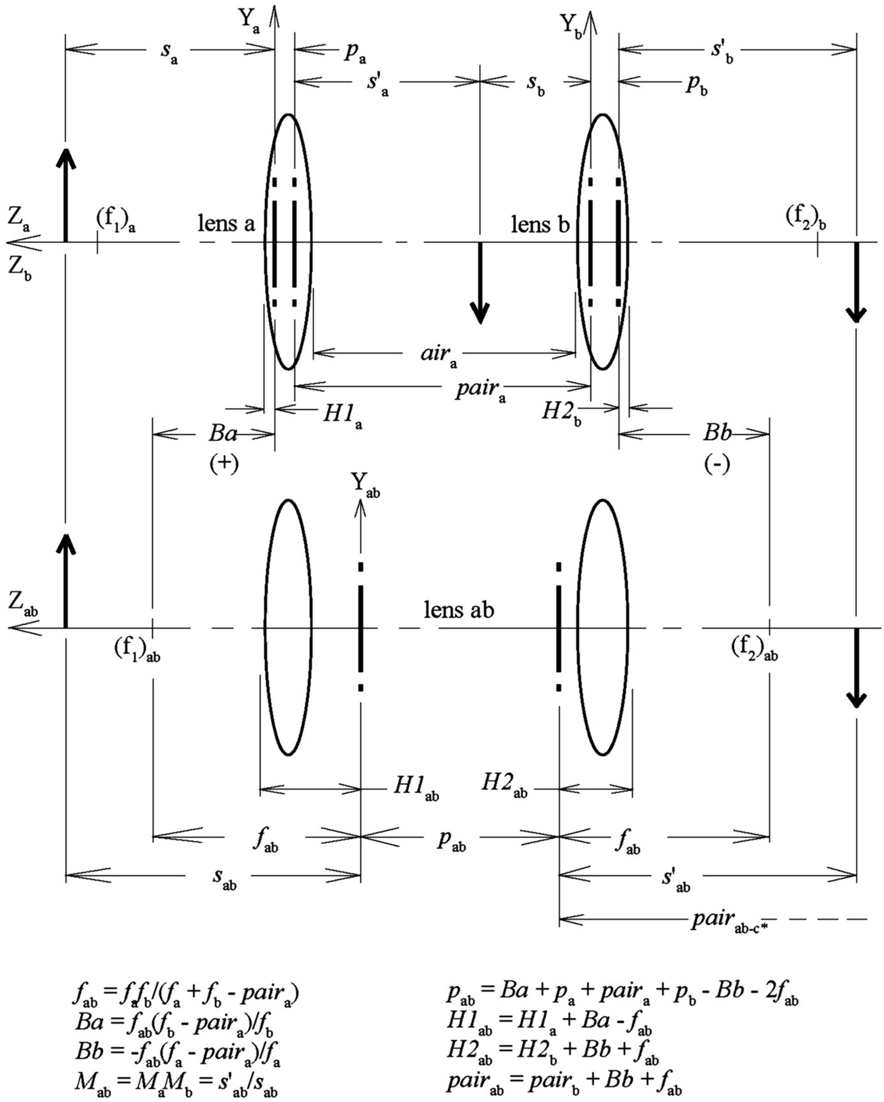

Figure 3.9 Gaussian properties of a lens doublet.[1] (Figure adapted from Ref. 3.)

The position of the doublet's principal points, H_{1ab} and H_{2ab}, with respect to the first and last vertices of the lenses can be determined from the geometry. The magnification of the doublet is

$$M_{ab} = M_a M_b.$$

The doublet can be increased to a triplet by adding another lens and recalculating the properties with the initial doublet as lens a, and the new lens

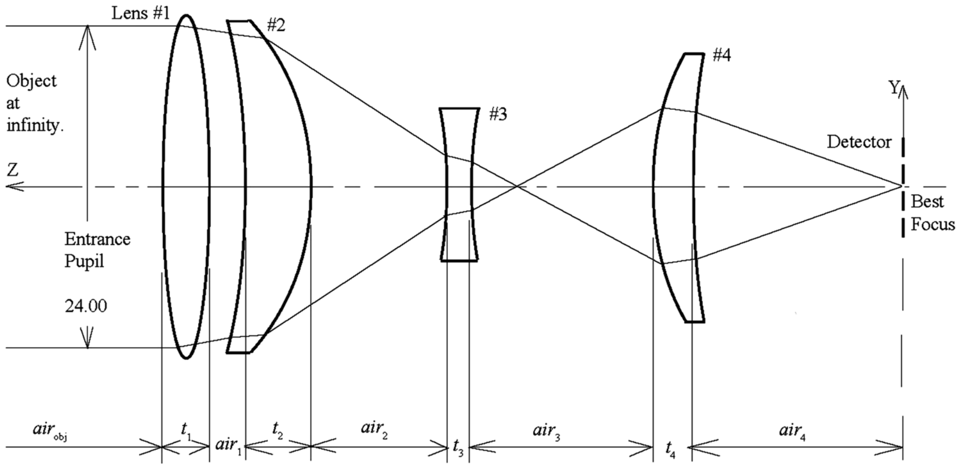

Figure 3.10 A four-lens infrared receiver.[1]

Table 3.4 Optomechanical prescription data for the infrared receiver.

Surface	Element	Radius	Index	Thickness
1	Obj.	Inf.	1.000	Inf.
2	1	−300	4.0026	2.000
3	1	300	1.0000	5.3566
4	2	110	4.0026	3.4500
5	2	55	1.0000	17.7750
6	3	310	4.0026	2.0000
7	3	−215	1.0000	11.9417
8	4	−11	4.0026	1.5000
9	4	−22	1.0000	20.4727
10	Det.	Inf.	1.0000	—

as lens b. The process is repeated, adding one lens at a time, until all of the lenses in the system have been included.

3.2.5 Example: An infrared receiver

A four-lens infrared receiver (Fig. 3.10) has been optically designed with the physical optical prescription provided in Table 3.4. The effective focal length of this system is reported to be −51.579012. The dimensional units of this prescription are inches and have been converted to the mechanical sign conventions. The engineer wants to develop the optomechanical constraint equations.

3.2.5.1 The Gaussian prescription

The first task is to derive the Gaussian prescription (Table 3.5) from the optomechanical prescription (Table 3.4) using the equations of Section 1.6:

Table 3.5 The Gaussian prescription data for the infrared receiver.

Element	f	H_1	H_2	p	pair
Obj.	Inf.	0.0	0.0	0.0	Inf.
1	50.081936	−0.2504639	0.2504639	1.4990722	7.2534706
2	34.98851	−1.6464068	−0.82320338	2.6267966	17.246002
3	−42.160333	−0.29420554	0.20404578	1.5017487	11.805767
4	6.6470266	0.33997836	0.67995673	1.1600216	21.152657
Det.	Inf.	0.0	0.0	0.0	0.0

$$\frac{1}{f} = (n-1)\left[\frac{1}{R_2} - \frac{1}{R_1} + \frac{t(n-1)}{nR_1R_2}\right],$$
$$H_1 = \frac{-ft(n-1)}{nR_2},$$
$$H_2 = \frac{-ft(n-1)}{nR_1},$$
$$p = t\left[1 - f(n-1)\left(\frac{1/R_2 - 1/R_1}{n}\right)\right].$$

The variable *pair* (the principal air thickness between lenses) is the distance between P_2 of one element and P_1 of the next element in Fig. 3.11. It is analogous to the air thickness, *air*, between the lens vertices (V_2 of one element and V_1 of the next element) in the physical optical prescription (see Fig. 3.10).

The data in Table 3.5 are then used to calculate the effective focal length of the four-lens system. For the infrared receiver quadruplet in Fig. 3.10, the focal length of the first element is

$$f_1 = 50.08.$$

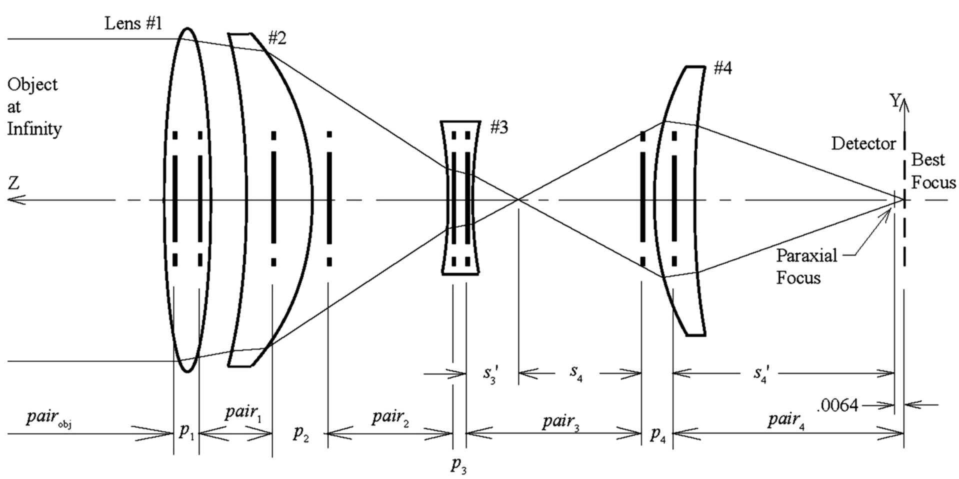

Figure 3.11 The principal air thicknesses *pair* for the receiver.[1]

Combining f_1 with the second lens, the effective focal length of the doublet is

$$f_{1\text{-}2} = 22.52.$$

Combining the 1-2 doublet with the third lens, the effective focal length of the resulting triplet is

$$f_{1\text{-}3} = 23.65.$$

Combining the 1-3 triplet with the fourth (and final) lens of the system, the system's effective focal length is

$$f_{1\text{-}4} = -51.58.$$

This effective focal length compares favorably with the effective focal length (*efl*) from the optical design code,

$$efl = -51.579012,$$

and provides confidence that the physical optical prescription has been properly interpreted.

3.2.5.2 Objects, images, and magnifications

Next, the engineer locates all of the intermediate objects and images, and calculates the element magnifications (Table 3.6) from the equations, noting that an element's object distance, s, is calculated from the properties s' and *pair* of the preceding element, as shown for elements 3 and 4 in Fig. 3.11:

$$\begin{aligned} s &= s'_{\text{elem-1}} + pair_{\text{elem-1}}, \\ s' &= 1/(1/s - 1/f), \\ M &= s'/s. \end{aligned}$$

The properties of element 4 are calculated here, as an example:

$$\begin{aligned} s_4 &= s'_3 + pair_3 = -2.111479 + 11.805767 = 9.694288, \\ s'_4 &= 1/(1/s_4 - 1/f_4) = 1/(1/9.694288 - 1/6.647027) = -21.14626, \\ M_4 &= s'_4/s_4 = -21.14626/9.694288 = -2.181311. \end{aligned}$$

Note that the Gaussian image does not register exactly on the detector; it is 0.0064 inches in front of the detector. This is because the optical

Table 3.6 Objects, images, and magnifications for the infrared receiver.

Element	f	s	s'	M
Obj.	Inf.	0.0	0.0	1.0
1	50.081936	Inf.	−50.08194	0.0
2	34.98851	−42.82846	−19.25678	0.4496257
3	−42.160333	−2.010775	−2.111479	1.050082
4	6.6470266	9.694288	−21.14626	−2.181311
Det.	Inf.	6.39518E-3	6.39518E-3	1.0

prescription locates the detector at the *plane of best focus* over the entire field of view, and this location will almost always be somewhat different from that of the paraxial or Gaussian focus. This difference suggests that the geometry of the system's image has been captured to an accuracy of about 6:51,000.

3.2.5.3 The element arrays

The engineer now has all of the focal lengths, magnifications, and principal thicknesses for all of the optical elements in the system. With these, the next step is to prepare the individual element arrays. The arrays for the first, second, third, and fourth elements are in Tables 3.7(a), (b), (c), and (d), respectively. The arrays for the detector are in Table 3.7(e). There are no lens design variables for the detector.

3.2.5.4 The optomechanical constraint equations

The optomechanical constraint equations are then generated by convolving and superimposing the element arrays in the process described earlier (in Sections 3.2.1 through 3.2.3). The results are in Tables 3.8(a) and (b), where Table 3.8(b) is a continuation of Table 3.8(a).

Two examples of the method for calculating the system influence coefficients for Lens 1 follow:

$$Tz_{\mathrm{i}}/Tz_1 = 1.0 \times 0.2022 \times 1.1027 \times 4.7581 \times 1.0 = 1.0607,$$

$$\begin{aligned}(\Delta M_{\mathrm{i}}/M)/Tz_1 &= 0.0 + 1.0 \times 0.01285 + 1.0 \times 0.2022 \times -0.02491 \\ &\quad + 1.0 \times 0.2022 \times 1.1027 \times -0.3282 \\ &= -0.06533.\end{aligned}$$

The reader will find these values in the Lens 1 array in Table 3.8(a). All of the other coefficients in the optomechanical constraint equations were calculated in a similar fashion.

Table 3.7(a) Element arrays for the first lens.

Image Motions	Object Motions						Lens Motions						
	Tx	Ty	Tz	Rx	Ry	Rz	Tx	Ty	Tz	Rx	Ry	Rz	Δf
Tx	0.0						1.0				−1.4991		
Ty		0.0						1.0		1.4991			
Tz			0.0						1.0				−1.0
Rx				0.0						1.0			
Ry					0.0						1.0		
Rz						1.0						0.0	
$\Delta M/M$			0.0						0.0				0.01997

	Lens Design Variables			
	Δt	ΔR_1	ΔR_2	Δn
Δf	0.627	−0.833	0.833	−16.67

Table 3.7(b) Element arrays for the second lens.

Image Motions	Object Motions						Lens Motions						
	Tx	Ty	Tz	Rx	Ry	Rz	Tx	Ty	Tz	Rx	Ry	Rz	Δf
Tx	0.4496						0.5504				−2.6268		
Ty		0.4496						0.5504		2.6268			
Tz			0.2022						0.7978				−0.3029
Rx				0.4496						0.5504			
Ry					0.4496						0.5504		
Rz						1.0						0.0	
$\Delta M/M$			0.01285						−0.01285				0.01573

	Lens Design Variables			
	Δt	ΔR_1	ΔR_2	Δn
Δf	−0.4558	−0.2895	1.2437	−11.78

Table 3.7(c) Element arrays for the third lens.

Image Motions	Object Motions						Lens Motions						
	Tx	Ty	Tz	Rx	Ry	Rz	Tx	Ty	Tz	Rx	Ry	Rz	Δf
Tx	1.0501						−0.0501				−1.5018		
Ty		1.0501						−0.0501		−1.5018			
Tz			1.1027						−0.1027				−0.00251
Rx				1.0501						−0.0501			
Ry					1.0501						−0.0501		
Rz						1.0						0.0	
$\Delta M/M$			−.02491						0.02491				0.00119

	Lens Design Variables			
	Δt	ΔR_1	ΔR_2	Δn
Δf	0.0601	−0.0559	0.1160	14.605

In multilens optical systems, it is often more convenient to arrange the equations so that they are vertically aligned, as in Table 3.9. The seven registration variables identifying each of the equations are shown across the top, and the independent mechanical variables are listed on the left side for each optical element. The two columns on the right show the sensitivity of each lens' focal length to the four lens design variables. From such a table it is relatively easy to identify the most sensitive optical elements for each of the registration variables.

In the Tx and Ty registration variables, the strongest is Element 4 with Tx_i/Tx_4 equal to 3.18. The next strongest is Element 2 at −1.26. Note that

Table 3.7(d) Element arrays for the fourth lens.

Image Motions	Object Motions *Tx*	*Ty*	*Tz*	*Rx*	*Ry*	*Rz*	Lens Motions *Tx*	*Ty*	*Tz*	*Rx*	*Ry*	*Rz*	Δf
Tx	−2.1813						3.1813				−1.1600		
Ty		−2.1813						3.1813		1.1600			
Tz			4.7581						−3.7581				−10.1207
Rx				−2.1813						3.1813			
Ry					−2.1813						3.1813		
Rz						1.0						0.0	
$\Delta M/M$			−0.3282						0.3282				0.4786

	Lens Design Variables Δt	ΔR_1	ΔR_2	Δn
Δf	−0.4112	−1.1525	0.2461	−2.2651

Table 3.7(e) Element arrays for the detector.

Image Motions	Object Motions *Tx*	*Ty*	*Tz*	*Rx*	*Ry*	*Rz*	Lens Motions *Tx*	*Ty*	*Tz*	*Rx*	*Ry*	*Rz*	Δf
Tx	1.0						−1.0						
Ty		1.0						−1.0					
Tz			1.0						−1.0				
Rx				1.0						−1.0			
Ry					1.0						−1.0		
Rz						1.0						−1.0	
$\Delta M/M$													−1.0

elements 2 and 3 have large influence coefficients in these equations but these are for rotations of the elements. The unit of rotation is the radian, a relatively large quantity that tends to inflate these influence coefficients, which are dimensioned by units of length/radian. In the *Tz* (focus) registration variable, the strongest influence is Element 2, followed closely by Element 4, at 4.18 and −3.76, respectively. If the design is concerned about focus resolution in the corners of the field of view, the *Rx* and *Ry* registration variables show that Element 4 with a coefficient of 3.18 has a strong influence on the tip-tilt of the image at the detector. These latter coefficients are dimensionless, dimensioned by units of radians/radian.

The mechanical variables, like tolerances, tend to vary independently by + and − amounts. At this initial level of observation, the absolute values are of interest, and −3 is considered to be larger than −2. At a later state of

Table 3.8(a) The optomechanical constraint equations for the infrared receiver.

Object Motions						Lens 1 Motions							Lens 2 Motions						
Tx	Ty	Tz	Rx	Ry	Rz	Tx	Ty	Tz	Rx	Ry	Rz	Δf	Tx	Ty	Tz	Rx	Ry	Rz	Δf
0.0						−1.0299				1.5439			−1.2607				6.0168		
	0.0						−1.0299		−1.5439					−1.2607		−6.0168			
		0.0						1.0607				−1.0607			4.1860				−1.5893
			0.0						−1.0299							−1.2606			
				0.0						−1.0299							−1.2606		
					1.0						0.0							0.0	
		0.0						−0.06533				0.08527			−0.32141				0.13287

Table 3.8(b) The optomechanical constraint equations for the infrared receiver.

Lens 3 Motions							Lens 4 Motions							Detector Motions							Registration Variables
Tx	Ty	Tz	Rx	Ry	Rz	Δf	Tx	Ty	Tz	Rx	Ry	Rz	Δf	Tx	Ty	Tz	Rx	Ry	Rz	Δf	
0.1092				3.2758			3.1813				1.1600			−1.0							$= Tx_i$
	0.1092		−3.2758					3.1813		1.1600					−1.0						$= Ty_i$
		−0.4885				−0.0119			−3.7576				−10.121			−1.0					$= Tz_i$
			0.1092							3.1813							−1.0				$= Rx_i$
				0.1092							3.1813							−1.0			$= Ry_i$
					0.0							0.0							−1.0		$= Rz_i$
		0.5860				0.00201			−0.3282				0.4786								$= \Delta M/M_i$

Table 3.9 The vertical arrangement of the optomechanical constraint equations for the infrared receiver.

OPTOMECHANICAL CONSTRAINT EQUATIONS

	REGISTRATION VARIABLES								
	TX	TY	TZ	RX	RY	RZ	DM/M	Df,p,G	LDesVar
Tx	0.0	0.0	0.0	0.0	0.0	0.0	0.0	0.0	Dt
Ty	0.0	0.0	0.0	0.0	0.0	0.0	0.0	0.0	DR1
Tz	0.0	0.0	0.0	0.0	0.0	0.0	0.0	0.0	DR2
Rx	0.0	0.0	0.0	0.0	0.0	0.0	0.0	0.0	Dn
Ry	0.0	0.0	0.0	0.0	0.0	0.0	0.0	0.0	
Rz	0.0	0.0	0.0	0.0	0.0	1	0.0	0.0	
Df,p,G	0.0	0.0	0.0	0.0	0.0	0.0	0.0	0.0	
SYSTEM-OBJECT									
Tx	−1.029893	0.0	0.0	0.0	0.0	0.0	0.0	6.277294E-2	Dt
Ty	0.0	−1.029893	0.0	0.0	0.0	0.0	0.0	−8.326065E-2	DR1
Tz	0.0	0.0	1.060679	0.0	0.0	0.0	−6.533874E-2	8.326065E-2	DR2
Rx	0.0	−1.543884	0.0	−1.029893	0.0	0.0	0.0	−16.66908	Dn
Ry	1.543884	0.0	0.0	0.0	−1.029893	0.0	0.0	0.0	
Rz	0.0	0.0	0.0	0.0	0.0	0.0	0.0	0.0	
Df,p,G	0.0	0.0	−1.060679	0.0	0.0	0.0	8.530602E-2	0.0	
ELEMENT-1									
Tx	−1.260663	0.0	0.0	0.0	0.0	0.0	0.0	−.4557727	Dt
Ty	0.0	−1.260663	0.0	0.0	0.0	0.0	0.0	−.289488	DR1
Tz	0.0	0.0	4.185968	0.0	0.0	0.0	−.321425	1.24372	DR2
Rx	0.0	−6.016825	0.0	−1.260663	0.0	0.0	0.0	−11.78357	Dn
Ry	6.016825	0.0	0.0	0.0	−1.260663	0.0	0.0	0.0	
Rz	0.0	0.0	0.0	0.0	0.0	0.0	0.0	0.0	
Df,p,G	0.0	0.0	−1.589272	0.0	0.0	0.0	.1328855	0.0	
ELEMENT-2									

(continued)

Table 3.9 Continued

Tx	.1092447	0.0	0.0	0.0	0.0	0.0	0.0	6.007042E-2	Dt
Ty	0.0	.1092447	0.0	0.0	0.0	0.0	0.0	−5.592452E-2	DR1
Tz	0.0	0.0	−.4885279	0.0	0.0	0.0	5.860023E-2	.116018	DR2
Rx	0.0	−3.275782	0.0	.1092447	0.0	0.0	0.0	14.05127	Dn
Ry	3.275782	0.0	0.0	0.0	.1092447	0.0	0.0	0.0	
Rz	0.0	0.0	0.0	0.0	0.0	0.0	0.0	0.0	
Df,p,G	0.0	0.0	−1.193441E-2	0.0	0.0	0.0	2.011003E-3	0.0	
ELEMENT-3									
Tx	3.181311	0.0	0.0	0.0	0.0	0.0	0.0	−.411237	Dt
Ty	0.0	3.181311	0.0	0.0	0.0	0.0	0.0	−1.152472	DR1
Tz	0.0	0.0	−3.75812	0.0	0.0	0.0	.3281635	.2460598	DR2
Rx	0.0	1.160022	0.0	3.181311	0.0	0.0	0.0	−2.265084	Dn
Ry	−1.160022	0.0	0.0	0.0	3.181311	0.0	0.0	0.0	
Rz	0.0	0.0	0.0	0.0	0.0	0.0	0.0	0.0	
Df,p,G	0.0	0.0	−10.12074	0.0	0.0	0.0	.4786067	0.0	
ELEMENT-4									
Tx	−1	0.0	0.0	0.0	0.0	0.0	0.0	0.0	Dt
Ty	0.0	−1	0.0	0.0	0.0	0.0	0.0	0.0	DR1
Tz	0.0	0.0	−1	0.0	0.0	0.0	0.0	0.0	DR2
Rx	0.0	0.0	0.0	−1	0.0	0.0	0.0	0.0	Dn
Ry	0.0	0.0	0.0	0.0	−1	0.0	0.0	0.0	
Rz	0.0	0.0	0.0	0.0	0.0	−1	0.0	0.0	
Df,p,G	0.0	0.0	0.0	0.0	0.0	0.0	0.0	0.0	
DETECTOR									

observation, say for structural deflections, coefficients of the opposite orientation might tend to compensate each other, but it is very rare that this can be made to occur intentionally and consistently.

With these initial insights, the mechanical engineer can begin to appreciate the challenges of aligning and stabilizing the image on the detector for this system.

This tabular arrangement is also importable into spreadsheet software for making other system-wide calculations. Figure 3.12 shows an evaluation of the focus effect of a tolerance of ±0.01 on the absolute Z position of each lens;

	TX	TY	TZ	RX	RY	RZ	DM/M	Df,p,G	LDesVar	**Z Axis Tolerance ±**	**Focus Error**	
Tx	0	0	0	0	0	0	0	0	Dt			
Ty	0	0	0	0	0	0	0	0	DR1			
Tz	0	0	0	0	0	0	0	0	DR2			
Rx	0	0	0	0	0	0	0	0	Dn			
Ry	0	0	0	0	0	0	0	0				
Rz	0	0	0	0	0	1	0	0				
Df,p,G	0	0	0	0	0	0	0	0				
SYSTEM-OBJECT												
Tx	-1.02989	0	0	0	0	0	0	6.28E-02	Dt			
Ty	0	-1.02989	0	0	0	0	0	-8.33E-02	DR1			
Tz	0	0	**1.060679**	0	0	0	-6.53E-02	8.33E-02	DR2	**0.01**	**0.010607**	
Rx	0	-1.54388	0	-1.02989	0	0	0	-16.6691	Dn			
Ry	1.543884	0	0	0	-1.02989	0	0	0				
Rz	0	0	0	0	0	0	0	0				
Df,p,G	0	0	-1.06068	0	0	0	8.53E-02	0				
ELEMENT-1												
Tx	-1.26066	0	0	0	0	0	0	-0.45577	Dt			
Ty	0	-1.26066	0	0	0	0	0	-0.28949	DR1			
Tz	0	0	**4.185968**	0	0	0	-0.32143	1.24372	DR2	**0.01**	**0.04186**	
Rx	0	-6.01683	0	-1.26066	0	0	0	-11.7836	Dn			
Ry	6.016825	0	0	0	-1.26066	0	0	0				
Rz	0	0	0	0	0	0	0	0				
Df,p,G	0	0	-1.58927	0	0	0	0.132886	0				
ELEMENT-2												
Tx	0.109245	0	0	0	0	0	0	6.01E-02	Dt			
Ty	0	0.109245	0	0	0	0	0	-5.59E-02	DR1			
Tz	0	0	**-0.48853**	0	0	0	5.86E-02	0.116018	DR2	**0.01**	**-0.00489**	
Rx	0	-3.27578	0	0.109245	0	0	0	14.05127	Dn			
Ry	3.275782	0	0	0	0.109245	0	0	0				
Rz	0	0	0	0	0	0	0	0				
Df,p,G	0	0	-1.19E-02	0	0	0	2.01E-03	0				
ELEMENT-3												
Tx	3.181311	0	0	0	0	0	0	-0.41124	Dt			
Ty	0	3.181311	0	0	0	0	0	-1.15247	DR1			
Tz	0	0	**-3.75812**	0	0	0	0.328164	0.24606	DR2	**0.01**	**-0.03758**	
Rx	0	1.160022	0	3.181311	0	0	0	-2.26508	Dn			
Ry	-1.16002	0	0	0	3.181311	0	0	0				
Rz	0	0	0	0	0	0	0	0				
Df,p,G	0	0	-10.1207	0	0	0	0.478607	0				
ELEMENT-4												
Tx	-1	0	0	0	0	0	0	0	Dt			
Ty	0	-1	0	0	0	0	0	0	DR1			
Tz	0	0	**-1**	0	0	0	0	0	DR2	**0.01**	**-0.01**	
Rx	0	0	0	-1	0	0	0	0	Dn			
Ry	0	0	0	0	-1	0	0	0				**Worst**
Rz	0	0	0	0	0	-1	0	0			**0.104933**	**Case**
Df,p,G	0	0	0	0	0	0	0	0				**Focus**
DETECTOR												**Error**

Figure 3.12 Focus errors evaluated in a spreadsheet.

this is not an airspace tolerance that can accumulate from airspace to airspace. The focus error contributed by each element is obtained by multiplying the Z tolerance by the Tz_i/Tz_i influence coefficient. These contributions are then summed on an absolute basis to obtain the "worst-case focus error" in the lower right of the figure. The worst-case focus error here is 0.1049 in., and about 80% of that is nearly evenly divided between Lenses 2 and 4. If this level of worst-case focus error is not acceptable, then tighter tolerances on the mounting of Lenses 2 and 4 offers the most return for a little tighter tolerances. On the other hand, if some attrition and/or on-line rework is appropriate, then perhaps a root-sum-square value would be acceptable.

Chapter 4
Other Optical Elements

All kinds of optical elements can be incorporated into the optomechanical constraint equations, following the same procedures as discussed in previous chapters. This chapter will present the flat-fold mirror, the powered mirror, the window, the diffraction grating, and the prism.

4.1 The Flat-Fold Mirror

The flat-fold mirror shown in Fig. 4.1 uses three coordinate systems: one for the object, one for the mirror, and one for the image. Since a flat-fold mirror changes the direction of the optical axis, these coordinate systems might not be either parallel or congruent. The magnification of the flat-fold mirror is 1.0.

With light coming from left to right, the object coordinate system has its origin at the point where the object crosses the incident optical axis (or its projection, as shown in the figure). Note that the object in this case is behind the mirror. Its positive Z axis is opposed to the direction of the incident light, and its Y-axis direction is upward. The X axis completes a right-handed coordinate system for the object of the mirror.

The mirror's coordinate system has its origin at the point where the optical axis intercepts the mirror surface; its positive Z axis is normal to the mirror surface on the incident side, and the Y-axis direction is upward (on the same side of the incident axis as the object's Y axis). The X axis completes a right-handed coordinate system for the mirror.

The image's coordinate system has its origin at the point where the image crosses the reflected optical axis. Its positive Z axis is against the imaging light (toward the mirror), and its Y axis is an image of the object's Y axis. The image's X axis completes a right-handed coordinate system. Note that the image's X axis has flipped to the opposite side of the mirror's Y-Z plane from the object's X axis.

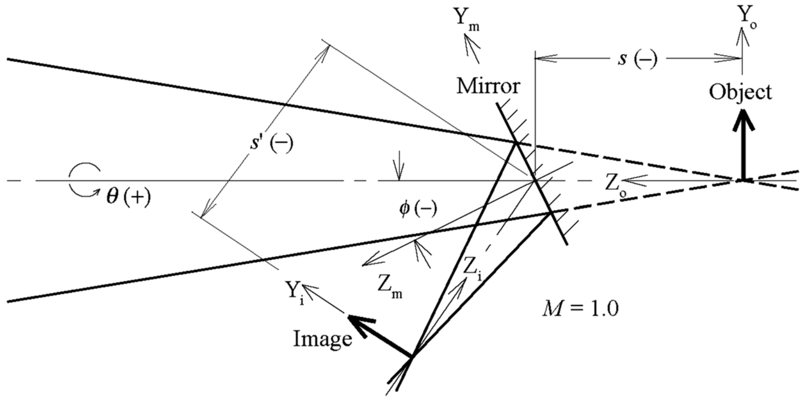

Figure 4.1 The flat-fold mirror.[4]

The angle of incidence, ϕ, is positive if the orientation of the object's Z axis is rotated (with respect to the mirror) in the direction of the mirror's Y axis into the mirror's Z axis (right-handed). The angle of reflection, ϕ', is equal to ϕ but opposite in orientation:

$$\phi' = -\phi.$$

The angle of rotation, θ, enables out-of-plane folding of the optical axis. This angle is positive if the object is rotated about its own Z axis in the direction of the object's X axis into the object's Y axis (right-handed).

The influence coefficients for the flat-fold mirror are simple geometric derivations from the geometry of the law of reflection. They can be summarized in two arrays: one for the object motions and one for the mirror motions (Table 4.1).

Note that the mirror has no influence on the image when the mirror is translated in its X-Y plane. Note also that a rotation of the mirror about its

Table 4.1 Influence coefficients for the flat-fold mirror.

Image Motions	**Object Motions**						**Mirror Motions**					
	Tx_o	Ty_o	Tz_o	Rx_o	Ry_o	Rz_o	Tx_m	Ty_m	Tz_m	Rx_m	Ry_m	Rz_m
Tx_i	$-\cos\theta$	$\sin\theta$									$2s'\cos\phi$	
Ty_i	$\sin\theta$	$\cos\theta$							$-2\sin\phi$	$2s'$		
Tz_i			1.0						$-2\cos\phi$			
Rx_i				$\cos\theta$	$-\sin\theta$					-2.0		
Ry_i				$-\sin\theta$	$-\cos\theta$						$2\cos\phi$	
Rz_i						-1.0					$-2\sin\phi$	
$\Delta M/M$												

Y axis contributes image rotations about both of the image's Y and Z axes. There are no deviation fractions for the flat-fold mirror.

4.2 The Powered Mirror

The powered mirror shown in Fig. 4.2 uses three coordinate systems: one for the object, one for the mirror, and one for the image. With light coming from left to right, the object coordinate system has its origin at the point where the object crosses the optical axis. Its positive Z axis is opposed to the direction of the object's emitted light, and its Y-axis direction is upward. The X axis completes a right-handed coordinate system for the object of the mirror.

The mirror's coordinate system has its origin at the point where the optical axis intercepts the mirror surface; its positive Z axis is normal to the mirror surface on the incident side, and the Y-axis direction is upward (on the same side of the incident axis as the object's Y axis). The X axis completes a right-handed coordinate system for the mirror.

The image's coordinate system has its origin at the point where the image crosses the reflected optical axis. Its positive Z axis is against the imaging light (toward the mirror), and its Y-axis direction is upward. The image's X axis completes a right-handed coordinate system. Note that the image's X axis has flipped to the opposite side of the Y-Z plane from the object's X axis in order to make the right-handed coordinate system.

The influence coefficients for the powered mirror (Table 4.2) are derived from the coefficients for the lens, noting three differences. The first is the change in orientations of the coordinate axis for the image. The second is that the image distance times two, $2s'$, replaces the lens' principal thickness, p, in the off-diagonal terms, giving Y and X translations of the image for X and Y

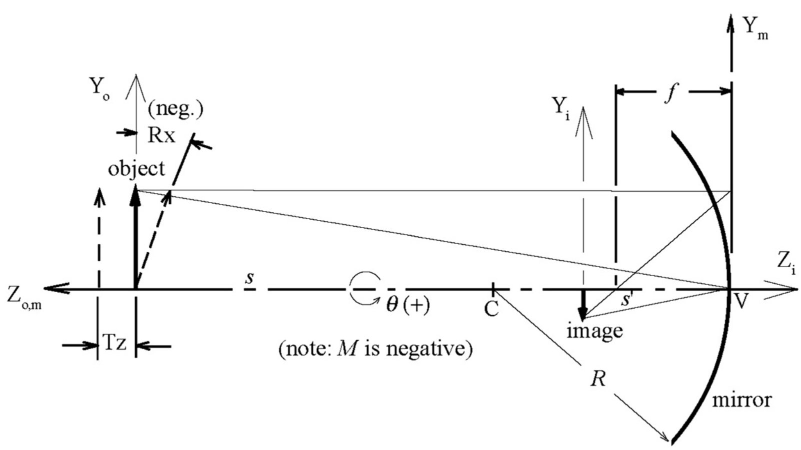

Figure 4.2 The powered mirror.[4]

Table 4.2 The influence coefficients for the powered mirror.

Image Motions	Tx_o	Ty_o	Tz_o	Rx_o	Ry_o	Rz_o	Tx_m	Ty_m	Tz_m	Rx_m	Ry_m	Rz_m	Δf
	Object Motions						**Mirror Motions**						
Tx_i	$-M\cos\theta$	$M\sin\theta$					$-(1-M)$				$2s'$		
Ty_i	$M\sin\theta$	$M\cos\theta$						$1-M$		$2s'$			
Tz_i			M^2						$-(1+M)^2$				$-(1-M)^2$
Rx_i				$M\cos\theta$	$-M\sin\theta$					$-(1+M)$			
Ry_i				$-M\sin\theta$	$-M\cos\theta$						$1+M$		
Rz_i						-1.0							
$\Delta M/M$			M/f						$-M/f$				$(1-M)/f$

Mirror Design Variable	ΔR
Δf	0.5

Table 4.3 Deviation fractions for the powered mirror.

Image Motions	Object Motions						Lens Motions						
	Tx_o	Ty_o	Tz_o	Rx_o	Ry_o	Rz_o	Tx_l	Ty_l	Tz_l	Rx_l	Ry_l	Rz_l	Δf_l
Tx_i													
Ty_i													
Tz_i			$-MTz_o/f$						$\dfrac{M^3 Tz_l}{f + MTz_l - fM^2}$				$M\Delta f/f$
Rx_i													
Ry_i													
Rz_i													
$\Delta M/M$			MTz_o/f						$-MTz_l/f$				$M\Delta f/f$

rotations of the mirror. The third is that the focal length is sensitive to only one variable, the radius, R, of the mirror.

The only Gaussian variable for the powered mirror is the focal length, which is a unique function of the radius of curvature: $f = 0.5R$. Consequently, only one influence coefficient affects the focal length. The object's rotation angle, θ, is positive if the object is rotated about its own Z axis in the direction of the object's X axis into its Y axis (right-handed).

The deviation fractions (Table 4.3) for the powered mirror are the same as those for the refractive lens. This array allows the engineer to estimate the magnitude of nonlinearities in the position, orientation, and size of the optical image and make any accommodations that seem appropriate.

4.3 The Optical Window

The optical window shown in Fig. 4.3 uses three coordinate systems: one for its object, one for the window, and one for its image. With light coming from left to right, the object coordinate system has its origin at the point where the

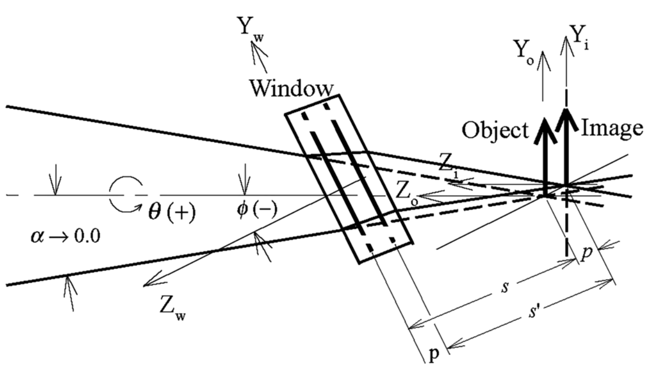

Figure 4.3 The optical window.[4]

object crosses the optical axis; its positive Z axis is against the light from the object, and its Y-axis direction is upward. Its X axis completes a right-handed coordinate system.

The window coordinate system has its origin at its first principal point. Its positive Z axis is normal to the first surface at the vertex, on the incident side of the window, and its Y-axis direction is upward. Its X axis completes a right-handed coordinate system. The magnification of an optical window is 1.0.

In theory, the locations of a window's principal points are indefinite. In the optomechanical constraint equations, they are assumed to be centered in the window's thickness. The principal thickness of a window is

$$p = t\left\{1 - \frac{\tan\sin^{-1}[(\sin\phi)/n]}{\tan\phi}\right\}$$

as a function of the angle of incidence, ϕ. As ϕ approaches 0.0,

$$p \to t\left(1 - \frac{1}{n}\right)$$

The image coordinate system has its origin at the point where the image crosses the transmitted optical axis; its positive Z axis is against the imaging light, and its Y-axis direction is upward. Its X axis completes a right-handed coordinate system.

The angle of incidence is positive if the orientation of the object's Z axis is rotated (with respect to the window) in the direction of the window's Y axis into the window's Z axis. The angle of rotation, θ, is positive if the object is rotated about its own Z axis in the direction of the object's X axis into its Y axis. The influence coefficients for the optical window are shown in Table 4.4. The only

Table 4.4 Influence coefficients for the optical window.

Image Motions	**Object Motions**						**Window Motions**						
	Tx_o	Ty_o	Tz_o	Rx_o	Ry_o	Rz_o	Tx_w	Ty_w	Tz_w	Rx_w	Ry_w	Rz_w	Δp
Tx_i	$\cos\theta$	$-\sin\theta$									$-p$		
Ty_i	$\sin\theta$	$\cos\theta$								$p\cos\phi$			$-\sin\phi$
Tz_i			1.0							$p\sin\phi$			$-\cos\phi$
Rx_i				$\cos\theta$	$-\sin\theta$								
Ry_i				$\sin\theta$	$\cos\theta$								
Rz_i						1.0							
$\Delta M/M$													

	Window Design Variables		
	Δt	$\Delta\phi$	Δn
Δp	$1 - \dfrac{\{\tan\sin^{-1}[(\sin\phi)/n]\}}{\tan\phi}$	$\dfrac{t[1-(n^2\cos^2\phi)/(n^2-\sin^2\phi)]}{(n^2-sin^2\phi)^{1/2}\sin\phi}$	$\dfrac{tn\cos\phi}{(n^2-\sin^2\phi)^{3/2}}$

Gaussian property of the optical window is its principal thickness, which is sensitive to the thickness, the angle of incidence, and the index of refraction.

4.4 The Diffraction Grating

If the flat-fold mirror of Section 4.1 is modified by ruling on the surface a series of narrow parallel grooves a distance d apart from one another, the incident light will be interrupted by the ruling, and the reflected light will display a series of spectra caused by the diffraction effects of the ruled grooves. The angle of diffraction, ϕ', of the spectra is controlled by the grating equation,

$$\sin\phi' = -\sin\phi + m\lambda/d,$$

where m is the order of the desired spectrum, λ is the wavelength of interest in that order, ϕ is the angle of incidence, and ϕ' is the angle of diffraction (Fig. 4.4). The wavelength and the ruling spacing are always positive. The order can be either a positive or a negative integer. The expression $m\lambda/d$ is called the *grating constant*, g:

$$g = m\lambda/d.$$

If the grating constant is 0.0, the order falls on the angle of reflection for the underlying flat mirror. If the grating constant is finite, the angle of diffraction for the desired wavelength in the desired order can be either greater than or less than the angle of reflection for the flat mirror, depending on the sense (+ or −) of the order of the desired spectrum.

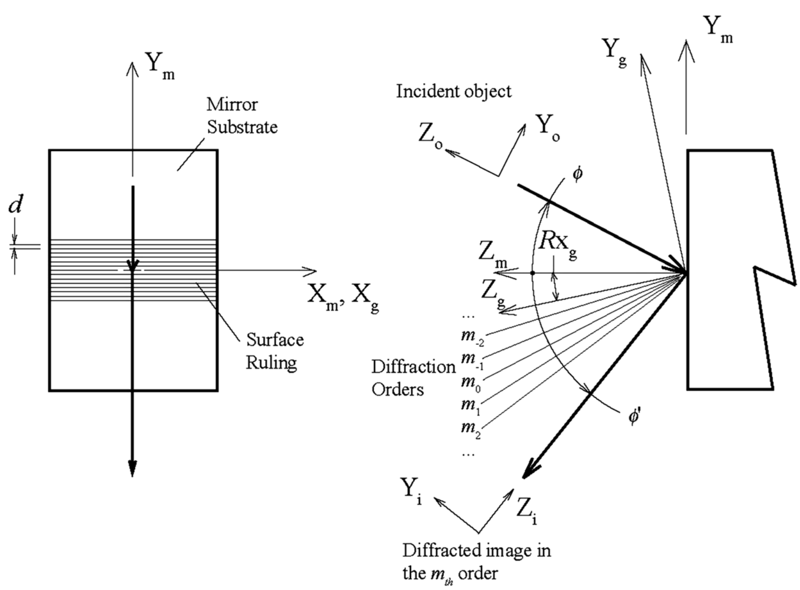

Figure 4.4 The diffraction grating.

The optomechanical behavior of the diffraction grating is similar to the behavior of the flat mirror on which it is ruled. We define a new coordinate system whose X axis is the same as the basic flat mirror but whose Z axis bisects the angle between the angle of incidence, ϕ, and the angle of diffraction, ϕ':

$$Rx_g = (\phi' + \phi)/2.$$

If the displacements and rotations of the diffraction grating are defined in this new coordinate system, the influence functions for the flat-fold mirror (Section 4.1) can be used to determine the effects on the image in the diffracted order and the desired wavelength that define g. Normally, for the flat mirror, the coordinate system would have its X-Y plane in the surface of the mirror. For the diffraction grating, however, its X-Y plane is rotated about its X axis by an angle Rx_g so that the grating's Z axis bisects the angle between the angle of incidence and the angle of diffraction. A two-dimensional coordinate transformation is required between the Y-Z planes of the mirror substrate and the diffraction grating.

4.5 The Prism

The prism shown in Fig. 4.5 uses three coordinate systems: one for its object, one for the reflective surface, and one for its image. Its geometry is defined by three surfaces: the incident surface, the reflective surface, and the exiting surface. All of these surfaces are flat. The incident and exiting surfaces are assumed to be normal to the local optical axis.

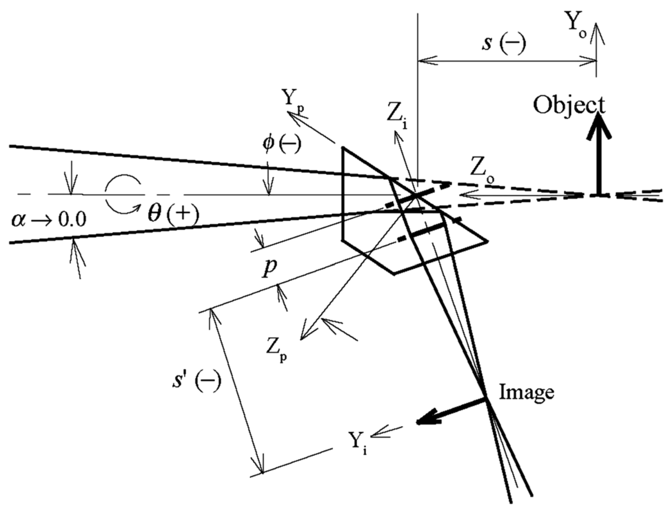

Figure 4.5 The prism.[4]

With light coming from left to right, the object coordinate system has its origin at the point where the object crosses the incident optical axis; its positive Z axis is against the light from the object, and its Y-axis direction is upward.

The prism's coordinate system has its origin where the incident optical axis intercepts the reflective surface, and its positive Z axis is normal to the reflective surface on the incident side. The Y-axis direction is upward (on the same side of the incident axis as the object's Y axis). The X axis completes a right-handed coordinate system for the prism.

The image's coordinate system has its origin at the point where the image crosses the reflected optical axis. Its positive Z axis is against the imaging light (toward the reflective surface), and its Y axis is an image of the object's Y axis. The image's X axis completes a right-handed coordinate system. Note that the image's X axis has flipped to the opposite side of the Y-Z plane from the object's X axis.

The physical optical prescription for the prism includes: (1) the distance from the first surface to the incident point on the reflective surface, (2) the angle of incidence at the reflective surface, (3) the distance from the reflective surface to the exiting surface, and (4) the index of refraction for the glass. The angle of incidence at the reflective surface is positive if the orientation of the object's Z axis is rotated (with respect to the reflective surface) in the direction of the surface's Y axis into the surface's Z axis (right-handed).

The angle of rotation, θ, enables out-of-plane folding of the optical axis. This angle is positive if the object is rotated about its own Z axis in the direction of the object's X axis into the object's Y axis (right-handed).

Unlike the flat-fold mirror, the prism has a finite principal thickness, p. Since the optical axis is assumed to be normal to the incident and exiting surfaces,

$$p = t(1 - 1/n),$$

where t is the total thickness of the glass from the incident surface to the exiting surface along the optical axis. Since all of the surfaces are flat, the position of the principal thickness is indeterminate. For convenience, P_1 is located at the reflective surface, and H_1 equals the distance from the first surface to the reflective surface. H_2 is the distance from the exiting surface to P_2. Note that H_2 can be either positive or negative, depending on the relative size of the principal thickness.

Variations in either the thickness t or the index of refraction n will have some effect on the principal thickness and therefore the Z position of the image. The influence coefficients of the prism design variables are derived by taking the first partial derivatives of p with respect to t and n (the design variables) in the above equation.

Table 4.5 Influence coefficients for the prism.

Image Motions	Tx_o	Ty_o	Tz_o	Rx_o	Ry_o	Rz_o	Tx_p	Ty_p	Tz_p	Rx_p	Ry_p	Rz_p	Δp_p
Tx_i	$-\cos\theta$	$\sin\theta$									$(2s'-p)\cos\phi$	$p\sin\phi$	
Ty_i	$\sin\theta$	$\cos\theta$							$-2\sin\phi$	$2s$			
Tz_i			1.0						$-2\cos\phi$				-1.0
Rx_i				$\cos\theta$	$-\sin\theta$					-2.0			
Ry_i				$-\sin\theta$	$-\cos\theta$						$2\cos\phi$		
Rz_i						-1.0					$-2\sin\phi$		
$\Delta M/M$													
	Object Motions						**Prism Motions**						

	Δt	Δn
Δp	$1-1/n$	t/n^2
	Prism Design Variables	

The influence coefficients for the prism (Table 4.5) are similar to those for the flat-fold mirror, with two extra terms that accommodate the effects of the principal thickness when the prism is rotated about its Y or Z axis.

Chapter 5
Computational Methods

In this section the optomechanical constraint equations will be developed for a two-lens simple telescope system using three different methods, presenting the strengths and weakness of each method. The telescope (Fig. 5.1) is defined by the physical optical prescription in Table 5.1. The dimensional units of the prescription are inches.

5.1 Longhand Method

The first method for developing the equations is the simple longhand, pencil-on-paper, method. Here, the author's hand-written notes were transcribed into a word processor file to make them more legible to the reader. All calculations were performed on a ten-key scientific calculator.

First, the prescription is converted from the optical designer's sign conventions (Table 5.1) to the optomechanical engineer's sign conventions presented in Section 1.11 (Table 5.2).

Then, the Gaussian prescription data are derived from the optomechanical prescription data (Table 5.2) using the methods shown in Section 3.2.5.1. The Gaussian prescription properties are shown in Table 5.3. Now, the

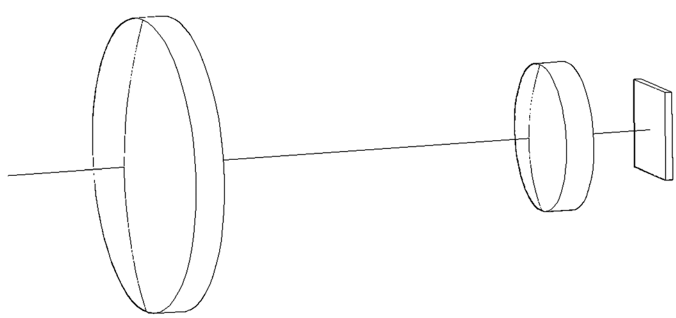

Figure 5.1. A two-lens simple telescope.

Table 5.1 Physical optical prescription for the two-lens telescope.

Surface	Element	Radius	Index	Thickness (mm)
1	Obj.	Inf.	1.000	Inf.
2	1	3.5	4.00024	0.25
3	1	5.0	1.0	2.67
4	2	1.5	4.00024	0.2
5	2	1.0	1.0	0.674
6	Det.	Inf.	1.0	0.0

Table 5.2 The physical optical prescription in optomechanical sign conventions.

Surface	Element	Radius	Index	Thickness (mm)
1	Obj.	Inf.	1.000	Inf.
2	1	–3.5	4.00024	0.25
3	1	–5.0	1.0	2.67
4	2	–1.5	4.00024	0.2
5	2	–1.0	1.0	0.674
6	Det.	Inf.	1.0	0.0

Table 5.3 The Gaussian properties of the telescope's elements.

Element	f	H_1	H_2	p	*pair*	Type
Obj.	Inf.	0.0	0.0	0.0	Inf.	Obj.
1	3.456	0.129	0.185	0.194	3.085	Lens
2	–1.459	–0.229	–0.153	0.133	0.510	Lens
Det.	Inf.	0.0	0.0	0.0	0.0	Det.

effective focal length of the system can be calculated using the method in Section 3.2.4:

$$f_{1\text{-}2} = 4.74,$$

which compares well with the focal length from the lens design: 4.7412. Next, from Section 3.2.5.2, the object positions and image positions, and magnifications for each of the optical elements are calculated (Table 5.4).

Note that the nominal deviation fractions have been entered in the final column of Table 5.4. For Lens 1 the nominal deviation fraction is 0.0 since the magnification is 0.0 (the object being at infinity). For Lens 2 the nominal deviation fraction is finite and negative. Now the engineer has the data to define the element arrays for the influence functions following Section 3.2.5.3 [Tables 5.5(a), (b), and (c)].

From these three element arrays the engineer can assemble the optomechanical constraint equations following the method of Section 3.2.5.4 (Table 5.6).

Table 5.4 The telescope's object positions, image positions, and magnifications.

Element	f	s	s'	M	Type	e/Tz_o
Obj.	Inf.	0.0	0.0	1.0	Obj.	0.0
1	3.456	Inf.	–3.456	0.0	Lens	0.0
2	–1.459	–0.371	–0.498	1.34	Lens	–0.918
Det.	Inf.	1.2×10^{-2}	1.2×10^{-2}	+1.0	Det.	0.0

Table 5.5(a) Element array for the first lens.

Image Motions	Object Motions: Tx	Ty	Tz	Rx	Ry	Rz	Element 1 Motions: Tx	Ty	Tz	Rx	Ry	Rz	Δf
Tx_i							1.0				–0.19		
Ty_i								1.0		0.19			
Tz_i									1.0				–1.0
Rx_i										1.0			
Ry_i											1.0		
Rz_i						1.0							
$\Delta M/M$													0.29

	Lens Design Variables: Δt	ΔR_1	ΔR_2	Δn
Δf_1	–1.54	–3.04	1.36	–1.18

Table 5.5(b) Element array for the second lens.

Image Motions	Object Motions: Tx	Ty	Tz	Rx	Ry	Rz	Element 2 Motions: Tx	Ty	Tz	Rx	Ry	Rz	Δf
Tx_i	1.37						–0.37				–0.13		
Ty_i		1.37						–0.37		0.13			
Tz_i			1.88						–0.88				–1.4
Rx_i				1.37						–0.37			
Ry_i					1.37						–0.37		
Rz_i						1.0							
$\Delta M/M$			–0.96						0.96				0.26

	Lens Design Variables: Δt	ΔR_1	ΔR_2	Δn
Δf_2	–3.06	–3.13	5.51	0.42

The longhand method is particularly useful with smaller optical systems and provides the engineer with early estimates of the sensitivity of the system's image to the stability of the optical elements. In this case, it can be seen that the first lens has the strongest influence, the detector is next strongest, and the

Table 5.5(c) Element array for the detector.

Image Motions	Object Motions						Detector Motions					
	Tx	*Ty*	*Tz*	*Rx*	*Ry*	*Rz*	*Tx*	*Ty*	*Tz*	*Rx*	*Ry*	*Rz*
Tx_i	1.0						–1.0					
Ty_i		1.0						–1.0				
Tz_i			1.0						–1.0			
Rx_i				1.0						–1.0		
Ry_i					1.0						–1.0	
Rz_i						1.0						–1.0
$\Delta M/M$												

second lens is the weakest. The object of the system, being at infinity, has no influence on the image except in rotation about the *Z* axis, and only the second lens contains nonlinear terms in the influence functions. These insights are often useful in evaluating early design concepts for construction of the telescope.

5.2 Spreadsheet Method

A computer-based spreadsheet program such as Microsoft Excel® offers a more flexible system for assembling the optomechanical constraint equations at the expense of a little more effort during setup of the spreadsheet. This starts with transcribing the physical optical prescription data into the spreadsheet (Fig. 5.2). These data are the same as those used in the manual calculations above.

The prescription data are then converted to the optomechanical sign conventions (Fig. 5.3). The highlighted cell shows the change in sign of the first radius of the second lens.

From the optomechanical prescription data, the Gaussian properties of the lenses plus the object distances, image distances, and magnifications can be calculated (Fig. 5.4). The highlighted cell shows the calculation of the location of the second principal point H_2 of the first lens. The Gaussian properties of the 1-2 doublet are shown just below the Gaussian prescription of the individual lenses. The *Ba* and *Bb* properties of the doublet are also shown.

The objects, images, and magnifications are then calculated. The calculations use the data from the Gaussian prescription. The location of each object and each image is calculated from the Gaussian prescription data. The magnification of each lens is the ratio of its image distance, s', to its object distance, s.

The individual element arrays are then prepared (Fig. 5.5). The highlighted cell shows the calculation of the Ty_i/Ty_2 influence coefficient for Element 2. Note that the properties (magnification, principal thickness, and focal length) used for the influence coefficients for each element have been transcribed to the heading area of each individual element array, facilitating the setup of the arrays.

Table 5.6 The telescope's optomechanical constraint equations.

	Object						Lens 1							Lens2							Detector					
	Tx	Ty	Tz	Rx	Ry	Rz	Tx	Ty	Tz	Rx	Ry	Rz	Δf	Tx	Ty	Tz	Rx	Ry	Rz	Δf	Tx	Ty	Tz	Rx	Ry	Rz
Tx_i							1.37				–0.27			–0.37				–0.13			–1.0					
Ty_i								1.37		0.27					–0.37		0.13					–1.0				
Tz_i									1.88				–1.88			–0.88			–0.014				–1.0			
Rx_i										1.37							–0.37							–1.0		
Ry_i											1.37							–0.37							–1.0	
Rz_i						1.0																				–1.0
$\Delta M/M_i$									–0.96				1.25			0.96				0.26						

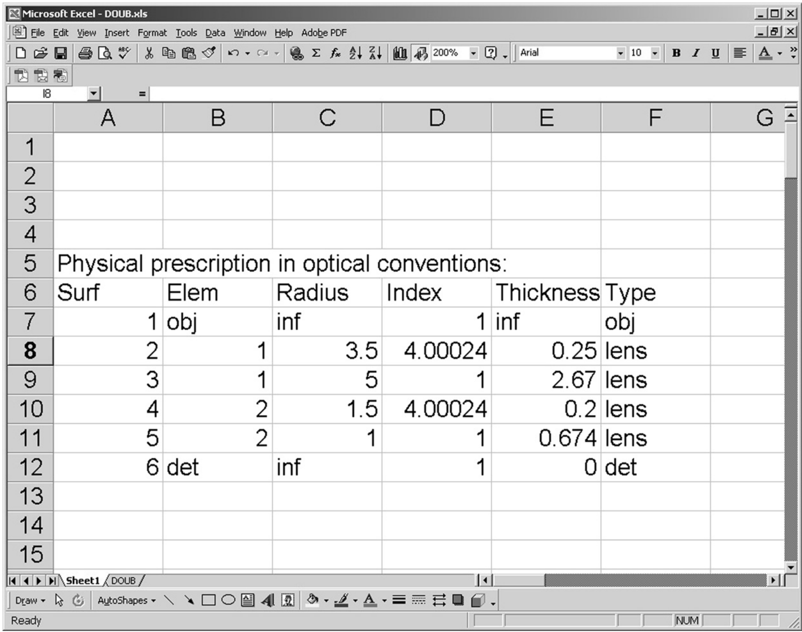

	A	B	C	D	E	F
5	Physical prescription in optical conventions:					
6	Surf	Elem	Radius	Index	Thickness	Type
7	1	obj	inf	1	inf	obj
8	2	1	3.5	4.00024	0.25	lens
9	3	1	5	1	2.67	lens
10	4	2	1.5	4.00024	0.2	lens
11	5	2	1	1	0.674	lens
12	6	det	inf	1	0	det

Figure 5.2 The optical prescription for a two-lens simple telescope.

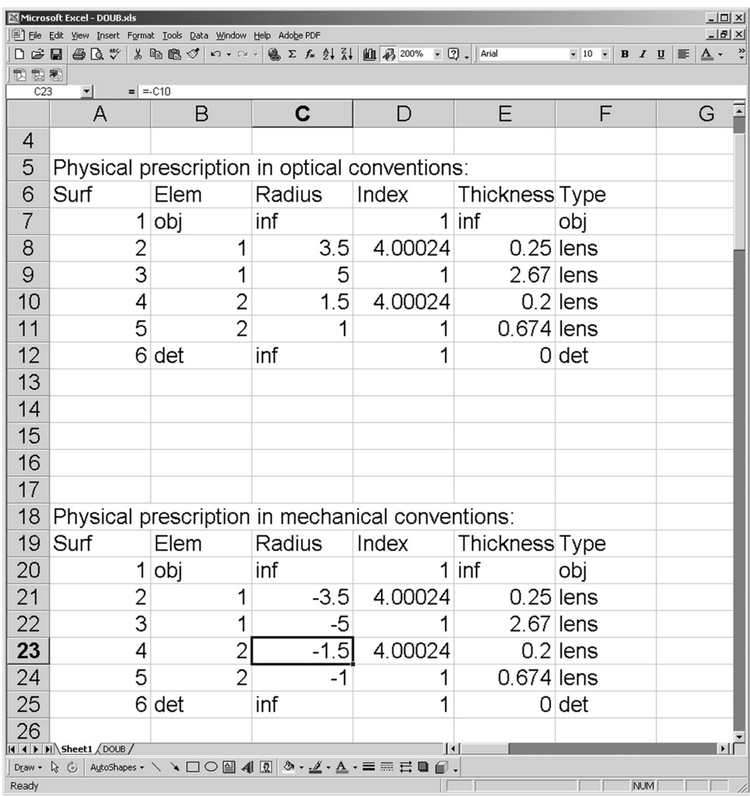

	A	B	C	D	E	F
5	Physical prescription in optical conventions:					
6	Surf	Elem	Radius	Index	Thickness	Type
7	1	obj	inf	1	inf	obj
8	2	1	3.5	4.00024	0.25	lens
9	3	1	5	1	2.67	lens
10	4	2	1.5	4.00024	0.2	lens
11	5	2	1	1	0.674	lens
12	6	det	inf	1	0	det
18	Physical prescription in mechanical conventions:					
19	Surf	Elem	Radius	Index	Thickness	Type
20	1	obj	inf	1	inf	obj
21	2	1	-3.5	4.00024	0.25	lens
22	3	1	-5	1	2.67	lens
23	4	2	-1.5	4.00024	0.2	lens
24	5	2	-1	1	0.674	lens
25	6	det	inf	1	0	det

Figure 5.3 The optical prescription converted to mechanical conventions.

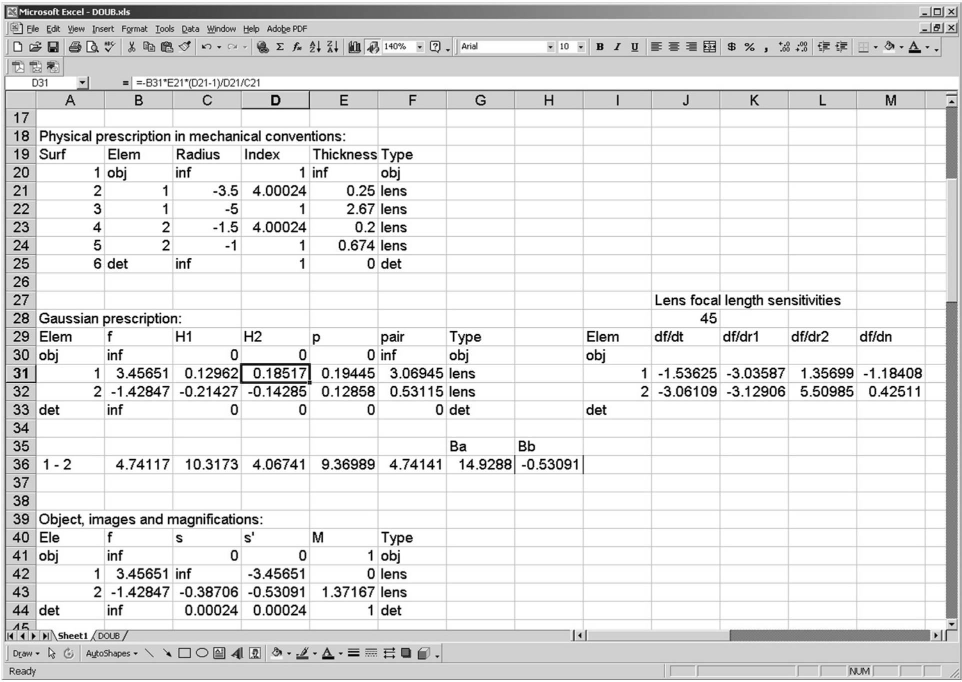
Microsoft Excel - DOUB.xls

D31 = =-B31*E21*(D21-1)/D21/C21

	A	B	C	D	E	F	G	H	I	J	K	L	M
17													
18	Physical prescription in mechanical conventions:												
19	Surf	Elem	Radius	Index	Thickness	Type							
20	1	obj	inf	1	inf	obj							
21	2	1	-3.5	4.00024	0.25	lens							
22	3	1	-5	1	2.67	lens							
23	4	2	-1.5	4.00024	0.2	lens							
24	5	2	-1	1	0.674	lens							
25	6	det	inf	1	0	det							
26													
27										Lens focal length sensitivities			
28	Gaussian prescription:									45			
29	Elem	f	H1	H2	p	pair	Type		Elem	df/dt	df/dr1	df/dr2	df/dn
30	obj	inf	0	0	0	inf	obj		obj				
31	1	3.45651	0.12962	0.18517	0.19445	3.06945	lens		1	-1.53625	-3.03587	1.35699	-1.18408
32	2	-1.42847	-0.21427	-0.14285	0.12858	0.53115	lens		2	-3.06109	-3.12906	5.50985	0.42511
33	det	inf	0	0	0	0	det		det				
34													
35							Ba	Bb					
36	1 - 2	4.74117	10.3173	4.06741	9.36989	4.74141	14.9288	-0.53091					
37													
38													
39	Object, images and magnifications:												
40	Ele	f	s	s'	M	Type							
41	obj	inf	0	0	1	obj							
42	1	3.45651	inf	-3.45651	0	lens							
43	2	-1.42847	-0.38706	-0.53091	1.37167	lens							
44	det	inf	0.00024	0.00024	1	det							

Figure 5.4 The Gaussian properties of the two-lens simple telescope.

Finally, the optomechanical constraint equations are assembled from the individual element arrays (Fig. 5.6). The highlighted cell in Fig. 5.6(a) shows the calculation of the $\Delta M/MTz_1$ influence coefficient (for Element 1) from the individual element arrays above it in the spreadsheet. The coefficients for the object and Element 1 are shown in Fig. 5.6(a), and the coefficients for Element 2 and the detector are shown in Fig. 5.6(b).

The spreadsheet provides an excellent tool for studying the effects of perturbations in the mechanical design. The engineer can perturb the radius of a lens element and immediately see the results in the image position, orientation, and size, and compare that result to the influence coefficients in the constraint equations. The engineer can also copy translations and displacements into the code from a structural analysis, and calculate the resulting registration errors at the detector.

The spreadsheet also offers higher precision (more decimal places) than might be convenient in the manual, ten-key calculator mode. It also permits the engineer to copy the equations onto multiple pages of the spreadsheet in support of calculating the results of different disturbances such as tolerances, load cases, or thermal effects.

5.3 Automated Method

The engineer might choose to prepare custom software that will relieve much of the iterative computational burden of preparing the optomechanical constraint equations, especially in larger optical systems. The author uses one such software

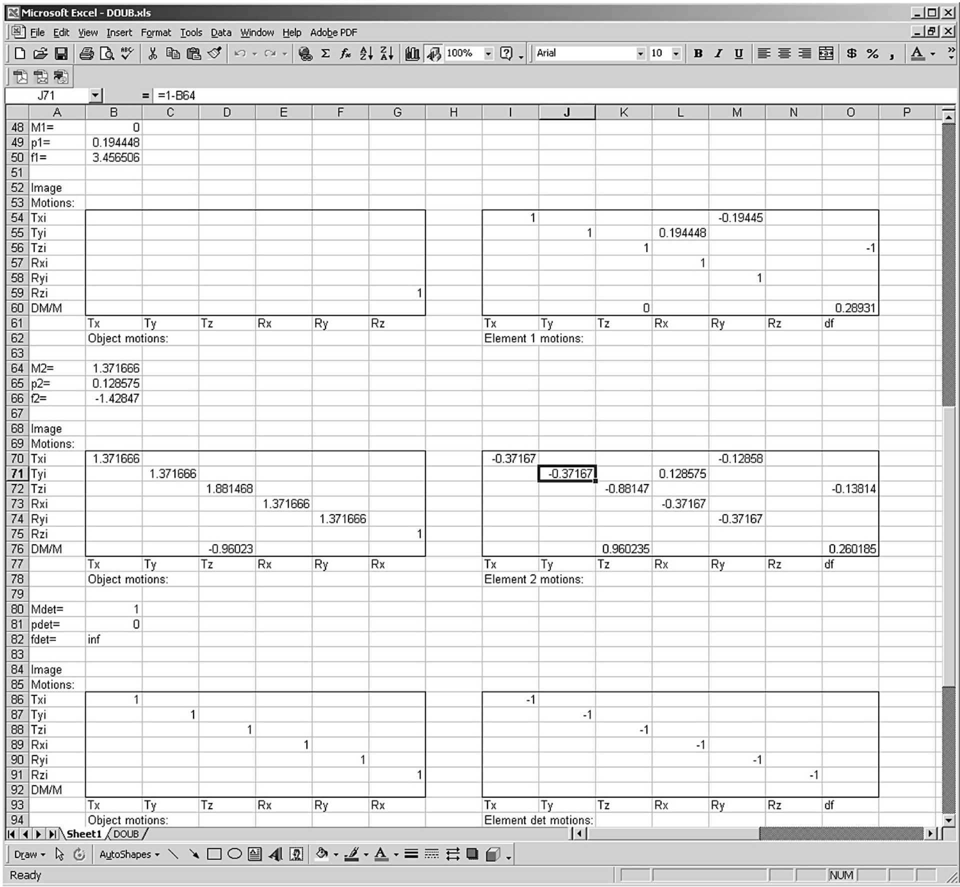

	A	B	C	D	E	F	G	H	I	J	K	L	M	N	O	P
48	M1=	0														
49	p1=	0.194448														
50	f1=	3.456506														
51																
52	Image															
53	Motions:															
54	Txi								1				-0.19445			
55	Tyi									1		0.194448				
56	Tzi										1				-1	
57	Rxi											1				
58	Ryi												1			
59	Rzi						1									
60	DM/M										0				0.28931	
61		Tx	Ty	Tz	Rx	Ry	Rz		Tx	Ty	Tz	Rx	Ry	Rz	df	
62		Object motions:							Element 1 motions:							
63																
64	M2=	1.371666														
65	p2=	0.128575														
66	f2=	-1.42847														
67																
68	Image															
69	Motions:															
70	Txi	1.371666							-0.37167				-0.12858			
71	Tyi		1.371666							-0.37167		0.128575				
72	Tzi			1.881468							-0.88147				-0.13814	
73	Rxi				1.371666							-0.37167				
74	Ryi					1.371666							-0.37167			
75	Rzi						1									
76	DM/M			-0.96023							0.960235				0.260185	
77		Tx	Ty	Tz	Rx	Ry	Rx		Tx	Ty	Tz	Rx	Ry	Rz	df	
78		Object motions:							Element 2 motions:							
79																
80	Mdet=	1														
81	pdet=	0														
82	fdet=	inf														
83																
84	Image															
85	Motions:															
86	Txi	1							-1							
87	Tyi		1							-1						
88	Tzi			1							-1					
89	Rxi				1							-1				
90	Ryi					1							-1			
91	Rzi						1							-1		
92	DM/M															
93		Tx	Ty	Tz	Rx	Ry	Rx		Tx	Ty	Tz	Rx	Ry	Rz	df	
94		Object motions:							Element det motions:							

Figure 5.5 The element arrays for the two-lens simple telescope.

code.[5] The code reads two text files, the first containing the optical geometry, and the second containing the index of refraction data. For the two-lens telescope system, the first file prepared by the engineer is the geometry file (Table 5.7).

The information in the right four columns (headed f1, f2, f3, and f4) for Surface 1 contains directions for the code: "f1" is a scale factor that converts the dimensions of the prescription (as from millimeters to inches). In this case, no conversion is necessary, and the scale factor is 1.0; the entry of 1.0 in "f2" tells the code that the information is in optical conventions so the code will need to convert the prescription to optomechanical conventions before proceeding.

The second text file is for the indices of refraction (Table 5.8).

These two files are read by the software code and produce an output file with all of the information developed in either the longhand or spreadsheet method (Table 5.9).

The output file opens with an echo of the original input files, in this case, using the optical sign conventions. This is followed by an echo of the prescription in optomechanical conventions, the Gaussian prescription for

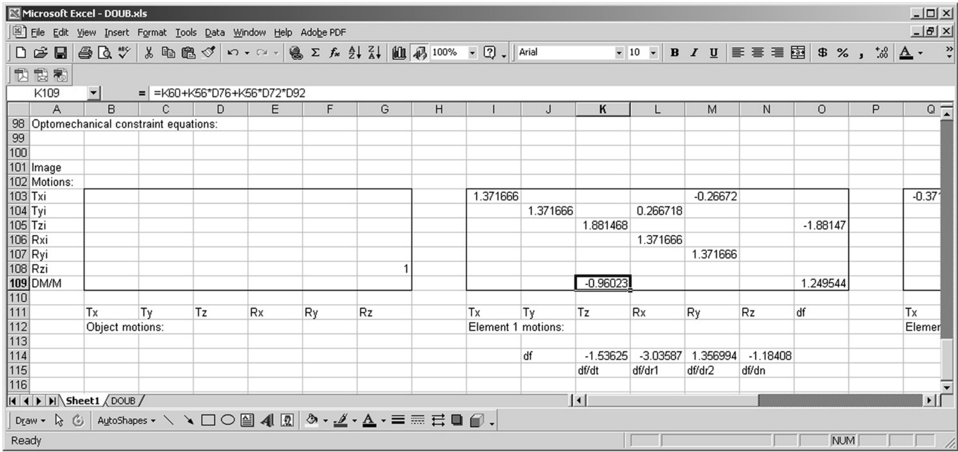

(a)

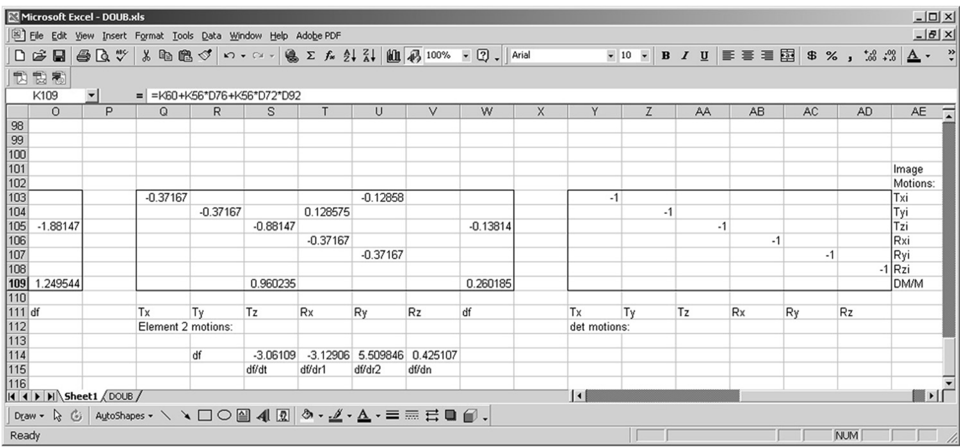

(b)

Figure 5.6 The optomechanical constraint equations for the two-lens simple telescope for (a) the object and Element 1 and for (b) Element 2 and the detector.

Table 5.7 The optical geometry file for the telescope.

Surf	Elem	Radius	Index	Thickness	Type	f1	f2	f3	f4
1	obj	inf	AIR	inf	obj	1.0000000	1.0000000	0.0000000	0.0000000
2	1	3.5	ge	.25	LENS	0.0000000	0.0000000	0.0000000	0.0000000
3	1	5	AIR	2.67	LENS	0.0000000	0.0000000	0.0000000	0.0000000
4	2	1.5	ge	.2	LENS	0.0000000	0.0000000	0.0000000	0.0000000
5	2	1	AIR	.674	LENS	0.0000000	0.0000000	0.0000000	0.0000000
6	det	inf	AIR	0.0	det.				

each of the elements in the system with the system's Gaussian properties at the bottom of the section, followed by the object positions, image positions, the magnifications, and the normalized deviation fractions for each element. There are no angles ϕ, ϕ', or θ in this design.

Table 5.8 The index of refraction file for the telescope.

MATERIAL	INDEX
AIR	1.0
ge	4.00024.

The code presents the optomechanical constraint equations in the vertical format with the seven registration variables across the top and the elements' independent mechanical degrees of freedom listed down the left-hand margin. The last two columns on the right are reserved for the sensitivities of the lens' focal lengths to the lens design variables of thickness, first radius, second radius, and index of refraction.

The code also prepares the individual element arrays [Tables 5.10(a), (b), and (c)].

The code then offers an option of preparing the optomechanical constraint equations in a format usable in Nastran finite element models. The Nastran model for this two-element telescope is shown in Table 5.11.

The text file can be imported into a Nastran structural model and attached to the optical elements. This utility is useful in demonstrating the optostructural stability of the mechanical design.

5.4 Rotating an Element's Object about Its Optical Axis

The formulation of the elements' influence functions (for lenses in Chapters 2 and for other elements in Chapter 4) defines an angle of rotation θ of an element's object about the element's incident optical axis. This feature allows the modeling of folded optical systems, including those in which the folds are out-of-plane with the rest of the elements. As an example, the object of a flat fold mirror, or possibly a prism, is rotated about the object's local Z axis by the amount of θ. This is equivalent to rotating the element (a mirror or prism) by the amount of $-\theta$ about the element's incident optical axis.

The angle of rotation and the angle of incidence, when combined at one element, will bend and rotate the optical axis into any orientation the engineer needs to duplicate the path of the optical axis in the optical designer's physical prescription. The quantities θ and ϕ are rotations about the local Z and X axes, respectively, and *defined in the optomechanical coordinate systems*. They are somewhat different from similar angles of rotation, α and β, used by optical designers to orient the optical surfaces in the system. The angles α and β are rotations about the local X and Y, axes, respectively, and *defined in the optical design coordinate systems*. These coordinate systems and their differences are explained in Chapter 1.

The θ-rotation feature also allows the engineer to align a system's detector with the far-field object so that the detector's coordinate system is parallel to

Table 5.9 The output file developing the telescope's optomechanical constraint equations.

PROJECT NAME: 'DOUB' TIME AND DATE: 12:39:20 03-29-2015

PHYSICAL PRESCRIPTION INPUT ECHO IN OPTICAL CONVENTIONS

Surf	Elem	Radius	Index	Thickness	Type	f1	f2	f3	f4
1	obj	inf	1.0	inf	obj	1	1	0	0
2	1	3.5	4.00024	.25	LENS	0	0	0	0
3	1	5	1.0	2.67	LENS	0	0	0	0
4	2	1.5	4.00024	.2	LENS	0	0	0	0
5	2	1	1.0	.674	LENS	0	0	0	0
6	det	inf	1.0	0	det				

INDEXES OF REFRACTION ARE RELATIVE TO THE VALUE OF 1.000292.

PHYSICAL PRESCRIPTION INPUT ECHO IN MECHANICAL CONVENTIONS

Surf	Elem	Radius	Index	Thickness	Type	f1	f2	f3	f4
1	obj	inf	1.0	inf	obj	1	0	0	0
2	1	−3.5	4.00024	.25	LENS	0	0	0	0
3	1	−5	1.0	2.67	LENS	0	0	0	0
4	2	−1.5	4.00024	.2	LENS	0	0	0	0
5	2	−1	1.0	.674	LENS	0	0	0	0
6	det	inf	1.0	0	det				

INDEXES OF REFRACTION ARE RELATIVE TO THE VALUE OF 1.000292.

GAUSSIAN PRESCRIPTION

ELE	F	H1	H2	P	P/AIR	PHI	THETA	TYPE	PHI'
obj	inf	0	0	0	inf	0	0	obj	
1	3.4565059	.12962156	.18517366	.1944479	3.0694484	0	0	LENS	
2	−1.4284694	−.21427469	−.1428498	.1285751	.5311502	0	0	LENS	
det	inf	0	0	0	0	0	0	det	
SYSTEM	4.741172	10.317298	4.0674085	9.3698891	4.7414085				

OBJECTS, IMAGES AND MAGNIFICATIONS

ELE	F	S	S'	M	PHI	THETA	TYPE	e/Tzo	PHI'
obj	inf	0	0	1.0	0	0	obj	0	0
1	3.456506	0	−3.456506	0	0	0	LENS	0	0
2	−1.428469	−.3870576	−.5309138	1.371666	0	0	LENS	−.9602	0
det	inf	2.36431E-4	2.36431E-4	+1.0	0	0	det	0	0

(*continued*)

Table 5.9. Continued

OPTOMECHANICAL CONSTRAINT EQUATIONS (ABSOLUTE VALUES SMALLER THAN 0 ARE PRINTED AS 0.0)

REGISTRATION VARIABLES

	TX	TY	TZ	RX	RY	RZ	DM/M	Df,p,G	LDesVar
Tx	0.0	0.0	0.0	0.0	0.0	0.0	0.0	0.0	Dt
Ty	0.0	0.0	0.0	0.0	0.0	0.0	0.0	0.0	DR1
Tz	0.0	0.0	0.0	0.0	0.0	0.0	0.0	0.0	DR2
Rx	0.0	0.0	0.0	0.0	0.0	0.0	0.0	0.0	Dn
Ry	0.0	0.0	0.0	0.0	0.0	0.0	0.0	0.0	
Rz	0.0	0.0	0.0	0.0	0.0	1	0.0	0.0	
Df,p,G	0.0	0.0	0.0	0.0	0.0	0.0	0.0	0.0	
SYSTEM-OBJECT									
Tx	1.371666	0.0	0.0	0.0	0.0	0.0	0.0	−1.536252	Dt
Ty	0.0	1.371666	0.0	0.0	0.0	0.0	0.0	−3.035868	DR1
Tz	0.0	0.0	1.881468	0.0	0.0	0.0	−.9602349	1.356994	DR2
Rx	0.0	.2667176	0.0	1.371666	0.0	0.0	0.0	−1.184077	Dn
Ry	−.2667176	0.0	0.0	0.0	1.371666	0.0	0.0	0.0	
Rz	0.0	0.0	0.0	0.0	0.0	0.0	0.0	0.0	
Df,p,G	0.0	0.0	−1.881468	0.0	0.0	0.0	1.249544	0.0	
ELEMENT-1									
Tx	−.3716662	0.0	0.0	0.0	0.0	0.0	0.0	−3.061093	Dt
Ty	0.0	−.3716662	0.0	0.0	0.0	0.0	0.0	−3.129063	DR1
Tz	0.0	0.0	−.8814681	0.0	0.0	0.0	.9602349	5.509846	DR2
Rx	0.0	.1285751	0.0	−.3716662	0.0	0.0	0.0	.4251073	Dn
Ry	−.1285751	0.0	0.0	0.0	−.3716662	0.0	0.0	0.0	
Rz	0.0	0.0	0.0	0.0	0.0	0.0	0.0	0.0	
Df,p,G	0.0	0.0	−.1381358	0.0	0.0	0.0	.2601849	0.0	
ELEMENT-2									
Tx	−1	0.0	0.0	0.0	0.0	0.0	0.0	0.0	Dt
Ty	0.0	−1	0.0	0.0	0.0	0.0	0.0	0.0	DR1
Tz	0.0	0.0	−1	0.0	0.0	0.0	0.0	0.0	DR2
Rx	0.0	0.0	0.0	−1	0.0	0.0	0.0	0.0	Dn
Ry	0.0	0.0	0.0	0.0	−1	0.0	0.0	0.0	
Rz	0.0	0.0	0.0	0.0	0.0	−1	0.0	0.0	
Df,p,G	0.0	0.0	0.0	0.0	0.0	0.0	0.0	0.0	
DETECTOR									

Table 5.10(a) Influence coefficient arrays for lens 1.

ELEMENT INFLUENCE COEFFICIENT ARRAYS

	TX	TY	TZ	RX	RY	RZ	TX	TY	TZ	RX	RY	RZ	DF
	OBJECT: : : : :						ELEMENT 1						
Tx							1				−.194448		
Ty								1		.194448			
Tz									1				−1
Rx										1			
Ry											1		
Rz						1							
DM/M													.28931

Table 5.10(b) Influence coefficient arrays for lens 2.

	TX	TY	TZ	RX	RY	RZ	TX	TY	TZ	RX	RY	RZ	DF
	OBJECT: : : : :						ELEMENT 2						
Tx	1.37167						−.371666				−.128575		
Ty		1.37167						−.371666		.128575			
Tz			1.88147						−.881468				−.138136
Rx				1.37167						−.371666			
Ry					1.37167						−.371666		
Rz						1							
DM/M			−.960235						.960235				.260185

Table 5.10(c) Influence coefficient arrays to the detector.

	TX	TY	TZ	RX	RY	RZ	TX	TY	TZ	RX	RY	RZ	DF
	OBJECT: : : : :						ELEMENT DET						
Tx	1						−1						
Ty		1						−1					
Tz			1						−1				
Rx				1						−1			
Ry					1						−1		
Rz						1						−1	
DM/M													

Table 5.11 The Nastran finite element model of the telescope's optomechanical constraint equations.

```
NASTRAN MESH
CEND
TITLE = DOUB'S IVORY(TM) UNIFIED OPTOMECHANICAL MODEL
$ SINGLE POINT CONSTRAINT SETS MUST BE CALLED OUT IN THE CASE CONTROL DECK.
SPC = 1000
$ MULTIPOINT CONSTRAINT SETS MUST BE CALLED OUT IN THE CASE CONTROL DECK.
MPC = 1000
BEGIN BULK

$ THE FOLLOWING GRID POINTS/DOFS HAVE BEEN ASSIGNED:
$ 1 THRU 2 /123456 ARE ASSIGNED TO THE OPTICAL ELEMENTS IN ASCENDING ORDER.
$ 3 /123456 IS ASSIGNED TO THE SYSTEM DETECTOR.
$ 4 /123456 IS ASSIGNED TO THE SYSTEM OBJECT.
$ 5 /123456 IS ASSIGNED TO THE REGISTRATION VARIABLES TX, TY, TZ, RX, RY, RZ.
$ 6 /1 IS ASSIGNED TO THE REGISTRATION VARIABLE DM/M.

GRID    5    3   0.       0.         0.         3
GRID    6    3   0.       0.         0.         3

MPC     1000 5   1        -1.        1          1    1.371666
             1   5        -.2667182             1    -.371666
             2   5        -.1285753             1    -1.

MPC     1000 5   2        -1.        1          2    1.371666
             1   4        .26671762             2    -.371666
             2   4        .12857513             2    -1.

MPC     1000 5   3        -1.        1          3    1.881468
             2   3        -.8814683             3    -1.

MPC     1000 5   4        -1.        1          4    1.371666
             2   4        -.3716663             4    -1.

MPC     1000 5   5        -1.        1          5    1.371666
             2   5        -.3716663             5    -1.

MPC     1000 5   6        -1.        3          6    -1.

MPC     1000 6   1        -1.        1          3    -.960235
             2   3        .9602349

SPC     1000 6   23456

$ DETECTOR
$ PRINCIPAL POINT
GRID    3    3   0.       0.         0.         3
$ DETECTOR COORDINATE SYSTEM
CORD2R  3    0   0.       0.         0.         0.   0.         1.
        1.   0.  0.
$ INCIDENT OPTICAL AXIS COORDINATE SYSTEM
CORD2R  6    3   0.       0.         0.         0.   0.         1.
        1.   0.  0.

$ ELEMENT 2
$ FIRST PRINCIPAL POINT
GRID    2    6   0.       0.         .65972532
$ ELEMENT COORDINATE SYSTEM
CORD2R  2    6   0.       0.         .65972530.      0.         1.659725
        1.   0.  .6597253
```

Table 5.11. Continued

```
$ INCIDENT OPTICAL AXIS COORDINATE SYSTEM
CORD2R  5    6    0.       0.       .65972530.   0.       1.659725
        1.   0.   .6597253

$ ELEMENT 1
$ FIRST PRINCIPAL POINT
GRID    1    5    0.       0.       3.2638961
$ ELEMENT COORDINATE SYSTEM
CORD2R  1    5    0.       0.       3.2638960.   0.       4.263896
        1.   0.   3.263896
$ INCIDENT OPTICAL AXIS COORDINATE SYSTEM
CORD2R  4    5    0.       0.       3.2638960.   0.       4.263896
        1.   0.   3.263896

$ OBJECT AT INFINITY AND NOT MODELED

ENDDATA
```

the object's coordinate system, simplifying the interpretation of the registration errors at the detector.

In assembling the optomechanical constraint equations for systems where the object is rotated about its optical axis, the convolution and superposition process must be modified slightly. This modification distributes the object's motions in its own (*X*-*Y*) coordinate system into the appropriate vector components of the image's (*X*-*Y*) coordinate system.

If the distant object of the two-lens telescope of Fig. 5.1 is re-orientated (rotated) through an angle θ_o equal to 30.0 deg as shown in Fig. 5.7, the engineer can recalculate the optomechanical constraint equation to obtain the appropriate vector components on the detector. To make the recalculation, the engineer will assume that the θ rotation occurs between the first and second lenses. This assumption is necessary because the magnification of the first lens is 0.0 (the object being at infinity), so the object motion array for lens 1 is empty, except for the Rz_i/Rz_o term [Table 5.10(a)]. Under the assumed conditions, θ_1 equals 30.0 deg. As shown in Fig. 5.8, the system's object and Lens 1 will be in parallel coordinate systems, and the coordinate transformation will be performed between Lens 1 and Lens 2, where the object motion array is full and finite [Table 5.10(b)].

The telescope's geometry file is revised (Table 5.12) by entering the rotation angle (30.0 deg) in the f2 column for the first surface of Lens 2 (Surface 4 in the table). The revision is shown in bold type. The telescope's index of refraction table remains unchanged (Table 5.13).

The code is then run with this data set to produce a new set of element influence coefficient arrays and the optomechanical constraint equations. In the element arrays for the system with a rotated object and a rotated Lens 1, both Lens 1 and the detector arrays [Tables 5.14(a) and (c)] are unchanged from their nonrotated condition [Tables 5.10(a) and (c)]. The element arrays

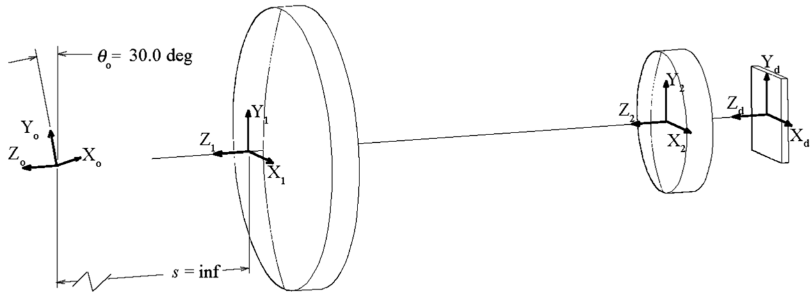

Figure 5.7 The two-lens telescope with the object only rotated about its *Z* axis.

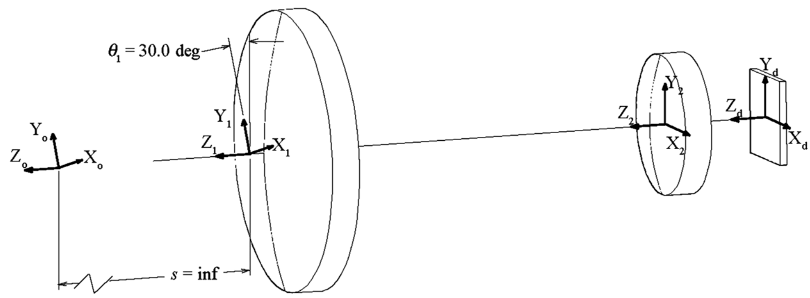

Figure 5.8 The two-lens telescope with both the object and lens 1 rotated about its *Z* axis.

Table 5.12 The optical geometry file for the telescope with the object and lens 1 rotated 30 deg.

Surf	Elem	Radius	Index	Thickness	Type	f1	f2	f3	f4
1	obj	inf	AIR	inf	obj	1.0000000	1.0000000	0.0000000	0.0000000
2	1	3.5	ge	.25	LENS	0.0000000	0.0000000	0.0000000	0.0000000
3	1	5	AIR	2.67	LENS	0.0000000	0.0000000	0.0000000	0.0000000
4	2	1.5	ge	.2	LENS	0.0000000	**30.000000**	0.0000000	0.0000000
5	2	1	AIR	.674	LENS	0.0000000	0.0000000	0.0000000	0.0000000
6	det	inf	AIR	0.0	det				

Table 5.13 Index of refraction file unchanged.

MATERIAL	INDEX
AIR	1.0
ge	4.00024

Table 5.14(a) Element arrays for the first lens with a rotated system object.

	TX	TY	TZ	RX	RY	RZ	TX	TY	TZ	RX	RY	RZ	DF
	OBJECT: : : : :						ELEMENT 1						
Tx							1				−.194448		
Ty								1		.194448			
Tz									1				−1
Rx										1			
Ry											1		
Rz						1							
DM/M													.28931

Table 5.14(b) Element arrays for the second lens with a rotated system object.

	TX	TY	TZ	RX	RY	RZ	TX	TY	TZ	RX	RY	RZ	DF
	OBJECT: : : : :						ELEMENT 2						
Tx	**1.1879**	**−.685833**					−.371666				−.128575		
Ty	**.685833**	**1.1879**						−.371666		.128575			
Tz			1.88147						−.881468				−.138136
Rx				**1.1879**	**−.685833**					−.371666			
Ry				**.685833**	**1.1879**						−.371666		
Rz						1							
DM/M			−.960235						.960235				.260185

Table 5.14(c) Element arrays for the detector with a rotated system object.

	TX	TY	TZ	RX	RY	RZ	TX	TY	TZ	RX	RY	RZ	DF
	OBJECT: : : : :						ELEMENT DET						
Tx	1						−1						
Ty		1						−1					
Tz			1						−1				
Rx				1						−1			
Ry					1						−1		
Rz						1						−1	
DM/M													

Table 5.15 The telescope's optomechanical constraint equations with the object rotated 30 deg about its Z axis.

OPTOMECHANICAL CONSTRAINT EQUATIONS (ABSOLUTE VALUES SMALLER THAN 0 ARE PRINTED AS 0.0)

	REGISTRATION VARIABLES								
	TX	TY	TZ	RX	RY	RZ	DM/M	Df,p,G	LDesVar
Tx	0.0	0.0	0.0	0.0	0.0	0.0	0.0	0.0	Dt
Ty	0.0	0.0	0.0	0.0	0.0	0.0	0.0	0.0	DR1
Tz	0.0	0.0	0.0	0.0	0.0	0.0	0.0	0.0	DR2
Rx	0.0	0.0	0.0	0.0	0.0	0.0	0.0	0.0	Dn
Ry	0.0	0.0	0.0	0.0	0.0	0.0	0.0	0.0	
Rz	0.0	0.0	0.0	0.0	0.0	1	0.0	0.0	
Df,p,G	0.0	0.0	0.0	0.0	0.0	0.0	0.0	0.0	
SYSTEM-OBJECT									
Tx	**1.187898**	**.6858331**	0.0	0.0	0.0	0.0	0.0	−1.536252	Dt
Ty	**−.6858331**	**1.187898**	0.0	0.0	0.0	0.0	0.0	−3.035868	DR1
Tz	0.0	0.0	1.881468	0.0	0.0	0.0	−.9602349	1.356994	DR2
Rx	**−.1333588**	**.2309842**	0.0	**1.187898**	**.6858331**	0.0	0.0	−1.280087	Dn
Ry	**−.2309842**	**−.1333588**	0.0	**−.6858331**	**1.187898**	0.0	0.0	0.0	
Rz	0.0	0.0	0.0	0.0	0.0	0.0	0.0	0.0	
Df,p,G	0.0	0.0	−1.881468	0.0	0.0	0.0	1.249544	0.0	
ELEMENT-1									
Tx	−.3716662	0.0	0.0	0.0	0.0	0.0	0.0	−3.061093	Dt
Ty	0.0	−.3716662	0.0	0.0	0.0	0.0	0.0	−3.129063	DR1
Tz	0.0	0.0	−.8814681	0.0	0.0	0.0	.9602349	5.509846	DR2
Rx	0.0	.1285751	0.0	−.3716662	0.0	0.0	0.0	.2720618	Dn
Ry	−.1285751	0.0	0.0	0.0	−.3716662	0.0	0.0	0.0	
Rz	0.0	0.0	0.0	0.0	0.0	0.0	0.0	0.0	
Df,p,G	0.0	0.0	−.1381358	0.0	0.0	0.0	.2601849	0.0	
ELEMENT-2									
Tx	−1	0.0	0.0	0.0	0.0	0.0	0.0	0.0	Dt
Ty	0.0	−1	0.0	0.0	0.0	0.0	0.0	0.0	DR1
Tz	0.0	0.0	−1	0.0	0.0	0.0	0.0	0.0	DR2
Rx	0.0	0.0	0.0	−1	0.0	0.0	0.0	0.0	Dn
Ry	0.0	0.0	0.0	0.0	−1	0.0	0.0	0.0	
Rz	0.0	0.0	0.0	0.0	0.0	−1	0.0	0.0	
Df,p,G	0.0	0.0	0.0	0.0	0.0	0.0	0.0	0.0	
DETECTOR									

Table 5.16 The telescope's Nastran model with the system's object rotated 30 deg about its *Z* axis.

```
NASTRAN MESH
CEND
TITLE = DOUBQ'S IVORY(TM) UNIFIED OPTOMECHANICAL MODEL
$ SINGLE POINT CONSTRAINT SETS MUST BE CALLED OUT IN THE CASE CONTROL DECK.
SPC = 1000
$ MULTIPOINT CONSTRAINT SETS MUST BE CALLED OUT IN THE CASE CONTROL DECK.
MPC = 1000
BEGIN BULK

$ THE FOLLOWING GRID POINTS/DOFS HAVE BEEN ASSIGNED:
$ 1 THRU 2 /123456 ARE ASSIGNED TO THE OPTICAL ELEMENTS IN ASCENDING ORDER.
$ 3 /123456 IS ASSIGNED TO THE SYSTEM DETECTOR.
$ 4 /123456 IS ASSIGNED TO THE SYSTEM OBJECT.
$ 5 /123456 IS ASSIGNED TO THE REGISTRATION VARIABLES TX, TY, TZ, RX, RY, RZ.
$ 6 /1 IS ASSIGNED TO THE REGISTRATION VARIABLE DM/M.

GRID    5          3   0.        0.          0.         3
GRID    6          3   0.        0.          0.         3

MPC     1000       5   1         -1.         1          1  1.187898
                   1   2         -.6858331              4  -.133359
                   1   5         -.2309842              1  -.371666
                   2   5         -.1285753              1  -1.

MPC     1000       5   2         -1.         1          1  .6858331
                   1   2         1.1878981              4  .2309842
                   1   5         -.1333592              2  -.371666
                   2   4         .12857513              2  -1.

MPC     1000       5   3         -1.         1          3  1.881468
                   2   3         -.8814683              3  -1.

MPC     1000       5   4         -1.         1          4  1.187898
                   1   5         -.6858332              4  -.371666
                   3   4         -1.

MPC     1000       5   5         -1.         1          4  .6858331
                   1   5         1.1878982              5  -.371666
                   3   5         -1.

MPC     1000       5   6         -1.         3          6  -1.

MPC     1000       6   1         -1.         1          3  -.960235
                   2   3         .9602349

SPC     1000       6   23456

$ DETECTOR
$ PRINCIPAL POINT
GRID    3          3   0.        0.          0.         3
$ DETECTOR COORDINATE SYSTEM
CORD2R  3          0   0.        0.          0.         0. 0.          1.
        1.         0.  0.
$ INCIDENT OPTICAL AXIS COORDINATE SYSTEM
CORD2R  6          3   0.        0.          0.         0. 0.          1.
        1.         0.  0.
```

Table 5.16. Continued

```
$ ELEMENT 2
$ FIRST PRINCIPAL POINT
GRID     2          6    0.         0.          .65972532
$ ELEMENT COORDINATE SYSTEM
CORD2R   2          6    0.         0.          .65972530.   0.   1.659725
         1.         0.   .6597253
$ INCIDENT OPTICAL AXIS COORDINATE SYSTEM
CORD2R   5          6    0.         0.          .65972530.   0.   1.659725
         1.         0.   .6597253

$ ELEMENT 1
$ FIRST PRINCIPAL POINT
GRID     1          5    0.         0.          3.2638961
$ ELEMENT COORDINATE SYSTEM
CORD2R   1          5    0.         0.          3.2638960.   0.   4.263896
         .8660254.5      3.263896
$ INCIDENT OPTICAL AXIS COORDINATE SYSTEM
CORD2R   4          5    0.         0.          3.2638960.   0.   4.263896
         .8660254.5      3.263896

$ OBJECT AT INFINITY AND NOT MODELED

ENDDATA
```

for the second lens [Table 5.14(b)] are changed [from Table 5.10(b)] to show the coordinate transformation between the X-Y coordinate systems of Lens 1 and Lens 2. This causes pure X or Y translations and rotations of Lens 1 to be passed to Lens 2 as the appropriate vector components in the Lens 2 coordinate system. These differences are highlighted in bold type in Table 5.14(b).

The optomechanical constraint equations are assembled from the changed element arrays. It may be seen in the element arrays that a translation in either X or Y of Lens 1 now creates a translation in both X and Y of the image of Lens 2 and on the registration at the detector. A similar effect can be seen between the rotations about X or Y of Lens 1 and the rotations about X and Y of the images of Lens 2 and at the registration at the detector. These differences in the optomechanical constraint equations are highlighted in bold type in Table 5.15.

The software also prepares a revised Nastran model of the telescope incorporating changes to both the influence coefficients and the geometry of the optical path (Table 5.16). The changes to the model are highlighted in bold type.

Chapter 6
Analysis Checkout

With regard to the quality of analyses performed using the optomechanical constraint equations, there are two considerations. The first is how well the constraint equations compare to physical theory, other computational methods such as lens design codes, and reported empirical test data. That is: How well do the equations simulate optical reality? The second consideration is: Considering all of the calculations going into the equations themselves, how can the engineer be sure that the equations as implemented are faithful to the original optical prescription?

6.1 The Quality of Simulation

The optomechanical constraint equations replicate the analyses made in optical design codes and tests made on optical brassboard setups. One of the most extensive evaluations of the constraint equations was performed on an optical image correlator.[6] The arrangement of the lenses, the spatial light modulators, the LED, and the detector is shown in Fig. 6.1. Alignment of the correlator was very delicate, so the technicians became very aware of the correlator's sensitivities to the position and orientation of the optical elements. A particularly sensitive element was L3, located between the spatial light modulators (SLM1 and SLM2) in Fig. 6.1. The image motions in the brassboard were measured when Tx and Ty displacements were applied to L3 by micrometer-driven translation stages. The agreement with the optomechanical constraint equations is shown in Fig. 6.2.

To determine the effects of rotating L3, the optical designer used the Zemax optical design code to rotate L3 about its first vertex V_1 and calculate the image's motion. The agreement with the optomechanical constraint equations is shown in Fig. 6.3. However, these data did not agree with the technicians' experience in attempting to align L3 in the brassboard. The slope is positive in the Zemax data, but the brassboard experience suggested that the slope should be negative. A review of the brassboard setup shows that the lens

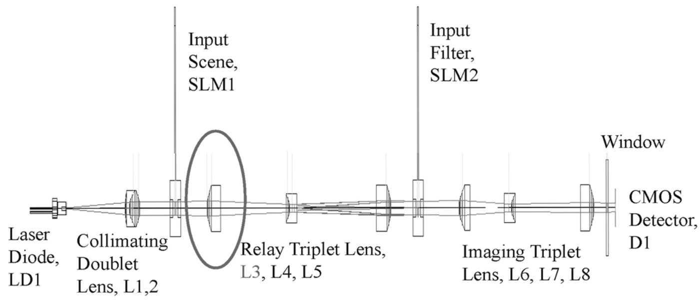

Figure 6.1 An optical image correlator.[1]

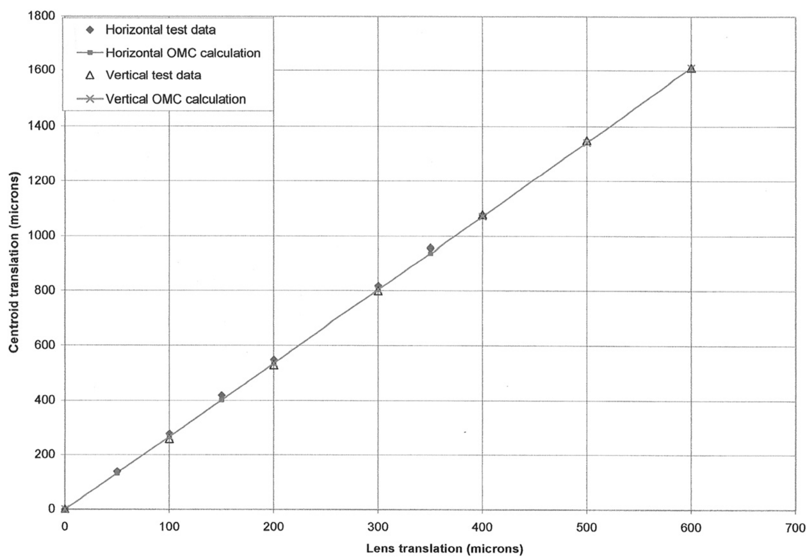

Figure 6.2 Verification of *Tx* and *Ty* motions of lens L3.[1]

holder for L3 was rotating the lens near the center of the lens thickness, about 1.55 mm behind the first vertex. Rotation about the first vertex is important because that was the location of the first principal point of the lens (a plano-convex form) and where the origin of coordinates for the lens was located for the optomechanical constraint equations.

Adjusting the test data for the 1.55 mm offset of the rotation axis (causing a simultaneous translation) resulted in Fig. 6.4, which shows the revised test data (with error bars) and compares the data to the corresponding curve for the optomechanical constraint equations when rotated 1.55 mm behind the vertex. This figure shows the slope of the curve to be reversed from Fig. 6.3, as anticipated by the technician, and the two curves to agree within the accuracy of the measurement error bars.

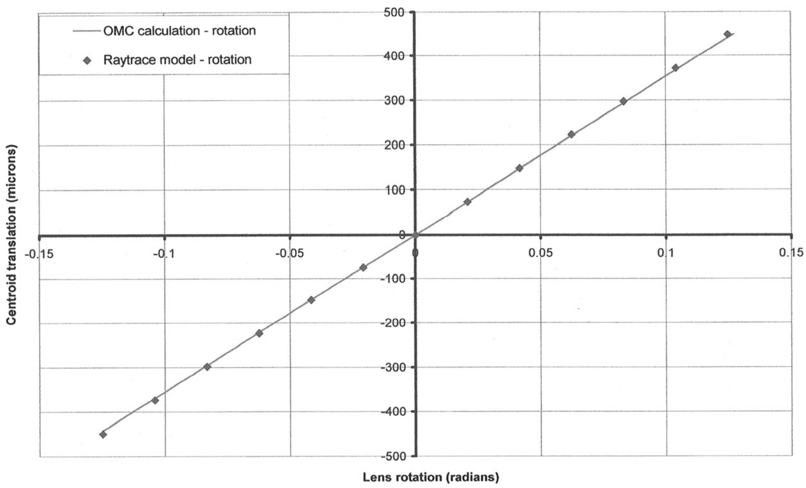

Figure 6.3 Verification of *Rx* and *Ry* motions of lens L3.[1]

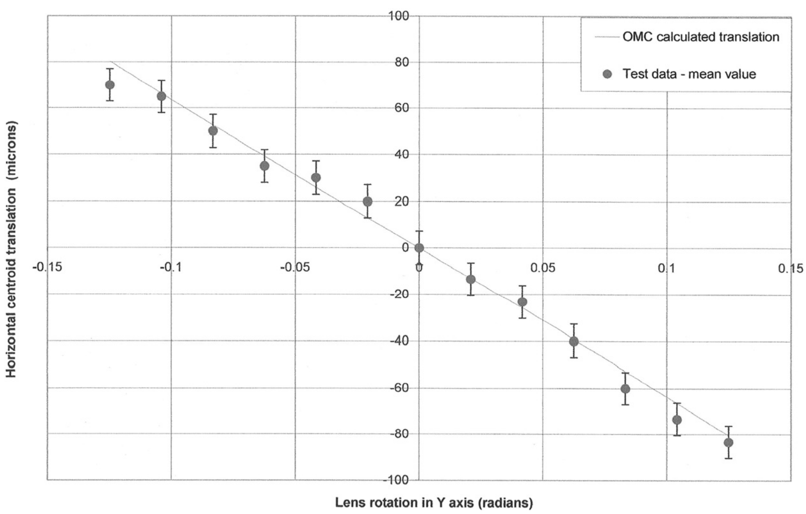

Figure 6.4 Verification of simultaneous *Ry* and *Tx* motions of lens L3.[1]

6.2 The Quality of Implementation

Preparation of the optomechanical constraint equations requires a number of mathematical operations, any of which can contribute errors in the resulting expressions. The engineer can check the quality of the calculations in a number of ways.

6.2.1 Effective focal length

In Section 3.2.5.1, the effective focal length of the infrared receiver was calculated as -51.58 based on the Gaussian properties of the lenses. This compared well with the value published by the lens design code: -51.579012. The two focal lengths will usually be somewhat different because they are calculated by different methods, but in well-corrected optical systems, they should be quite close. In this case, the error appears to be about 1:5,000. This is consistent with the four-place accuracy of the calculations.

6.2.2 Gaussian registration error at the detector

In the four-element infrared receiver mentioned above, the initial registration error at the detector (Section 3.2.5.2) was found to be 0.006395 in. The Gaussian focus was slightly in front of the detector. This registration error was the final value in the s' column when the magnifications were being calculated. In a perfectly corrected system, its value would be 0.000000. From the optical prescription, it is known that the effective focal length is -51.579012 in. Therefore, this initial registration error represents the difference between the paraxial focal plane and the plane of best focus over the entire field of view. It represents an uncertainty of about 1 part in 10,000 in the position of the image and is consistent with the 3- to 5-place precision of the physical optical prescription data.

6.2.3 Validation sums

After the optomechanical constraint equations have been prepared, the engineer can make a quick check to see if the influence coefficients are consistent. Along the major diagonal, from Tx_i/Tx to Rz_i/Rz, the sum of the coefficients of all of the elements should equal 0.0. Assuming that there are n elements in the system, including the object and the detector,

$$\begin{aligned}
\sum Tx_\mathrm{i}/Tx_n &= 0.0,\\
\sum Ty_\mathrm{i}/Ty_n &= 0.0,\\
\sum Tz_\mathrm{i}/Tz_n &= 0.0,\\
\sum Rx_\mathrm{i}/Rx_n &= 0.0,\\
\sum Ry_\mathrm{i}/Ry_n &= 0.0,\\
\sum Rz_\mathrm{i}/Rz_n &= 0.0,
\end{aligned}$$

and for the off-diagonal term,

$$\sum(\Delta M/M_\mathrm{i})/Tz_n = 0.0.$$

For the infrared receiver example shown above (Section 3.2.5.4), the sums are

$$\sum Tx_{\mathrm{i}}/Tx_n = 0.0 - 1.0299 - 1.2607 + 0.1093 + 3.1812 - 1.0 = 0.0001,$$
$$\sum Ty_{\mathrm{i}}/Ty_n = 0.0 - 1.0299 - 1.2607 + 0.1093 + 3.1812 - 1.0 = 0.0001,$$
$$\sum Tz_{\mathrm{i}}/Tz_n = 0.0 + 1.0603 + 4.1859 - 0.4886 - 3.7576 - 1.0 = 0.0,$$
$$\sum Rx_{\mathrm{i}}/Rx_n = 0.0 - 1.0299 - 1.2606 + 0.1093 + 3.1812 - 1.0 = 0.0001,$$
$$\sum Ry_{\mathrm{i}}/Ry_n = 0.0 - 1.0299 - 1.2606 + 0.1093 + 3.1812 - 1.0 = 0.0001,$$
$$\sum Rz_{\mathrm{i}}/Rz_n = 1.0 + 0.0 + 0.0 + 0.0 + 0.0 - 1.0 = 0.0,$$
$$\sum (\Delta M/M_{\mathrm{i}})/Tz_n = 0.0 - 0.06530 - 0.32141 + 0.05861 + 0.3281 = 0.0,$$

which are consistent with the round-off precision in the analysis.

If the optical system is folded, the appropriate coordinate transformations need to be applied in the process.

6.2.4 Rigid body sums

A more comprehensive check on the quality of the optomechanical constraint equations involves rotating the entire system through some angle, usually 1.0 rad. Then, the rotations of all of the elements are easily calculated as 1.0 rad. The Y displacements of the elements will depend on each element's distance from the origin of rotation.

The -2x reticle projector (Section 3.1.1) might be rotated 1.0 rad about its X axis at the CCD. The Y displacements of the system's elements (Fig. 6.5) are

$$Ty\,\text{reticle} = -677.5\ \text{mm},$$
$$Ty\,\text{lens} = -452.5\ \text{mm},$$
$$Ty\,\text{CCD} = 0.0\ \text{mm}.$$

The registration errors caused by this rotation are

$$\sum Tx_{\mathrm{i}}/Tx_n = 0.0,$$
$$\sum Ty_{\mathrm{i}}/Ty_n = 0.0,$$
$$\sum Tz_{\mathrm{i}}/Tz_n = 0.0,$$
$$\sum Rx_{\mathrm{i}}/Rx_n = 0.0,$$
$$\sum Ry_{\mathrm{i}}/Ry_n = 0.0,$$
$$\sum Rz_{\mathrm{i}}/Rz_n = 0.0,$$
$$\sum (\Delta M/M_{\mathrm{i}})/Tz_n = 0.0.$$

These results are again consistent with the round-off precision in the analysis. This method also checks the accuracy of the off-axis terms that are dependent on the principal thickness p of the lenses.

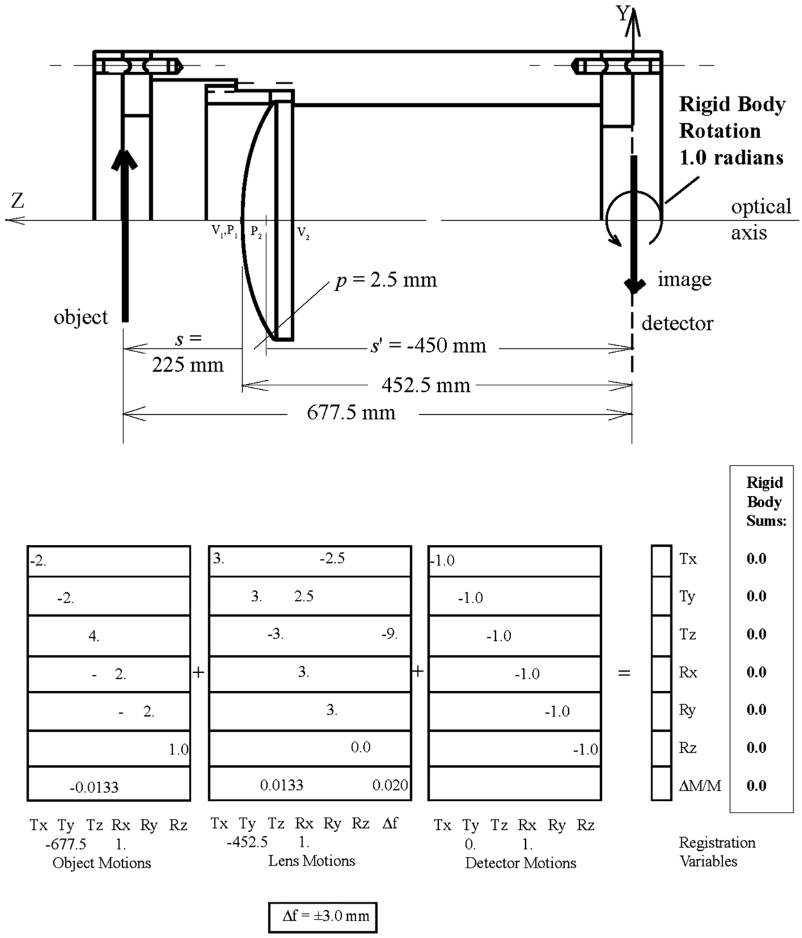

Figure 6.5 Rigid body sums for the reticle projector.

This method is very similar to the "rigid body checks" that are often performed to validate finite element structural models. If the optomechanical constraint equations are incorporated in a finite element structural model, this is a good way to validate them.

Another example of the rigid body sums is provided for the infrared receiver. If the system is rotated 1.0 rad about its detector's X axis (Fig. 6.6), the rotations will all be 1.0 rad, and the translations will be

$$Ty_1 = -64.25 \text{ in.}$$

$$Ty_2 = -55.49 \text{ in.}$$

$$Ty_3 = -35.62 \text{ in.}$$

$$Ty_4 = -22.31 \text{ in.}$$

$$Ty_d = 0.0 \text{ in.}$$

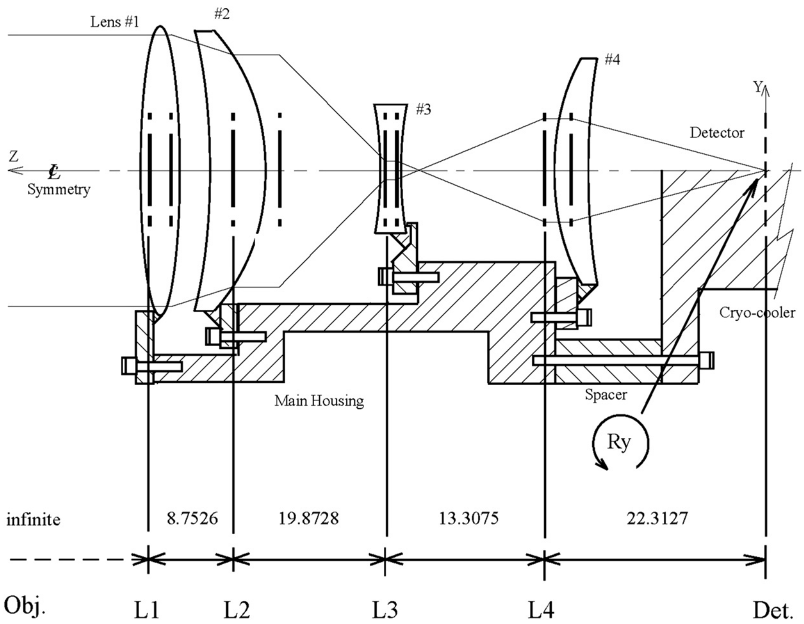

STATIC ANALYSIS SUBCASE NO. 1: ROTATED ABOUT THE X AXIS AT THE DETECTOR

NODE	X TRANS	Y TRANS	Z TRANS	X ROT	Y ROT	Z ROT
1	0.0000E-01	-6.4246E+01	0.0000E-01	1.0000E+00	0.0000E-01	0.0000E-01
2	0.0000E-01	-5.5493E+01	0.0000E-01	1.0000E+00	0.0000E-01	0.0000E-01
3	0.0000E-01	-3.5620E+01	0.0000E-01	1.0000E+00	0.0000E-01	0.0000E-01
4	0.0000E-01	-2.2313E+01	0.0000E-01	1.0000E+00	0.0000E-01	0.0000E-01
5(d)	0.0000E-01	0.0000E-01	0.0000E-01	1.0000E+00	0.0000E-01	0.0000E-01

Figure 6.6. Rigid body displacements for *Ry* motion of the infrared receiver.[1]

When these translations and rotations are applied to the infrared receiver (Fig. 6.7), the registration errors between the image and the detector are

$$\sum Tx_{\mathrm{i}} = 0.0,$$
$$\sum Ty_{\mathrm{i}} = 51.59 \text{ in.}$$
$$\sum Tz_{\mathrm{i}} = 0.0,$$
$$\sum Rx_{\mathrm{i}} = 0.0,$$
$$\sum Ry_{\mathrm{i}} = 0.0,$$
$$\sum Rz_{\mathrm{i}} = 0.0,$$
$$\sum \Delta M/M_{\mathrm{i}} = 0.0.$$

Note that the object, which is at infinity, was not included in the analysis and was therefore assumed to be stationary. The result is that the image on the detector moved as the instrument was rotated. For a 1.0-rad rotation, that

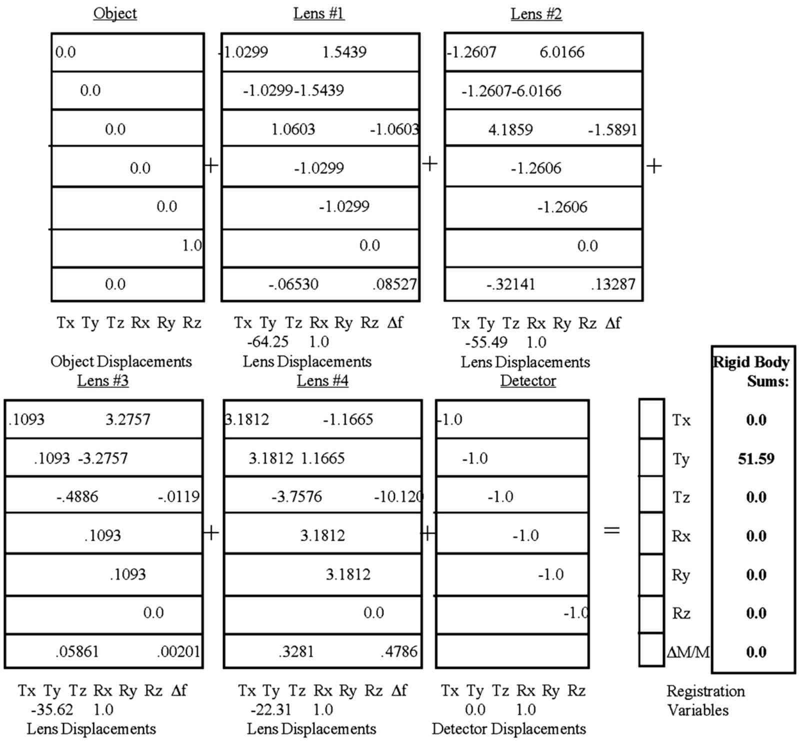

Figure 6.7 Rigid body sums for the infrared receiver.[1]

motion should numerically equal the focal length of the system, which is -51.579012 in. according to the Gaussian prescription. The coordinate systems change the sign from $-$ to $+$.

These results are again consistent with the round-off precision in the analysis, ~1:5,000, from the rigid body sums.

6.3 A System's Deviation Fractions

This section describes how the individual elements' properties (influence coefficients and deviation fractions) can be used to quantify a system's nonlinearities between each optical element and the system's image. The deviation fractions that quantify the nonlinearities in the individual optical elements' influence functions have been described in Chapter 2.

The nonlinearities occur in the influence functions relating the Z-axis motions, Tz_l, of an element and the change in focal length, Δf, of an element to both the Z-axis motion of the system's image, Tz_i, and the change in size $\Delta M/M$ of the system's image (Sections 2.2.8 and 2.2.9). The effects of a Z-axis motion of an element, Tz_l, will be described here. The Tz_i and $\Delta M/M$ influence functions are somewhat different and will be treated separately. The effects on Δf of an element can be described by following the procedures for the effects of Tz_1.

6.3.1 Deviation fraction for Z-axis motion of a system's image

Among the expressions for a four-lens system's influence coefficients (A through K in Section 3.2.2), the expression C defines the Z-axis image motion, Tz_i, at the detector caused by a Z-axis motion, Tz_1, of the system's first lens:

$$Tz_i/Tz_1 = (1 - M_1{}^2)(M_2{}^2)(M_3{}^2)(M_4{}^2),$$

which can be contracted to

$$Tz_i/Tz_1 = (1 - M_1{}^2)(M_2{}^2)(M_3{}^2)(M_4{}^2) = c_1c_2c_3c_4 \equiv C_{Tzi},$$

where each lower-case c_n represents the influence coefficient for the corresponding element among the four lenses. The value of this expression for C_{Tzi} is reported as an influence coefficient in the optomechanical constraint equations (Section 3.2.2).

The image motion caused by the translation of a lens in the Z direction is one of the nonlinear influence functions. The full influence function can be written as

$$Tz_i/Tz_1 = [c_1/(1+e_1)][c_2/(1+e_2)][c_3/(1+e_3)][c_4/(1+e_4)] \equiv IF_{Tzi},$$

where each of the lower-case e_n is the deviation fraction for the corresponding element's influence on its own image, and IF_{Tzi} is the full influence function.

The full influence function can be rearranged to

$$\begin{aligned} IF_{Tzi} &= [c_1c_2c_3c_4]/[(1+e_1)(1+e_2)(1+e_3)(1+e_4)] \\ &= C_{Tzi}/[(1+e_1)(1+e_2)(1+e_3)(1+e_4)], \end{aligned}$$

where C_{Tzi} is the first lens's influence coefficient at the system's image. If e_1, e_2, e_3, and $e_4 \ll 1.0$, the product of two or more deviation fractions will be much smaller and can be ignored; in this case, the influence function can be rewritten as

$$IF_{Tzi} = C_{Tzi}/(1 + e_1 + e_2 + e_3 + e_4).$$

From the definition of the form for the influence function in Chapter 1,

$$IF_j = c_j/(1 + e_j),$$

and if E_{Tzi} is the first lens's deviation fraction at the system's image, it follows that

$$IF_{Tzi} = C_{Tzi}/(1 + E_{Tzi}) = C_{Tzi}/(1 + e_1 + e_2 + e_3 + e_4),$$

and

$$(1 + E_{\mathrm{Tzi}}) = (1 + e_1 + e_2 + e_3 + e_4),$$

in which case

$$E_{\mathrm{Tzi}} = e_1 + e_2 + e_3 + e_4.$$

This expression for the system's deviation fraction can be evaluated using the individual lens's deviation fractions developed in Section 2.2:

$$\begin{aligned}
e_1 &= -M_1{}^3[Tz_1]/(f_1 + M_1 - f_1 M_1{}^2)\\
e_2 &= -M_2[(1 - M_1{}^2)Tz_1]/f_2\\
e_3 &= -M_3[M_2{}^2(1 - M_1{}^2)Tz_1]/f_3\\
e_4 &= -M_4[M_3{}^2 M_2{}^2(1 - M_1{}^2)Tz_1]/f_4.
\end{aligned}$$

Note that the terms in square brackets [ ] are the local Z-axis displacements for the particular local deviation fraction being calculated. In the case of e_1, this term is Lens 1's displacement, Tz_1. In the case of e_2, it is the motion of Lens 1's image (which is Lens 2's object) caused by the motion of Lens 1 itself $(1 - M_1{}^2)Tz_1$. In the cases of e_3 and e_4, they are the image motions of Lenses 2 and 3 (which are the object motions for Lenses 3 and 4) caused again by the motion of Lens 1 itself, $M_2{}^2(1 - M_1{}^2)Tz_1$ and $M_3{}^2M_2{}^2(1 - M_1{}^2)Tz_1$. All of these local displacements are calculated from the local displacement Tz_1 of the lens being evaluated, Lens 1 in this case.

The deviation fraction E_{Tz1} for the influence function between the Z-axis motion of Lens 1 and the Z-axis motion of the image at the detector is the sum of these four terms: $e_1 + e_2 + e_3 + e_4$.

6.3.2 Deviation fraction for change in size of a system's image

Also among the expressions for a four-lens element system's influence coefficients (Section 3.2.2), the expression J defines the change in size of the image at the detector, $\Delta M/M$, caused by a Z-axis motion, Tz_1, of the system's first lens:

$$\frac{\Delta M}{MTz_1} = -\left(\frac{M_1}{f_1}\right) + (1 - M_1^2)\left(\frac{M_2}{f_2}\right) + (1 - M_1^2)M_2^2\left(\frac{M_3}{f_3}\right) + (1 - M_1^2)M_2^2M_3^2\left(\frac{M_4}{f_4}\right).$$

If c'_n is assigned as the influence coefficient for the $\Delta M/M$ registration variable, and c_n is assigned as the influence coefficient for the Tz_i registration variable, the equation can be rewritten as

$$\Delta M/MTz_1 = c'_1 + c_1c'_2 + c_1c_2c'_3 + c_1c_2c_3c'_4 \equiv C_{\Delta\mathrm{M/M}},$$

where $C_{\Delta M/M}$ is defined as the influence coefficient between the Z-axis motion of Lens 1 and the change in size of the image at the detector. The value of the expression $C_{\Delta M/M}$ is reported as an influence coefficient in the optomechanical constraint equations.

The change in size of the image caused by the translation of a lens in the Z direction is one of the nonlinear influence functions.

If e'_n and e_n are assigned as the deviation fractions for the influence coefficients c'_n and c_n, respectively, the full influence function can be written as

$$\frac{\Delta M}{MTz_1} = \frac{c'_1}{1+e'_1} + \frac{c_1 c'_2}{(1+e_1)(1+e'_2)} + \frac{c_1 c_2 c'_3}{(1+e_1)(1+e_2)(1+e'_3)} + \frac{c_1 c_2 c_3 c'_4}{(1+e_1)(1+e_2)(1+e_3)(1+e'_4)}.$$

If the deviation fractions e'_n and $e_n \ll 1.0$, the product of two or more deviation fractions will be much smaller and can be ignored. Then, the full influence function can be simplified to

$$\frac{\Delta M}{MTz_1} = \frac{c'_1}{1+e'_1} + \frac{c_1 c'_2}{1+e_1+e'_2} + \frac{c_1 c_2 c'_3}{1+e_1+e_2+e'_3} + \frac{c_1 c_2 c_3 c'_4}{1+e_1+e_2+e_3+e'_4} \equiv IF_{\Delta M/M}.$$

where $IF_{\Delta M/M}$ is the full influence function between the Z-axis motion of Lens 1 and the change in size of the image at the detector.

The value of this influence function $IF_{\Delta M/M}$ can be calculated as shown from the influence coefficients c'_n, and c_n and the deviation fractions e'_n and e_n for the individual optical elements.

In Chapter 1, the influence function was defined in the form

$$IF_j = \frac{c_j}{1+e_j},$$

which can be rearranged to

$$e_j = \frac{c_j}{IF_j} - 1.$$

From the system-level influence coefficient for Element 1, $C_{\Delta M/M}$, and the system-level influence function for Element 1, $IF_{\Delta M/M}$, the deviation fraction for the influence function between the Z-axis motion of Element 1 and the change in size of the image at the detector (as developed in Section 1.1) can be determined from

$$E_{\Delta M/M} = \frac{C_{\Delta M/M}}{IF_{\Delta M/M}} - 1.$$

The deviation fraction $E_{\Delta M/M}$ for the influence function between the Z-axis motion, Tz_1, of Lens 1 and the change in size, $\Delta M/M$, of the image at the detector is uniquely determined from the influence coefficients and the deviation fractions of the individual optical elements.

6.3.3 Summary of a system's deviation fractions

Every optical element with optical power has four nonlinear influence functions. Two of these influence the Tz position of the image (the focus), and the other two influence the image size (magnification). These two image properties are affected by both the translation in Z of the optical element (illustrated in Section 6.3.2) and by a change in focal length of the optical element due to variations in its dimensions and properties (not illustrated here). In general, the nonlinearities in the change in focus (Tz_{i}) of the system are considerably easier to assess than those in the change in magnification, $\Delta M/M$, of the system, but both are determined by the influence functions (influence coefficients and deviation fractions) of the individual elements, as illustrated above. The nonlinear effects caused by a translation in Z of one element have been illustrated. The effects caused by a change in focal length are evaluated by identical processes.

Chapter 7
Applications

This chapter looks at three different applications of the optomechanical constraint equations to solve nettlesome problems in optomechanical system design, analysis, and manufacture. The first application discusses an optical image correlator that had been designed optically to use commercially available optical elements but had run into trouble during brassboard development. The optomechanical constraint equations were used to determine the sensitivity of the correlator's performance to all of the dimensional and thermal variables in the system and to maximize the correlator's performance and minimize the assembly and test labor required for manufacture.

The second application discusses a fiber optic spread-spectrum encoder system for fiber optic communication security that demonstrated 60% transmission loss during environmental tests. A maximum to 10% loss was allowable. The optomechanical constraint equations modeled the optical-structural-thermal behavior versus the transmission efficiency, η, of the system. The model identified the principal contributors to the losses and identified design changes that brought the system into acceptable performance.

The final application discusses a suite of instruments mounted on an airborne two-axis gimbal set with strict boresight and line-of-sight requirements. The optomechanical constraint equations were incorporated into a Nastran finite element model of the imager, the laser, and the laser receiver in the gimbal. The engineer used the Nastran model to guide the initial structural CAD design of the gimbal and achieve the required dynamic pointing stability for the system.

7.1 An Optical Image Correlator

The optomechanical constraint equations were used in the design of an optical image correlator.[6] Although the correlator relies on diffractive effects to achieve its purpose, it can be approached as being two overlapping imaging

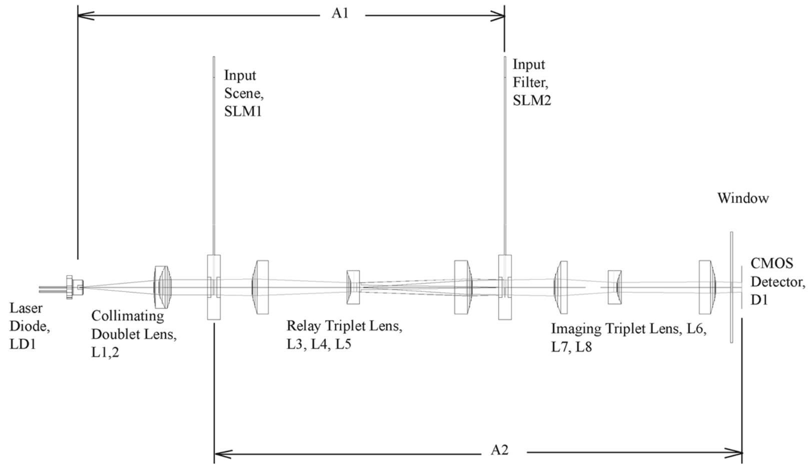

Figure 7.1 An optical image correlator.[1]

systems that need to be very carefully aligned (Fig. 7.1). The first system (A1) runs from the laser diode light source (LD1) to the second spatial light modulator (SLM2).

In the A1 listing (Table 7.1) there are 16 surfaces including the laser diode (Obj.) and the second spatial light modulator (Det.). The purpose of A1 is to deliver the diffracted wavefront from SLM1 to SLM2 at a sharply defined focal plane and numerical aperture.

The second system (A2) runs from SLM1 through SLM2 to the detector. In the A2 listing (Table 7.2) there are 22 surfaces, including the first spatial light modulator (Obj.) and the CMOS detector (Det.). SLM2 is treated as a

Table 7.1 The physical optical prescription for the A1 imaging system.

Surface	Element	Radius	Index	Thickness	Type
1	Obj.	Inf.	1	18.185	Obj.
2	1	−33.6	1.612	1.100	Lens
3	1	−8.5	1	0	Lens
4	2	−8.5	1.514	3.2	Lens
5	2	11.97	1	9.374	Lens
6	3	Inf.	1.456	1.4	Wind.
7	3	Inf.	1	8.374	Wind.
8	4	−16.962	1.514	3.9	Lens
9	4	Inf.	1	19.7874	Lens
10	5	7.78	1.514	2	Lens
11	5	Inf.	1	22.7688	Lens
12	6	Inf.	1.514	4.2	Lens
13	6	18.155	1	7.0996	Lens
14	7	Inf.	1.456	0.7	Wind.
15	7	Inf.	1	0	Wind.
16	Det.	Inf.	1	0	Det.

Table 7.2 The physical optical prescription for the A2 imaging system.

Surface	Element	Radius	Index	Thickness	Type
1	Obj.	Inf.	1	0	Obj.
2	1	Inf.	1.456	0.7	Wind.
3	1	Inf.	1	8.374	Wind.
4	2	−16.962	1.514	3.9	Lens
5	2	Inf.	1	19.7874	Lens
6	3	7.78	1.514	2	Lens
7	3	Inf.	1	22.7688	Lens
8	4	Inf.	1.514	4.2	Lens
9	4	18.155	1	7.0996	Lens
10	5	Inf.	1.456	1.4	Wind.
11	5	Inf.	1	10.9493	Wind.
12	6	−12.55	1.52	3.2	Lens
13	6	Inf.	1	4.4457	Lens
14	7	Inf.	1.514	3.55	Wind.
15	7	Inf.	1	3	Wind.
16	8	Inf.	1.514	2	Lens
17	8	−7.78	1	19.7874	Lens
18	9	Inf.	1.514	3.9	Lens
19	9	16.962	1	3.5061	Lens
20	10	Inf.	1.514	0.5588	Wind.
21	10	Inf.	1	2.1082	Wind.
22	Det.	Inf.	1	0	Det.

window (Element 5 in Table 7.2). The purpose of A2 is to collect the diffracted wavefront from SLM1 and deliver it to the detector. The A1 and A2 optical systems are dimensioned in millimeters.

The physical optical prescription data were imported into Microsoft Excel®, and the optomechanical constraint equations were assembled in a spreadsheet (Fig. 7.2). The equations for A1 and for A2 were arranged to overlap on the spreadsheet, allowing simultaneous solutions for registration errors in both imaging systems. The figure shows the results for a rigid body check of the equations, and, as can be seen in the bottom right corner of the figure, the correlator passed with all registration errors being 0.0 in the check.

The next step was to develop a detailed tolerance allocation plan with the mechanical design team. This plan had four levels of tolerances. The first level was the catalog tolerances on commercial optical components. The second was a tolerance in mounting the elements in their cells. The third was for mounting the cells in modules. The fourth was the mounting the modules in the system. These sources were then summed to determine the net worst-case tolerances for the position, orientation, and focal length of all of the elements in the system (Fig. 7.3).

The resulting registration errors were compared to the required registration accuracy (Table 7.3) by the design team. It was agreed that the

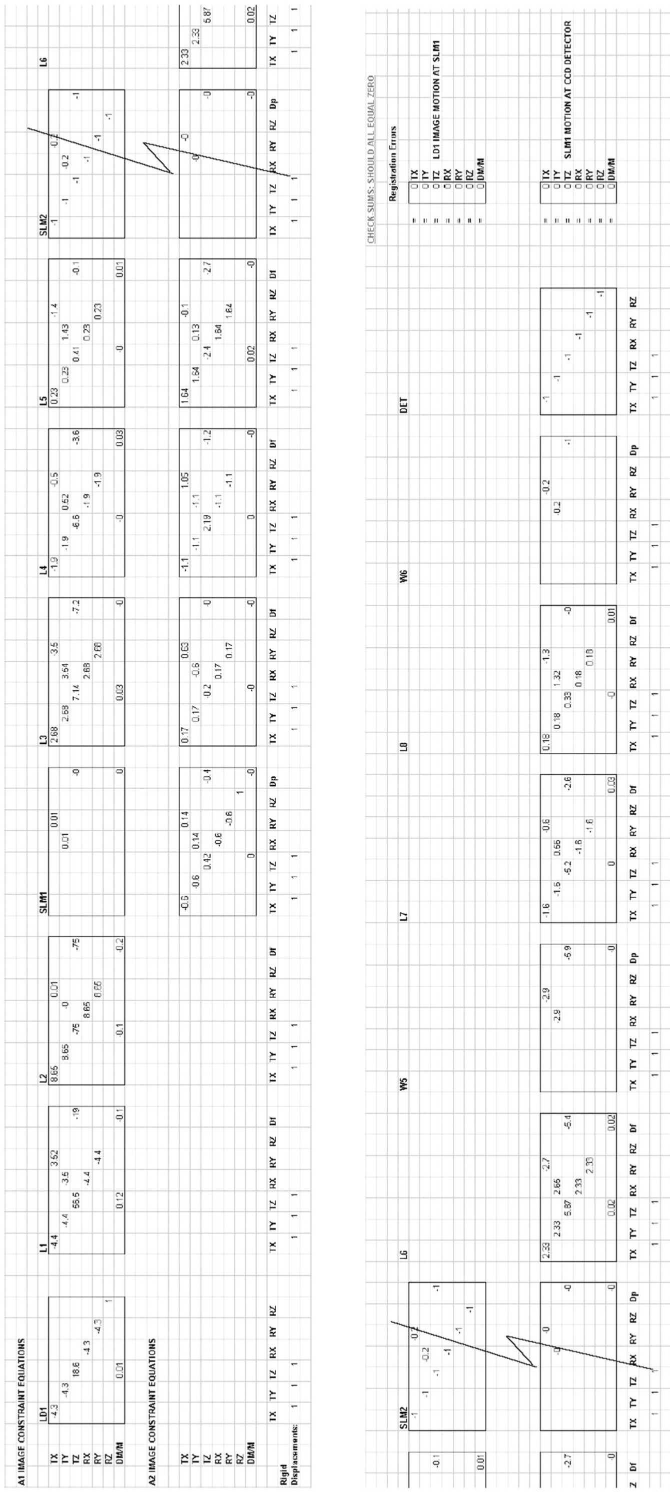

Figure 7.2 The optomechanical constraint equations for the optical image correlator.

NET OF ALL TOLERANCES (Tabular Form)

Element	Tx	Ty	Tz	Rx	Ry	Rz	Df,p	Wavelength
LD1	0.455	0.455	0.455	0.063	0.063	0.0018		
L1,2	0.125	0.125	0.125	0.0018	0.0018	0.0018	0.413943508	
L2								
W1	0.189965	0.189965	0.125	0.0036	0.0036	0.0036	-1.25644E-06	
BL1	0.193641	0.193641	0.125	0.0036	0.0036	0.0036		
W2	0.194198	0.194198	0.125	0.0036	0.0036	0.0036	-4.4577E-07	
SLM1	0.395025	0.395025	0.275	0.0036	0.0036	0.0036		0.03
W3	0.195458	0.195458	0.125	0.0036	0.0036	0.0036	-4.4577E-07	
BL2	0.196344	0.196344	0.125	0.0036	0.0036	0.0036		
W4	0.198251	0.198251	0.125	0.0036	0.0036	0.0036	-1.25644E-06	
L3	0.33825	0.33825	0.325	0.0036	0.0036	0.0036	0.654061634	
L4	0.255887	0.255887	0.125	0.0036	0.0036	0.0036	0.14997173	
L5	0.430465	0.430465	0.325	0.0036	0.0036	0.0036	0.700065969	
W5	0.321244	0.321244	0.125	0.0036	0.0036	0.0036	4.953E-09	
SLM2	0.522071	0.522071	0.275	0.0036	0.0036	0.0036		0.03
W6	0.322504	0.322504	0.125	0.0036	0.0036	0.0036	-4.4577E-07	
L6	0.538398	0.538398	0.5	0.0054	0.0054	0.0036	0.23907306	
L7	0.46492	0.46492	0.25	0.0054	0.0054	0.0036	0.14997173	
L8	0.672918	0.672918	0.45	0.0054	0.0054	0.0036	0.654061634	
W7	0.571915	0.571915	0.25	0.0054	0.0054	0.0036	-2.34115E-07	
det	0.824908	0.824908	0.65	0.0054	0.0054	0.0054		

Figure 7.3 Net tolerances for the optical image correlator.

Table 7.3 Worst-case image registration errors on initial assembly.

	Assembly Errors	**±Registration Accuracy**
A1 Image:		
Tx	4.508229	0.015
Ty	4.508229	0.015
Tz	27.05065	0.260
Rx	0.298267	0.144
Ry	0.298267	0.144
Rz	0.0054	0.0083
$\Delta M/M$	0.054786	0.0083
A2 Image:		
Tx	4.281985	0.01
Ty	4.281985	0.01
Tz	10.06271	0.112
Rx	0.040398	0.062
Ry	0.040398	0.062
Rz	0.009	0.0055
$\Delta M/M$	0.65066	0.0083

Tz focus errors in both A1 and A2 were untenable, making initial alignment very difficult. It was agreed to tighten the tolerances on focal lengths of L3 and L8 from ±2% to ±0.5%.

In order to fold the correlator into a compact form, it was necessary to evaluate the influences of fold mirrors on the registration errors. The optomechanical constraint equations were re-formulated with a fold mirror between each optical element in both imaging systems, as shown in Fig. 7.4.

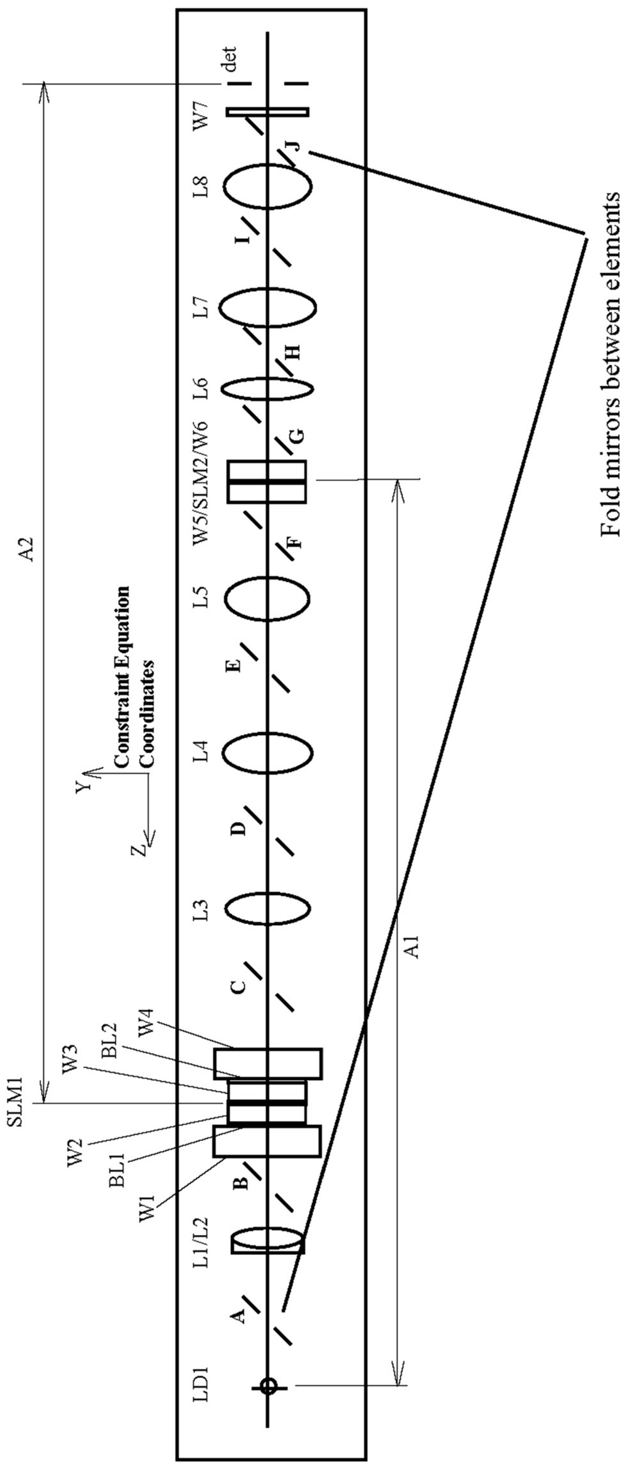

Figure 7.4 Fold mirrors modeled between all optical elements in the correlator.[1]

Table 7.4 Sensitivity of A1 and A2 image registration to adjustable fold mirrors in the system.

	A1 Imaging Coefficients			A2 Imaging Coefficients		
Mirror	Ty_i/Rx_m	Tx_i/Ry_m	Tz_i/Tz_m	Ty_i/Rx_m	Tx_i/Ry_m	Tz_i/Tz_m
A	6.20	−89.7	−26.2			
B	**−125.0**	**−176.7**	**−0.00024**			
C	125.2	−177.1	−0.00024	5.35	−7.57	−0.593
D	−74.8	−105.8	−10.1	−17.1	−24.1	−0.318
E	**26.6**	**−37.6**	**−0.829**	**51.8**	**−73.3**	**−3.41**
F	−5.90	−8.53	−1.41	−81.6	−115.4	−0.0116
G				80.3	−113.6	−0.0116
H				**−56.0**	**−79.2**	**−8.31**
I				**21.8**	**−30.9**	**−0.951**
J				−3.93	−5.56	−1.41

The influences of each of the mirrors on the A1 and A2 images were tabulated as shown in Table 7.4.

Mirrors B and E, shown in bold type, were chosen to fold the A1 imaging system and control the registration between the spatial light modulators. Mirrors H and I, also shown in bold type, were selected to fold the A2 imaging system and present its image to the detector. Note that mirror E also has influences in the A2 optical path; these influences need to be corrected by mirrors H and I. These four mirrors were re-identified as M1, M2, M3, and M4 in Fig. 7.5.

M1 and M2 were crucial for aligning the spatial light modulators in Tx, Ty, and Rz. M1 dominated the Tx and Ty alignment, and M2 controlled the Rz alignment. The solution to the A1 alignment problem is outlined in Table 7.5, which shows the influence coefficients of both mirrors on the A1 image, the required adjustment capability of each mirror-mount based on the influence coefficients, and the actual performance achieved in meeting the alignment requirements. The resolution "achieved" for the M1 mirror mount is only an estimate, but it was demonstrated to be well under the 8.5 μrad requirement. The M1 and M2 mirror mounts had to be custom designed to meet the alignment and stability requirements for the system's operation.

Finally, the optomechanical constraint equations were used to select the material for the optical bench. The thermal effects were studied in the spreadsheet with the equations. The thermal expansion properties of the metal bench and the glasses were listed in the spreadsheet. The dn/dT values for the glasses were also listed in the spreadsheet. The thermal expansion of the bench was used for calculating the change in the air spaces between elements. The thermal expansion and dn/dT properties of the glasses were used for calculating the change in focal length of each lens

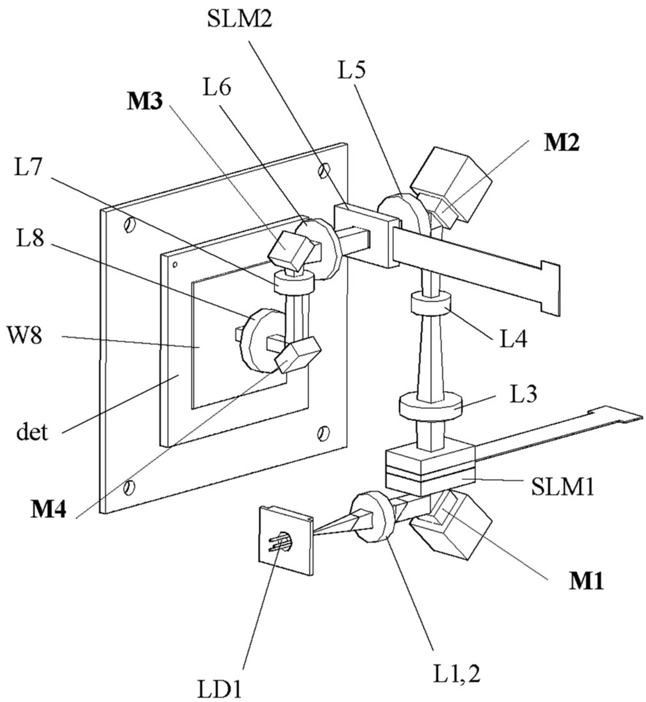

Figure 7.5 The correlator's initial layout as folded.

Table 7.5 The M1 and M2 influence coefficients on the registration of the A1 image.

Registration Variables	M1 Motions						M2 Motions					
	Tx	Ty	Tz	Rx	Ry	Rz	Tx	Ty	Tz	Rx	Ry	Rz
Tx					125.0						−26.6	
Ty			0.0184	−176.8					1.083	−37.6		
Tz			−0.00024						−0.829			
Rx										−1.53		
Ry					0.018						1.083	
Rz					1.414						1.414	
$\Delta M/M$			0.000298						−0.031			

	M1 (Rx)	M1 (Ry)	M2 (Rx)	M2 (Ry)
Required:				
Stroke, mrad (±)	8.5	11.1		42.
Resolution, μrad (±)	8.5	12.		589.
Achieved:				
Stroke, mrad (±)	17.	17.	52.	52.
Resolution, μrad (±)	0.26	0.26	556.	556.

with temperature. These data were then input to the optomechanical constraint equations to calculate the thermal sensitivity of focus $Tz/\Delta T$ and the thermal sensitivity of image size $\Delta M/M\Delta T$ (a proxy for numerical aperture). Table 7.6 lists these data.

Table 7.6 Sensitivity of A1 and A2 image registration to optical bench materials.

Bench Material	Aluminum	CRES	Titanium	Invar
A1				
$Tz/\Delta T$ (mm/°C)	−0.023	−0.013	−0.012	−0.0053
$\Delta M/M\Delta T$ (°/C)	0.00030	0.00032	0.00033	0.00034
A2				
$Tz/\Delta T$ (mm/°C)	−0.0041	−0.0039	−0.0039	−0.0038
$\Delta M/M\Delta T$ (°/C)	0.00036	0.00036	0.00036	0.00036

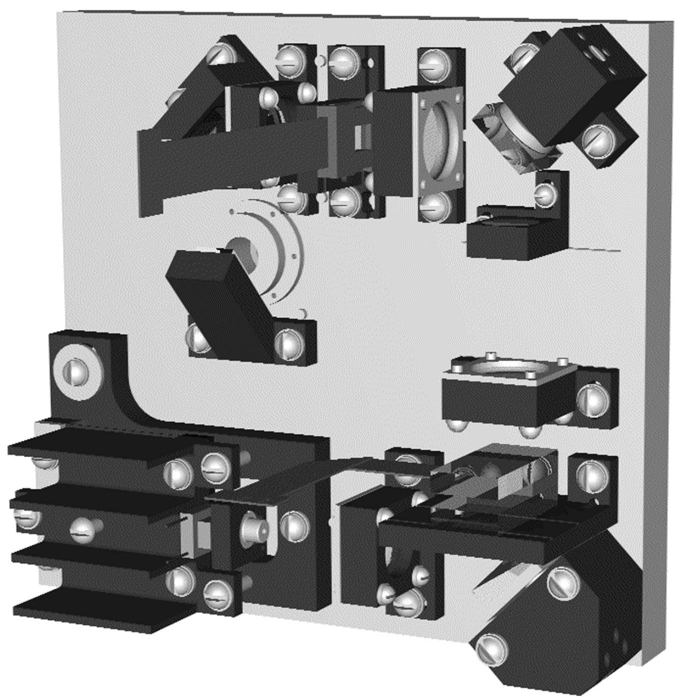

Figure 7.6 The correlator's final configuration.[1]

The CRES (corrosion-resistant steel) bench was adequately stable over the anticipated environment, so the cost of a titanium or Invar bench was avoided. The final design (Fig. 7.6) was successfully built, tested, and put into service. This design reduced assembly time by two-thirds and operating power by 6 dB. The optomechanical constraint equations were also shown (in Section 6.1) to agree very well with both physical test data and the Zemax optical design code.

7.2 A Fiber Optic Spread-Spectrum Encoder

The optomechanical constraint equations were used to stabilize a fiber optic spread-spectrum encoder against the effects of temperature changes. In the fiber optic encoder (Fig. 7.7), the light (1.541 μm wavelength) from the input fiber is first collimated and split between the P and S polarizations. It is then dispersed by a diffraction grating, and the spectrum is refocused on a spatial filter (mask) that encodes it. The encoded spectrum is then re-collimated, and the diffracted orders recombined at a second grating. Finally, a focusing lens re-launches the light into the output fiber.

The mechanical layout of the encoder is shown in Fig. 7.8. The radiation from the input single-mode fiber (F_{in}) is collimated at a lens (L1) and directed through a series of beamsplitters (P1, P2, P3, and P4) that separate the P and S polarization states. After passing through the beamsplitters, the light is directed by a mirror (M1) to a grating (G1) that disperses the spectrum contained in the radiation. The dispersed spectrum is then focused by lenses L2 and L3 on the encoding mask (W1). The radiation transmitted by the mask is re-collimated by lenses L4 and L5, and directed to another grating (G2) that reverses the dispersion effects of G1. The recombined radiation is then directed by a mirror (M2) to a focusing lens (L6) so that the beam can be injected into the output single-mode fiber (F_{out}).

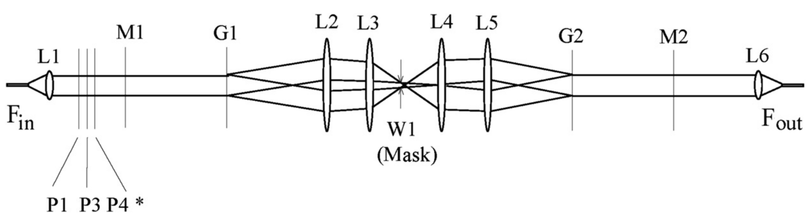

Figure 7.7 A fiber optic spread-spectrum encoder.[1]

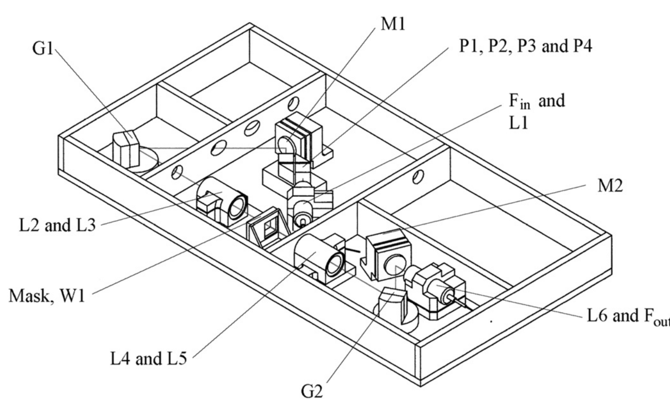

Figure 7.8 The fiber optic encoder mechanical layout.[1]

The plan form of the optical bench is 228.6 mm (9 in.) wide by 431.8 mm (17 in.) long and is laid out to accommodate a duplicate channel (for S polarization) of encoding components configured as a mirror image of the one shown in Fig. 7.8 (for P polarization). The two channels then encode the orthogonal polarization states of the input radiation and share the input fiber (F_{in}), the collimating lens (L1), and portions of the beamsplitter array (P1, P2, P3, and P4).

The core of the single-mode fibers is about 9.1 μm in diameter, and the end of the input fiber (F_{in}) is imaged at the output fiber (F_{out}) with unity magnification (the image is the same size as the output fiber, 9.1 μm in diameter). The registration errors between the image and the output fiber must be kept small with respect to the diameter of the fiber to assure efficient coupling of the power in the image to the output fiber. The optical path length is about 0.75 m.

One challenge for the mechanical engineer is to maximize the efficiency, η, of re-inserting the 1.541 μm light into the fiber network at the output fiber (F_{out}). Early thermal tests were indicative of the problem: The best test article dropped to 40% efficiency between 25° C and 45° C, as shown in Fig. 7.9. This loss in efficiency was considered excessive.

A thermo-elastic optical analysis was performed in three steps. First, the optomechanical constraint equations for the encoder were prepared from the physical optical prescription of the encoder's optics. The constraint equations calculate the position, orientation, and size of the image (of the input fiber) with respect to the output fiber (registration errors) based on changes in the position, orientation, and properties of the optical elements. Second, the registration errors were used to calculate the coupling efficiency at the output fiber following handbook equations.[7] Finally, a simple finite element model was prepared that would calculate the position and orientation changes of all of the optical elements in the system.

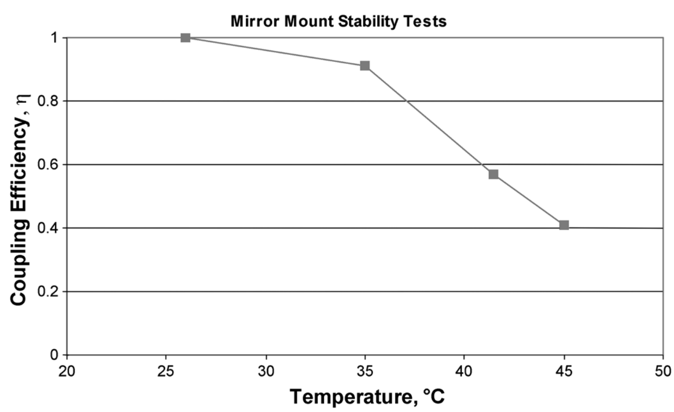

Figure 7.9 Thermal test of coupling efficiency of the encoder.

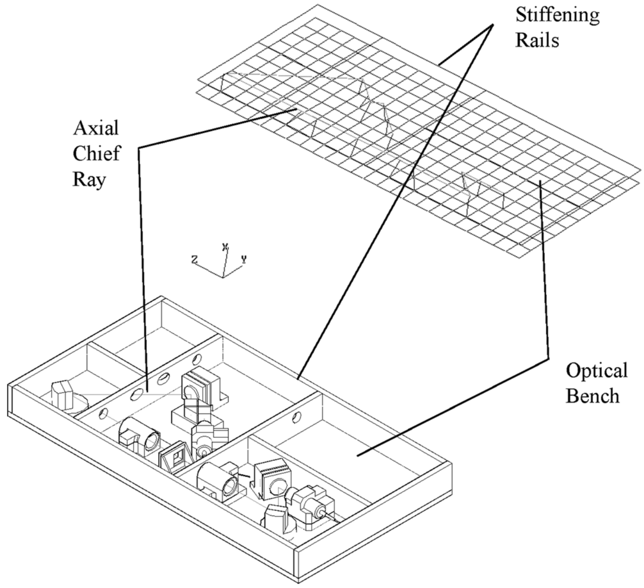

Figure 7.10 A simple thermo-elastic model of the encoder.[2]

The finite element model was made to accurately calculate the mechanical displacements and rotations of the principal points of all of the optical elements in the encoder (Fig. 7.10). In rigid body checks and isothermal checks the model was well behaved, and in static gravity checks it gave reasonable values for deflections. The lowest eigenvalues agreed well with laboratory tests.

A computational spreadsheet program (Microsoft Excel) was used to process the calculations; the optomechanical constraint equations (including changes in optical properties with temperature) and coupling efficiency equations were recorded in the spreadsheet. A block in the spreadsheet was reserved to copy the displacement vector from the finite element analysis output file to the spreadsheet. The analysis temperature was also entered in the spreadsheet next to the finite element displacement data. The spreadsheet automated all of the interpretive calculations and prepared graphical output. Only three acts were required by the analyst: (1) prepare the optomechanical constraint equations, (2) run the finite element model, and (3) print the graphical output data. The results of the analysis are shown in Fig. 7.11 and compared to the early test results.

One of the advantages of the optomechanical constraint equations is that all of the calculations are open and available for inspection. A review of individual contributors in the spreadsheet, as summarized in Table 7.7, discloses two major contributors to the coupling loss problem.

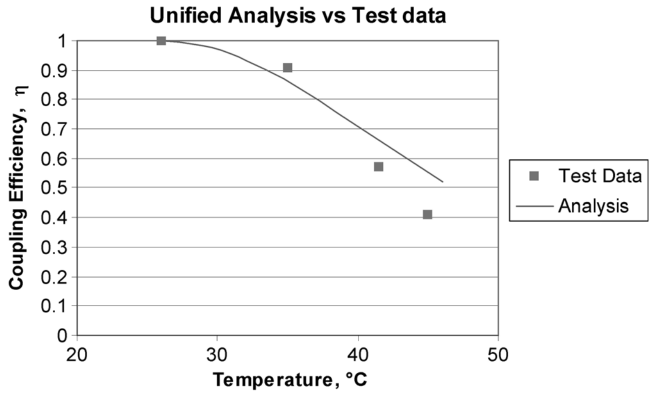

Figure 7.11 Analysis versus test results for the encoder.[1]

Table 7.7 Contributors to the coupling losses in the encoder.

		Contributors		
Registration Variables	**Net Errors**	**Mirror Mounts**	**Aluminum Bench**	**Lens Thermal**
Tx	0.003443	0.003443		
Ty	0.000312	1.51×10^{-6}		
Tz	0.035492		0.040696	−0.00518
Rx	2.72×10^{-11}			
Ry	4.97×10^{-12}			
Rz	-2.7×10^{-16}			
$\Delta M/M$	0.00594		0.005715	0.000225
η as analyzed	0.522			
η stabilized mounts		0.846		
η with CRES bench			0.985	

The largest contributors are the fold mirror mounts, in which the adjusting screws are stainless steel in otherwise all-aluminum assemblies. Replacing the stainless steel screws with aluminum screws (of the same alloy as the mount itself) would increase the coupling efficiency from 0.522 to 0.846.

The table also lists the contributions of the lens thermal sensitivities and the thermal expansion of the aluminum optical bench. Since their contributions to the Tz error were of opposite sign, it was possible to nullify the effects of the lens thermal sensitivities by selecting a suitable low-thermal-expansion material for the optical bench. If 416 stainless steel was used (a reasonably good match to nullify the lens effects), the Tz registration error could be reduced by over 70%. Combined with correcting the mirror mounts, the resulting coupling efficiency would be 0.985.

7.3 An Infrared Imager

The optomechanical constraint equations were used for designing the structure of the inner (elevation) gimbal for a suite of instruments, including an infrared imager (Fig. 7.12).

The outline of the inner gimbal had been defined for the proposal effort in CAD software, and the optical physical prescriptions for the imager, the laser, and the laser receiver had been completed in Code V. It was necessary to stabilize the line of sight (LOS) of the suite to less than 10 μrad (rms) in a random vibration environment. The stability of the imager was considered to be the most difficult problem, so the imager was addressed first. The gimbal was to be mounted on an isolated platform with a resonant frequency of 25 Hz and a peak resonant transmissibility of 2.5. The random response in the frequency band of interest was estimated to be about 1.0 g (rms) (g is the normal gravitational acceleration: 1.0 g = 9.8 m/s^2). Therefore, it was decided to first stabilize the imager in 1.0 g static gravity.

The imager's optical design as developed in Code V is shown in Fig. 7.13. The units of the physical optical prescription were inches. The prescription data were used to develop the optomechanical constraint equations using the Ivory Optomechanical Modeling Tools software.[5] Ivory produced two output files: the "imager.out" file containing the constraint equations in a form to import to Microsoft Excel, and the "imager.nas" file containing the same information in a form to import to a Nastran finite element model.

The *.stp files for the imager were imported from Code V into Patran and meshed with solid finite elements (Fig. 7.14); the "imager.nas" file was also imported to Patran and attached to the solid optical elements so that any time one of the optical elements moved, the image at the detector would move also. The optical elements were "framed" with bar elements in Patran to form cells for each of the elements (Fig. 7.15).

Then the CAD solid model of the proposal's inner gimbal structure was imported to Patran as well, as shown in Fig. 7.16(a), which also

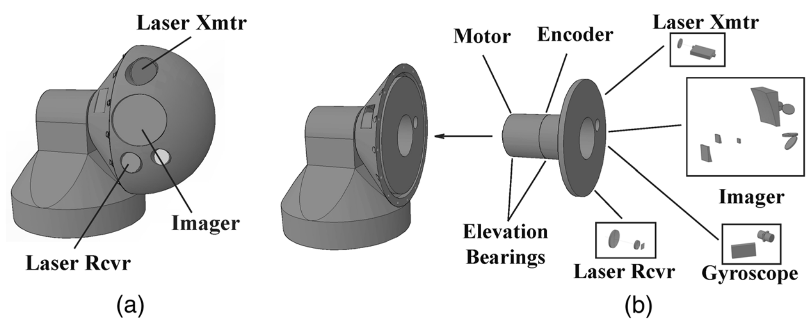

Figure 7.12 A suite of infrared instruments: (a) external view of the system and (b) exploded view of optical components (reprinted from Ref. 8).

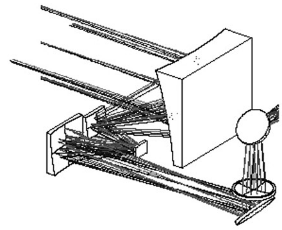

ELT NO.	SUR NO.	SURFACE DESCRIPTION RADIUS X Y	SHAPE	THICKNESS OR SEPARATION	APERTURE DESCRIPTION DIMENSION X	Y	SHAPE	MATERIAL
OBJECT		INF	FLT	INFINITY				
				1.3000		7.405	CIR	
				0.0000		7.417	CIR	
				0.0000		7.417	CIR	
				4.4564		7.417	CIR	
1	1	-10.6445	A-1	-4.4555	3.400	2.798	C-1	REFL
2	2	-3.4340	A-2	1.5854	0.900	0.634	C-2	REFL
3	3	INF	FLT	-2.8516	0.500	0.338	C-3	REFL
4	4	5.3737	A-3	7.3000	1.540	1.240	C-4	REFL
		DECENTER(1)						
5	5	INF	FLT	0.0000		1.316	CIR	REFL
		BEND(1)						
				-0.5020		1.161	CIR	
6	6	-2.7639 CX	SPH	-0.1351		1.241	CIR	GERMMW
		HOLOGRAM(1)						
6	7	-3.9269	A-4	-2.0528		1.206	CIR	
		DECENTER(2)						
7	8	INF	FLT	2.0528		1.026	CIR	REFL
		BEND(2)						
8	9	1.8290 CX	SPH	0.1621		0.745	CIR	GERMMW
		HOLOGRAM(2)						
8	1							
9	1							
9	1							
	1							
10	1							
10	1							
IMAG								

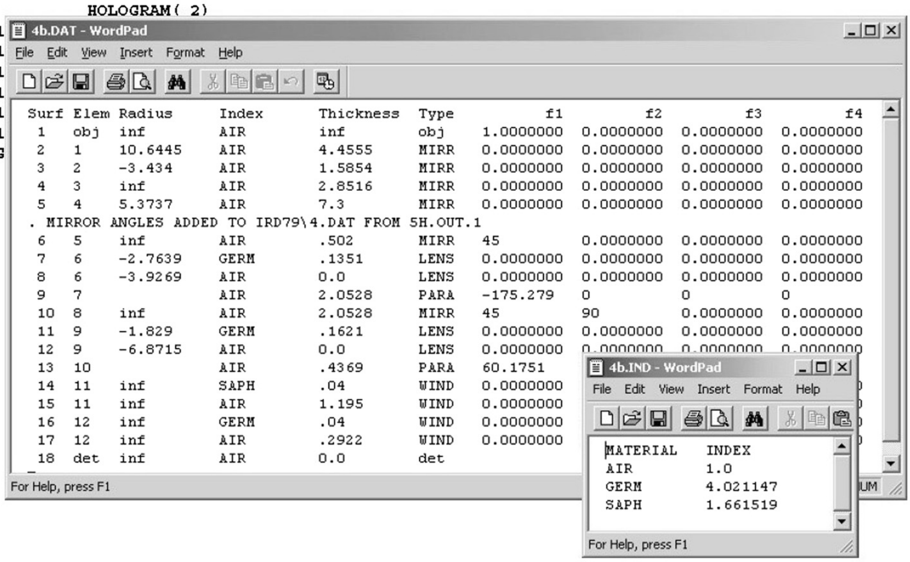

4b.DAT - WordPad

File Edit View Insert Format Help

Surf	Elem	Radius	Index	Thickness	Type	f1	f2	f3	f4
1	obj	inf	AIR	inf	obj	1.0000000	0.0000000	0.0000000	0.0000000
2	1	10.6445	AIR	4.4555	MIRR	0.0000000	0.0000000	0.0000000	0.0000000
3	2	-3.434	AIR	1.5854	MIRR	0.0000000	0.0000000	0.0000000	0.0000000
4	3	inf	AIR	2.8516	MIRR	0.0000000	0.0000000	0.0000000	0.0000000
5	4	5.3737	AIR	7.3	MIRR	0.0000000	0.0000000	0.0000000	0.0000000
. MIRROR ANGLES ADDED TO IRD79\4.DAT FROM 5H.OUT.1									
6	5	inf	AIR	.502	MIRR	45	0.0000000	0.0000000	0.0000000
7	6	-2.7639	GERM	.1351	LENS	0.0000000	0.0000000	0.0000000	0.0000000
8	6	-3.9269	AIR	0.0	LENS	0.0000000	0.0000000	0.0000000	0.0000000
9	7		AIR	2.0528	PARA	-175.279	0	0	0
10	8	inf	AIR	2.0528	MIRR	45	90	0.0000000	0.0000000
11	9	-1.829	GERM	.1621	LENS	0.0000000	0.0000000	0.0000000	0.0000000
12	9	-6.8715	AIR	0.0	LENS	0.0000000	0.0000000	0.0000000	0.0000000
13	10		AIR	.4369	PARA	60.1751			
14	11	inf	SAPH	.04	WIND	0.0000000			
15	11	inf	AIR	1.195	WIND	0.0000000			
16	12	inf	GERM	.04	WIND	0.0000000			
17	12	inf	AIR	.2922	WIND	0.0000000			
18	det	inf	AIR	0.0	det				

For Help, press F1

4b.IND - WordPad

File Edit View Insert Format Help

MATERIAL	INDEX
AIR	1.0
GERM	4.021147
SAPH	1.661519

For Help, press F1

Figure 7.13 Optical prescription for the infrared imager (reprinted from Ref. 8).

shows the meshed and framed optical cells positioned on the CAD model solids. Next, the inner gimbal CAD solids were meshed with shell elements [Fig. 7.16(b)], simulating the thickness of the structural walls, and the imager's optical cells were mounted to the inner gimbal structure with

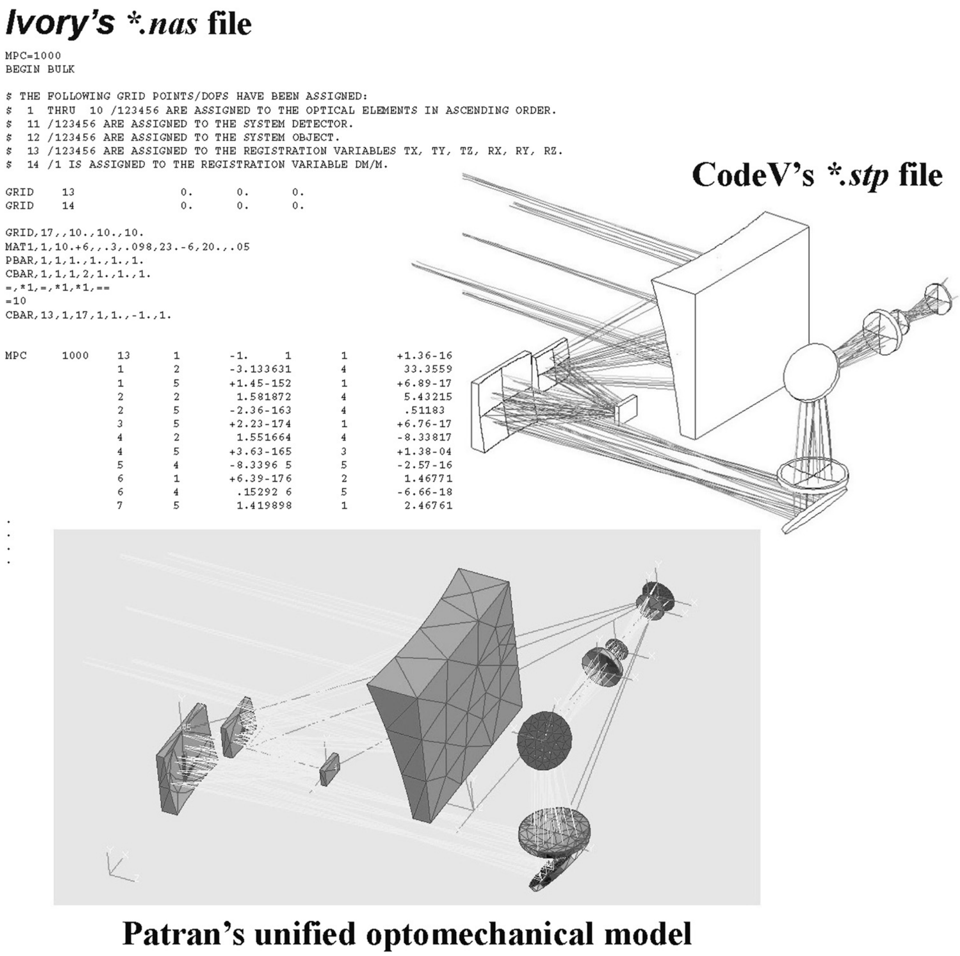

Figure 7.14 The optical elements and optomechanical constraint equation in Patran (reprinted from Ref. 8).

more bar elements [Figs. 7.17(a) and (b)]. This configuration is a complete opto-structural model of the imager on the elevation gimbal's structure.

The model was tested in a 6-degree-of-freedom (1.0 in. in each of *Tx*, *Ty*, *Tz*, and 1.0 rad in each of *Rx*, *Ry*, *Rz*) rigid body check. The Nastran output file is shown in Table 7.8.

In the Nastran output file, grid point 3454 is the base point at which the displacements were input to the model. Grid point 2123 shows the six image motions on the detector. They are all small values except for T1 in *Rx* displacement and T2 in *Ry* displacement, where the reported values of 16.679 and −16.677 agree well with the effective focal length of 16.678 from the Ivory output file. The grid point 2124 shows the change in image size $\Delta M/M$ in the T1 column. The multipoint constraints on degrees of freedom R1 and

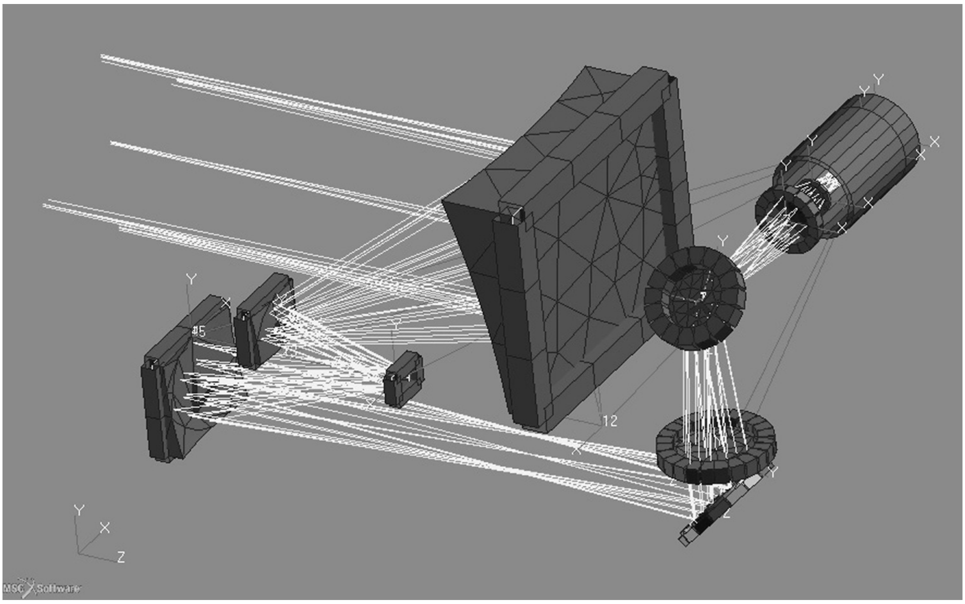

Figure 7.15 The optical elements modeled into cells (framed) in Patran.[9]

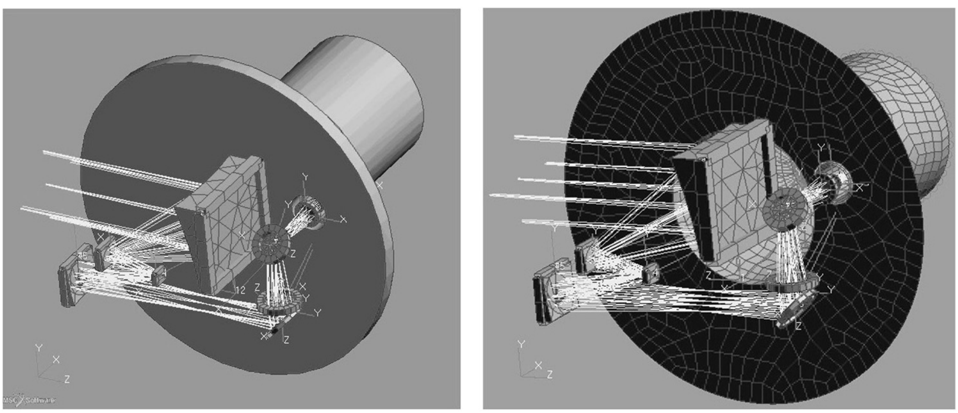

(a) (b)

Figure 7.16 (a) The inner gimbal CAD solids with the meshed optical cells properly located. (b) The inner gimbal structure meshed with shell elements and the CAD solids removed.[9]

R2 of grid point 2124 were modified to directly calculate the LOS errors in radians as follows:

$$2124\,\mathrm{R1} = (2123\,\mathrm{T1})/16.678$$
$$2124\,\mathrm{R2} = (2123\,\mathrm{T2})/-16.678,$$

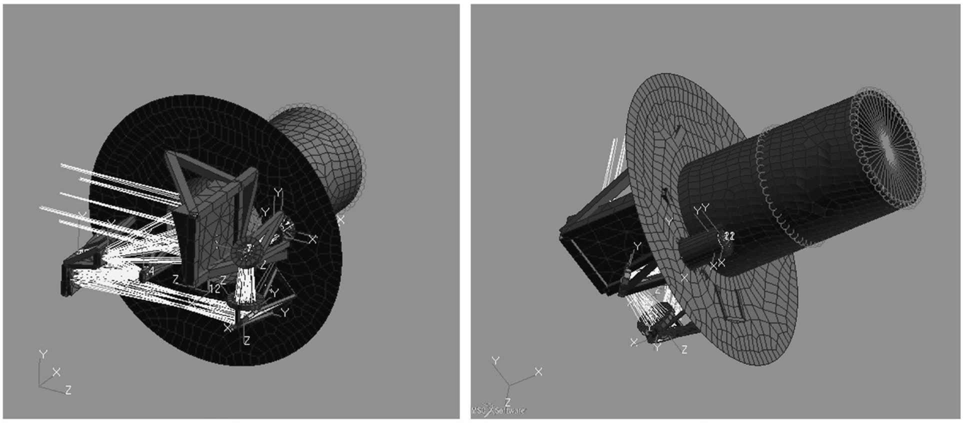

(a) (b)

Figure 7.17 (a) The optical cells initially mounted to the face of the elevation gimbal. (b) A back view of the initial elevation gimbal (reprinted from Ref. 8).

where 16.678 is the effective focal length of the optical system, and the far-field LOS rotations *Rx* and *Ry* are in the R1 and R2 columns, respectively. It can be seen that the far-field LOS calculations agree with the imposed rotations to about 3 parts in 100,000.

Stabilizing the imager on the inner gimbal began with a simple three-axis (*X*, *Y*, and *Z*) static gravity loading of 1.0 gs. Nastran calculated the image motions and the far-field LOS errors in the displacement vectors shown in Table 7.9. The grid points 3454 and 3456 represent the centers of the elevation axis ball bearings that constrain the gimbal in gravity loading.

The far-field LOS errors are summarized in the Table 7.10. The *Rx* and *Ry* values are taken from the Nastran displacements (Table 7.9) for grid point 2124, R1 and R2, for each of the loading cases. The net value is the root-sum-square value of *Rx* and *Ry* for each of the loading cases. The LOS errors exceeded the budget by over three-fold in the *Z* axis of gravity, so it was necessary to substantially stiffen the structural support.

To determine the elements that contribute most to the LOS error, it is helpful to look at the cumulative contributions of all of the degrees of freedom of all of the optical elements. This was performed by importing both the optomechanical constraint equations and the Nastran displacement vectors into Microsoft Excel. Then, the individual influence coefficients (from the optomechanical constraint equations) were multiplied by the individual displacement components (from Nastran) to determine the individual image motion contributions on an element-by-element and degree-of-freedom-by-degree-of-freedom basis. These values were then summed and charted to disclose the largest contributors to the LOS errors.

The results of plotting the *Z*-axis gravity loading case are shown in Figs. 7.18(a) and (b) for *Rx* and *Ry* components of the LOS errors,

Table 7.8 Image registration errors in the Nastran displacement vectors for the 6-degree-of-freedom rigid body check.

DISPLACEMENT VECTOR (TX)

POINT ID.	TYPE	T1	T2	T3	R1	R2	R3
2123	G	−4.495383E-09	−2.804798E-06	1.535378E-06	−8.338841E-12	4.617249E-10	4.605635E-12
2124	G	1.157860E-07	0.0	0.0	−2.695207E-10	1.681897E-07	0.0
3454	G	1.000000E+00	0.0	0.0	0.0	0.0	0.0

DISPLACEMENT VECTOR (TY)

POINT ID.	TYPE	T1	T2	T3	R1	R2	R3
2123	G	2.489022E-06	2.804443E-06	−1.531967E-06	1.458557E-11	−7.180084E-11	6.401721E-12
2124	G	3.411351E-06	0.0	0.0	1.492293E-07	−1.681684E-07	0.0
3454	G	0.0	1.000000E+00	0.0	0.0	0.0	0.0

DISPLACEMENT VECTOR (TZ)

POINT ID.	TYPE	T1	T2	T3	R1	R2	R3
2123	G	−2.348945E-06	−7.698533E-10	1.999892E-05	7.981358E-11	−1.151832E-10	−1.155364E-11
2124	G	1.876438E-03	0.0	0.0	−1.408310E-07	4.616426E-11	0.0
3454	G	0.0	0.0	1.000000E+00	0.0	0.0	0.0

DISPLACEMENT VECTOR (RX)

POINT ID.	TYPE	T1	T2	T3	R1	R2	R3
2123	G	1.667934E+01	−7.940791E-06	−2.036467E-05	9.572198E-11	6.800884E-06	2.518961E-06
2124	G	−2.309178E-03	0.0	0.0	1.000010E+00	4.761695E-07	0.0
3454	G	0.0	0.0	0.0	1.000000E+00	0.0	0.0

DISPLACEMENT VECTOR (RY)

POINT ID.	TYPE	T1	T2	T3	R1	R2	R3
2123	G	2.328079E-02	−1.667689E+01	2.076247E-04	2.350952E-06	2.803869E-06	7.069737E-04
2124	G	1.907376E-02	0.0	0.0	1.395799E-03	1.000030E+00	0.0
3454	G	0.0	0.0	0.0	0.0	1.000000E+00	0.0

DISPLACEMENT VECTOR (RZ)

POINT ID.	TYPE	T1	T2	T3	R1	R2	R3
2123	G	−2.529502E-05	−1.178215E-01	1.429845E-05	1.248827E-05	2.497396E-10	9.992900E-01
2124	G	−3.477024E-05	0.0	0.0	−1.516563E-06	7.065168E-03	0.0
3454	G	0.0	0.0	0.0	0.0	0.0	1.000000E+00

Table 7.9 Image registration errors in the Nastran displacement vectors for *X*-, *Y*-, and *Z*-axis gravitational loading.

DISPLACEMENT VECTOR (X GRAVITY)

POINT ID.	TYPE	T1	T2	T3	R1	R2	R3
2123	G	−4.992433E-05	2.669824E-04	7.401585E-04	1.224534E-04	1.137726E-05	−5.847887E-05
2124	G	−6.120696E-04	0.0	0.0	−2.993424E-06	−1.600805E-05	0.0
3454	G	0.0	0.0	0.0	0.0	3.829348E-08	−3.936964E-08
3456	G	0.0	0.0	0.0	−4.206286E-11	7.107967E-08	−7.302642E-08

DISPLACEMENT VECTOR (Y GRAVITY)

POINT ID.	TYPE	T1	T2	T3	R1	R2	R3
2123	G	2.339886E-04	3.158928E-04	4.181697E-04	4.730350E-05	2.639247E-05	−2.648768E-06
2124	G	−3.468143E-04	0.0	0.0	1.402977E-05	−1.894068E-05	0.0
3454	G	0.0	0.0	0.0	0.0	−3.548640E-10	−6.136999E-07
3456	G	0.0	0.0	0.0	−8.670319E-08	4.243269E-10	−1.117305E-06

DISPLACEMENT VECTOR (Z GRAVITY)

POINT ID.	TYPE	T1	T2	T3	R1	R2	R3
2123	G	3.268024E-04	3.839157E-04	−1.930393E-04	−8.001957E-05	−6.618082E-05	1.248440E-05
2124	G	1.295611E-04	0.0	0.0	1.959481E-05	−2.301928E-05	0.0
3454	G	0.0	0.0	0.0	0.0	6.137461E-07	−2.179917E-10
3456	G	0.0	0.0	0.0	8.850597E-08	1.117723E-06	−3.177722E-10

Table 7.10 Initial far-field imager line-of-sight errors for *X*-, *Y*-, and *Z*-axis gravitational loading.

	LOS Errors (μrad)		
	Rx	*Ry*	Net
X Gravity	−2.9934	−16.0081	16.2855
Y Gravity	14.0298	−18.9407	23.5708
Z Gravity	19.5948	−23.0193	30.2299

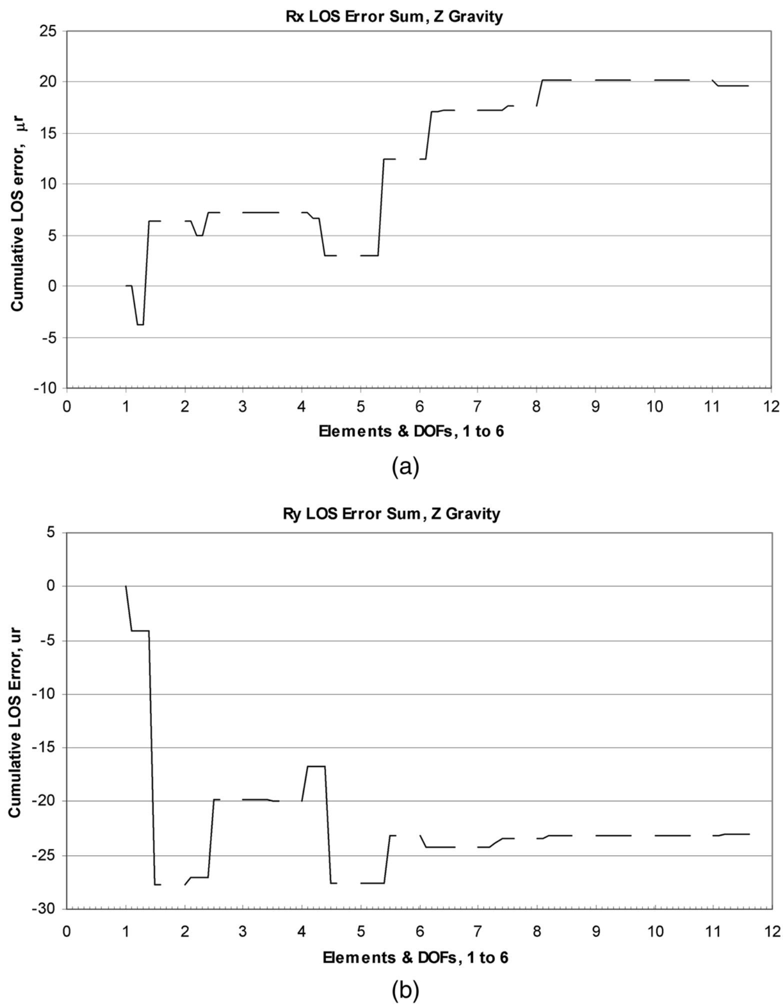

Figure 7.18 Cumulative, element-by-element, LOS error charts for *Z*-axis gravity for the (a) *Rx* and (b) *Ry* components.

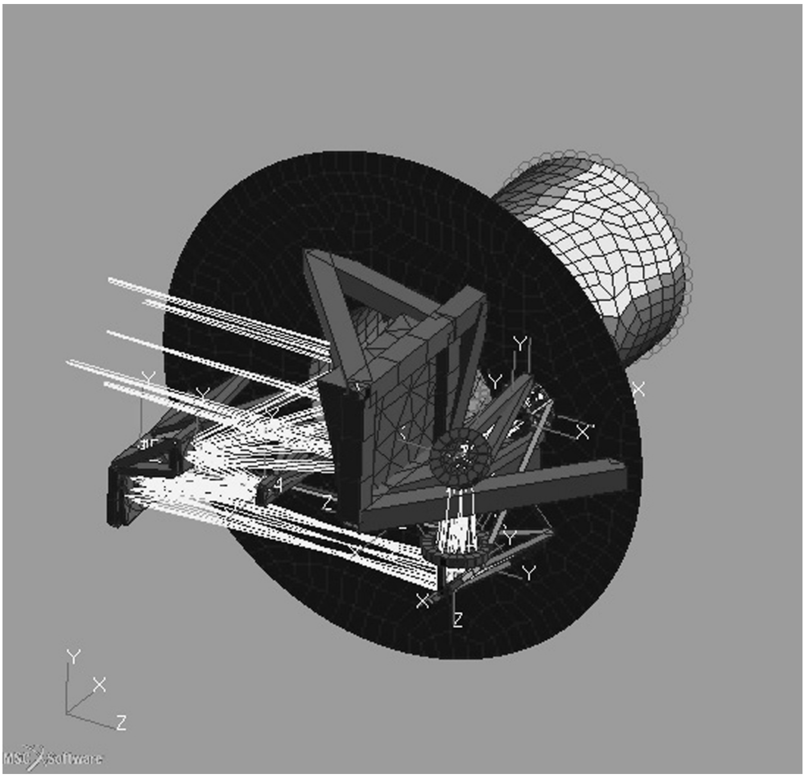

Figure 7.19 Additional stiffening for the infrared imager mounting.

respectively. It is clear from these plots that the *Ry* displacement (degree of freedom 5) of Element 1 is the greatest contributor to the *Ry* LOS error, and its *Rx* displacement a significant contributor to the *Rx* LOS error.

Additional stiffening of the mounting of Element 1 (Fig. 7.19) produced a material improvement in the LOS stability in the next Nastran run for the *Z* axis of gravity (Table 7.11) but had little effect on the *Y*-axis response and actually worsened the *X*-axis response. The reader can see that one of the braces for Element 1 actually obscures part of the light path. It will be seen that this was corrected in a later iteration.

Table 7.11 Imager line-of-sight errors for the first revision to the structural support of the imager.

	LOS Errors (μrad)		
	Rx	*Ry*	Net
X Gravity	17.0123	8.23231	18.89945
Y Gravity	17.68992	−15.3495	23.42095
Z Gravity	9.980825	16.55372	19.32984

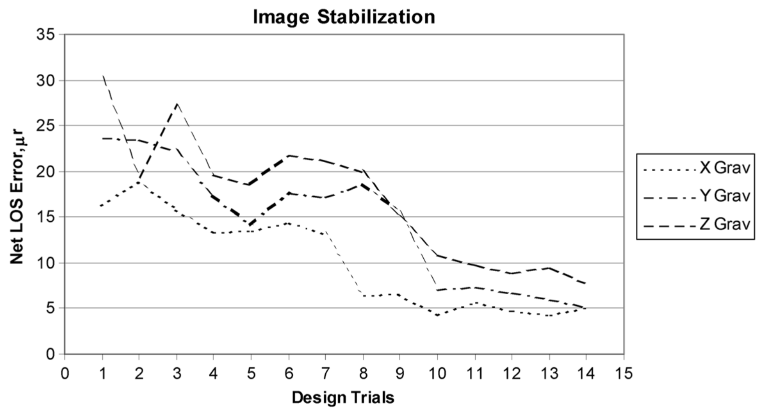

Figure 7.20 The history of reducing the LOS errors in Patran/Nastran (reprinted from Ref. 10).

This design process is an iterative one involving several trials before the engineer becomes sensitive to the structural and optical interactions involved.

In this particular design, 14 trials were used to finally reduce the net LOS errors to less than 10 μrad in all three gravity vectors. The results of these trial optomechanical designs are plotted in Fig. 7.20, and the numerical results after the 14th trial are shown in Table 7.12.

The final structural configuration of the imager on the elevation gimbal is shown in Fig. 7.21 with front- and rear-quarter views. Substantial stiffening was required on the opposite side of the optical mounting plate in addition to the stiffening of the optical cells and mounts, themselves. In this figure one can see the adjustment to Element 1's back brace to avoid obscuring the optical path.

The final step in the analysis was to verify that this configuration would perform as expected in the random vibration environment. This required the addition of the laser, the laser receiver, and the gyroscope to the elevation gimbal. The configuration of their mounting is shown in Fig. 7.22. The gimbal was then excited by the random vibration spectrum [Fig. 7.23(a)], and the random LOS errors for the imager were calculated

Table 7.12 Imager line-of-sight errors for the 13th revision to the structural support of the imager.

	LOS Errors (μrad)		
	Rx	*Ry*	Net
X Gravity	−0.79157	4.972313	5.034926
Y Gravity	3.34836	−3.92354	5.158069
Z Gravity	5.486229	−5.56046	7.811364

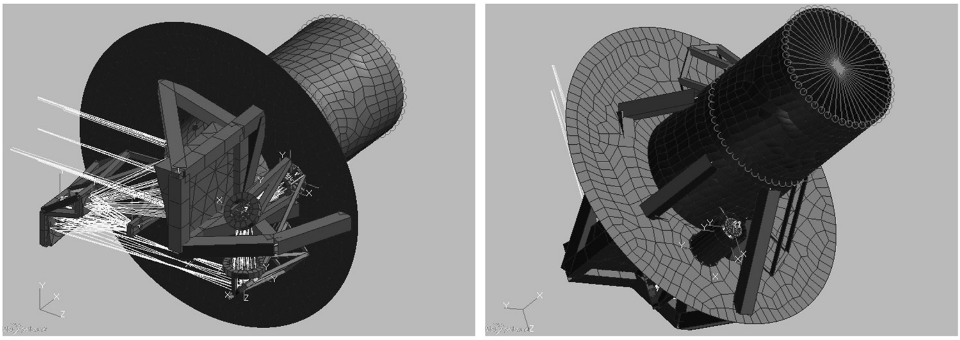

(a) (b)

Figure 7.21 The final structural configuration of the imager: (a) front view and (b) rear view.

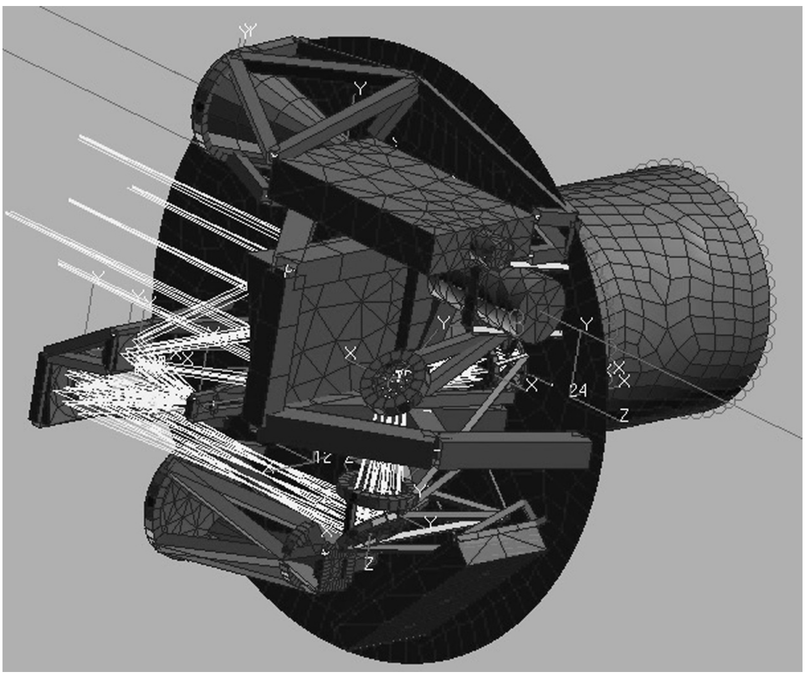

Figure 7.22 The configuration of the full suite of instruments.

by the Nastran model. The response power spectral density (PSD) for the imager's LOS under vibration in the X axis is also shown in Fig. 7.23(b). The net response for all three instruments is shown in Table 7.13 for each of the three axes of vibration. This effort provided the CAD engineer a workable initial concept for the structure of the inner gimbal of the system.

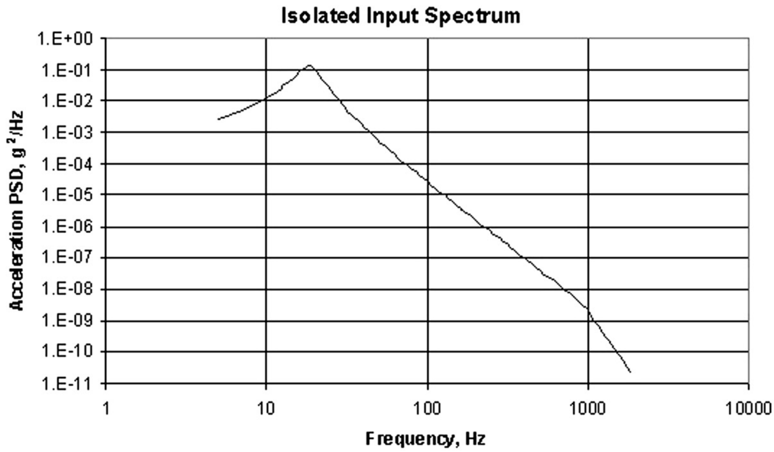

(a)

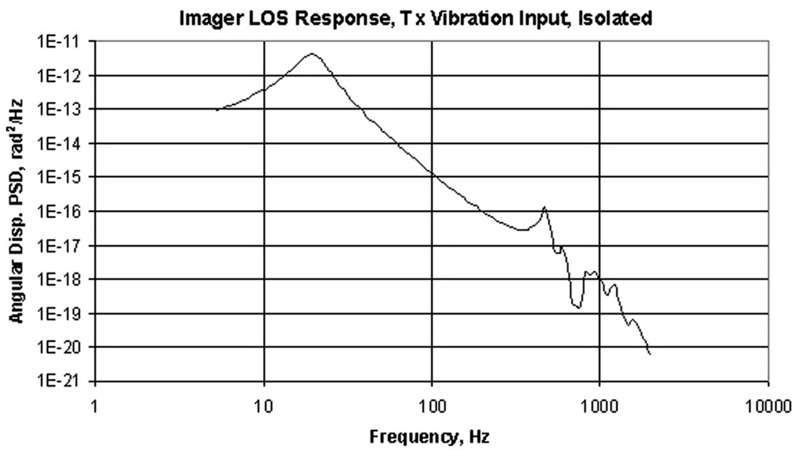

(b)

Figure 7.23 (a) Excited *X*-axis acceleration PSD. (b) LOS angular response PSD (reprinted from Ref. 11).

Table 7.13 Imager and laser line-of-sight errors and gyroscope pointing errors for in-service random vibration environments.

Vibration loading vector	*Tx*	*Ty*	*Tz*
Net pointing errors (rms μrad)			
Imager (2124)	6.4	5.5	8.9
Laser (21663)	7.5	0.9	6.8
Gyroscope (10286)	1.7	2.2	16.9

References

1. A. E. Hatheway, *Optomechanical Analysis*, Tutorial, Alson E. Hatheway, Inc., Pasadena (2015).
2. A. E. Hatheway, *Optomechanics and the Tolerancing of Instruments*, Tutorial, Alson E. Hatheway, Inc., Pasadena (2015).
3. W. J. Smith, *Modern Optical Engineering*, McGraw-Hill, New York, pp. 58–85 (1990).
4. A. E. Hatheway, *Ivory User's Guide*, Alson E. Hatheway, Inc., Pasadena (2015).
5. A. Hatheway, *Ivory Optomechanical Modeling Tools*, Alson E. Hatheway Inc., Pasadena (2015).
6. P. Burke, A. Caneer, A. Whitehead, and A. Hatheway, "Optical correlator system design using opto-mechanical constraint equations to determine system sensitivities," *Proc. SPIE* **5176**, 44–52 (2003) [doi: 10.1117/12/507542].
7. F. C. Allard, *Fiber Optics Handbook for Engineers and Scientists*, McGraw-Hill, New York (1990).
8. A. E. Hatheway, "Linking a laser and an optical imager to a gyro's axis of rotation in MSC Nastran," *MSC Software 2011 Users Conference*, MSC Software Corporation, Santa Ana (2011).
9. A. E. Hatheway, "Off-axis imager modeling," *AEH IR&D Report* **73**, Alson E. Hatheway Inc., Pasadena (2010).
10. A. E. Hatheway, "Controlling lines of sight and lines of propagation in stable systems," *Proc. SPIE* **8125**, 81520V (2011) [doi: 10.1117/12.895545].
11. A. E. Hatheway, "Unified optomechanical modeling: Stabilizing the line-of-sight of an IR imager," *Proc. SPIE* **9577**, 957705 (2015) [doi: 10.1117/12.2186870].

Index

Alson E. Hatheway is Chair (and a co-founder) of the International Technical Group on Optomechanical Engineering, and President of his own company, Alson E. Hatheway Inc. He has a Bachelor of Science degree in Mechanical Engineering from the University of California, Berkeley. He managed mechanical engineering departments for Xerox Corporation, Hughes Aircraft Company, and Gould Corporation before opening his own firm to concentrate on the mechanical design and analysis of optical systems. He has published more than 70 technical papers with numerous technical societies (SPIE, OSA, ASME, AIAA, ASPE, and IES) and edited 12 volumes of the *Proceedings of SPIE*.

Mr. Hatheway is a Fellow of both SPIE and OSSC, a senior member of AIAA, and a life member of ASME. He is listed in *Who's Who in Science and Engineering*, *Who's Who in America*, and *Who's Who in the World*. He has been a part-time faculty member at the University of La Vern (California) and taught various industrial tutorials on aspects of optomechanical engineering.